UNIVERSITY OF CALIFORNIA
RIVERSIDE

Novel Insights Into the Mechanisms of Atherosclerosis

A Dissertation submitted in partial satisfaction
of the requirements for the degree of

Doctor of Philosophy

in

Biomedical Sciences

by

Rebecca Hernandez

September 2024

Dissertation Committee:
Dr. Changcheng Zhou, Chairperson
Dr. Meera Nair
Dr. Marcus Kaul

The Dissertation of Rebecca Hernandez is approved:

Committee Chairperson

University of California, Riverside

ACKNOWLEDGEMENTS

I would like to express my gratitude to the School of Medicine Core at the University of California, Riverside, and to Mary Hamer for her invaluable assistance with the 10x Genomics platform. I also acknowledge the UC San Diego IGM Genomics Center for sequencing the PANDORA-seq, single-cell RNA, and RNA-seq samples. I am grateful to Dr. Wenxin Zhao for preparing the recombinant AlkB, and to Dr. Sihem Cheloufi's lab for providing the mESCs.

Importantly, I wish to acknowledge the Zhou lab members, both past and present, for their support and assistance. I extend my deepest thanks to Dr. Zhou for his mentorship and for trusting me to lead these projects. I would like to also thank my funding sources: the NIH T32 training program and the American Heart Association Pre-doctoral fellowship program.

Lastly, I would like to acknowledge everyone who has supported me through this journey, especially my mom and dad. It’s because of your courage and sacrifices that I’ve been able to achieve my dreams. As I continue on my journey, please know that every accomplishment I achieve is as much yours as it is mine.

Por último, quiero dar las gracias a todos los que me han apoyado en este camino, especialmente a mi mamá y papá. Gracias a sus valentías y sacrificios he podido alcanzar mis sueños. Mientras continúo mi camino, sepan que cada logro que obtengo es tanto suyo como mío.

DEDICACIÓN/DEDICATION

Esta disertación está dedicada a todas las estudiantes latinas en ciencias de primera generación. Asumimos el desafío, luchamos, nunca nos rendimos, y sí se pudo!

This dissertation is dedicated to all first-generation Latina students in science. We took on the challenge, we struggled, never gave up, and we did it!

ABSTRACT OF THE DISSERTATION

Novel Insights Into the Mechanisms of Atherosclerosis

by

Rebecca Hernandez

Doctor of Philosophy, Graduate Program in Biomedical Sciences
University of California, Riverside, September 2024
Dr. Changcheng Zhou, Chairperson

Atherosclerosis is a chronic inflammatory disease characterized by the accumulation of lipids, immune cells, necrotic cells, and other fibrous material in the sub-intimal space of large arteries. The lack of medical intervention or lifestyle changes can lead to advanced plaque development and plaque rupture, causing complete obstruction of blood flow, and ultimately death. Novel small noncoding RNAs (sncRNAs) including tRNA-derived small RNAs (tsRNAs) and rRNA-derived small RNAs (rsRNAs) have emerged as new players in regulating biological processes in various diseases but their role in atherosclerosis remains unknown. Using a novel PANDORA-seq method for the detection of highly modified sncRNAs, we identified many dysregulated tsRNAs and rsRNAs in the intima of high cholesterol diet (HCD)-fed LDL receptor-deficient ($LDLR^{-/-}$) mice as compared with traditional small RNA sequencing results. HCD-induced intimal tsRNA-Arg-CCG may contribute to atherosclerosis by stimulating endothelial dysfunction. Emerging studies also suggest paternal dietary exposures may affect offspring health via tsRNA/rsRNA-mediated intergenerational transmission of paternal phenotypes. We found

that paternal HCD feeding can increase atherosclerosis in F1 female, but not F1 male, offspring, which was associated with increased intimal inflammation in the F1 females. Using PANDORA-seq, we confirmed that tsRNAs and rsRNAs were also altered in the sperm of HCD-fed mice, which correlated with expression changes in sncRNA-biogenesis related genes in the epididymis. These studies highlight the function of tsRNA/rsRNA in disease development and the transmission of diseased phenotypes. In addition to the discovery of tsRNAs and rsRNAs in mediating atherosclerosis development, we also investigated the effects of adventitial fibroblast IκB kinase β (IKKβ) in regulating plaque stability. The involvement of the adventitia on plaque development has been largely overlooked. IKKβ is a known pro-inflammatory molecule and has been previously demonstrated to promote plaque development. Interestingly, we found that deficiency of IKKβ in fibroblasts rendered $LDLR^{-/-}$ mice to develop unstable plaques characterized with thin fibrous caps, large necrotic cores, and reduced collagen content. Single cell-sequencing analysis revealed decreased smooth muscle cell population in fibroblast IKKβ deficient aortas, possibly due to reduced fibroblast to smooth muscle cell differentiation. These results indicate that fibroblasts are crucial for maintaining the plaque stability in an IKKβ-dependent manner. Collectively, these studies revealed new contributors of atherosclerosis development, including novel tsRNAs/rsRNAs, paternal diet, and fibroblast IKKβ on atherosclerosis development and plaque stability.

Table of Contents

List of Tables

List of Figures

1. Chapter 1: Introduction

1.1 Atherosclerosis – an Overview

Atherosclerosis, or plaque development in the arteries, is the major contributor of cardiovascular disease (CVD) and death worldwide. It is a multifactorial disease causing narrowing of large and medium arteries, which reduces blood flow to major organs resulting in deadly outcomes such as carotid artery disease, coronary artery disease, peripheral artery disease, and chronic kidney disease. There are several risk factors associated with atherosclerosis development including hypertension, elevated cholesterol, diabetes, obesity, substance use, inactivity, and genetic factors. However, despite medical intervention and lifestyle changes, atherosclerosis remains a significant health crisis worldwide.

Atherosclerosis was initially believed to be associated with dysregulated lipid and cholesterol storage, but in the 19th century Rudolf Virchow proposed that inflammation may be the primary contributor to atherosclerosis (1). However, this idea was not explored until the 1970s when Russel Ross introduced the "Response to injury" hypothesis, which considers all of the interactions and inflammatory responses from the cells involved in atherosclerosis and was later combined with his "Inflammation hypothesis" (2, 3). Since then, the link between atherosclerosis and inflammation has been extensively studied and proven to be important in atherosclerosis development like Virchow first hypothesized. Today, atherosclerosis is characterized by the uncontrolled accumulation of lipids, immune

cells, and other fibrous material into the sub-intimal space that is driven by chronic inflammation (4-8).

At the cellular level, atherosclerosis is initiated when the inner intimal layer, composed of endothelial cells, undergoes a phenotypic change, termed endothelial dysfunction, stimulated by modified LDL such as oxidized-LDL (oxLDL) and the presence of other risk factors. The endothelium fails to maintain vascular homeostasis during endothelial dysfunction like vasodilation, eliminating reactive oxygen species, and maintaining an appropriate inflammatory balance. Various chemotactic factors and adhesion molecules are expressed by endothelial cells undergoing endothelial dysfunction, which aids in monocyte migration and infiltration. Ox-LDL is rapidly taken up by monocyte scavenger receptors upon monocyte infiltration, leading to the conversion of monocytes into lipid-filled macrophage foam cells. The lesional foam cells can release inflammatory factors to further contribute to the monocyte infiltration, lipid build-up, and a vicious inflammatory cycle (Figure 1.1) (6-9).

While acute vessel wall inflammation leads to asymptomatic fatty streaks on the vessel wall, chronic inflammation and the gradual, uncontrolled accumulation of foam and necrotic cells develop into symptomatic plaques. If left untreated, the plaque increases in size and may eventually rupture, exposing the thrombogenic core and giving rise to a thrombus, or blood clot. Thrombosis can be life-threatening, causing complete blockage in the brain, heart, or other major organs. Thus, controlling the stability of the plaque is necessary to prevent thrombotic events. Though the mechanisms behind plaque instability remain elusive, the characteristics of rupture prone plaques include a thin fibrous cap, small

extracellular matrix (ECM) component, large immune cell infiltrate, and a large necrotic core (10).

It has been recognized for decades that vascular smooth muscle cells (VSMCs) in the middle, or medial, layer undergo bi-directional phenotypic switching between contractile to synthetic during atherosclerosis progression, enabling VSMCs to proliferate and migrate to the cap of the plaque (also termed, fibrous cap) (11). It is also believed that VSMCs contribute to ECM deposition, such as collagen, to reinforce cap stability (11). Therefore, dysregulation in VSMC phenotypic switching, or the lack of VSCMs at the cap may contribute to plaque instability. Indeed, it has been documented that VSMCs are nearly absent in human samples of ruptured plaque, further contributing to the notion that VSMCs are essential for maintaining plaque stability (12). Besides their role in plaque stability, VSMCs are also believed to uptake lipids, rendering them foam cells, which may necrotize and contribute to the necrotic core (11). Though this topic remains controversial, it suggests that VSMCs can be both beneficial and detrimental to plaque stability and the mechanisms dictating the fate of VSMCs are unknown and require further investigation. Interestingly, other origins of VSMCs have been reported such as circulating or adventitial progenitor cells (13, 14), alluding to the fact that cellular contributions to plaque stability is complex and requires more research to trace the origins of fibrous cap cells.

1.1.1 Generational inheritance of CVD

The discovery and wide production of drugs targeting risk factors of CVD Such as elevated cholesterol, hypertension, and glucose intolerance have decreased CVD age-specific death rates (15, 16). Unfortunately, this declining trend is stabilizing, and CVD

remains the world's leading cause of death despite the various medical interventions available to treat the risk factors associated with disease progression (16). Thus, the presence of atherogenic risk factors alone cannot fully explain the epidemiology of this disease. Studies have demonstrated that parental suboptimal exposures such as an unhealthy diet, ageing, or environmental toxicants can modify the germline epigenome, affecting embryonic and fetal development resulting in adverse health outcomes in adult offspring. Furthermore, various epidemiological studies, such as the Överkalix cohorts of Northern Sweden and the Dutch famine of 1994, have provided evidence of generational epigenetic inheritance through multigenerational analysis of these cohorts. For example, studies of the Överkalix cohorts of Northern Sweden demonstrates that early life reduction of food supply was correlated with decreased mortality rates in grandchildren (17). Interestingly, these were sex-specific observations where grandson mortality was associated with grandfather food supply, and granddaughter mortality was associated with grandmother food supply (17, 18). Additionally, during the Dutch famine of 1994, offspring from mothers who were in their last trimester during the famine became less obese, whereas mothers who were in their early pregnancy resulted in higher obesity rates in their offspring (19). These landmark studies provided some of the initial evidence of nonmendelian inherited traits, which drove for a deeper exploration behind the mechanisms of these inherited phenotypes.

In relation to cardiovascular disease, longitudinal cohort studies, such as the Framingham cohort study, the Physicians' Health study, and the Women's Health Study provide evidence that parental history of CVD or presence of associated risk factors in

parents serve as an independent risk factor for atherosclerosis development in offspring (20-23). Though we cannot ignore familial lifestyles as a contributor of CVD trends in a family group, rodent models have made it possible to investigate the association between parental suboptimal exposures, such as diet, to CVD outcomes in a controlled environment. A series of studies by Napoli and colleagues have demonstrated that maternal hypocholesterolemia in human or rodent models increase fatty streak and subsequent plaque size in fetal and postnatal offspring (24-26). Interestingly, early maternal antioxidant or lipid lowering intervention can reverse maternal hypercholesterolemia-elicited increase atherosclerosis development in their offspring (27, 28). The mechanism behind maternal hypercholesterolemia-induced cardiometabolic disease in offspring have not been fully investigated, but it has been suggested that maternal hypercholesterolemia alters the macrophage epigenetic state, inhibiting LXRa and PPARg expression. In turn, this promoted macrophage polarization toward an M1 inflammatory phenotype in the offspring (29).

Besides maternal effects, paternal suboptimal diets can also affect offspring health. For example, paternal high-fat diet (HFD) feeding in rodents can induce a range of metabolic disorders in the offspring (30-32) Paternal low-protein diet can also affects offspring health and impair vascular function and metabolic disorders in offspring (33-36). Besides dietary challenges, environmental toxicants can also elicit inter- and trans-generational adverse health effects in the offspring (37-40). For example, it was demonstrated that maternal in utero exposure to lipopolysaccharides (LPS) in rats triggered hypertension in F1 through F5 progeny (41), proving that environmental exposures may be

imprinted in the epigenome across multiple generations. Together these studies support the concept that parental environmental exposures may interfere with offspring epigenetic signatures resulting in adverse cardiometabolic phenotypes. Various well-known epigenetic regulators have been proposed to contribute to intergenerational inheritance of environment-induced phenotypes in mammals (42). Interestingly, sperm small non-coding RNAs (sncRNAs) especially tRNA-derived small RNAs (tsRNAs) and rRNA-derived small RNAs (rsRNAs) have been shown to directly contribute to the transmission paternal metabolic phenotypes(32, 43-45).

1.2 Small noncoding RNAs- an Overview

It was originally thought that the noncoding regions of DNA do not contain any function or benefit to the organism (46). However, when scientists discovered that only <2% of the human genome encodes for protein, it was presumed that the remaining ~98% must have a functional purpose. It quickly became evident that ncRNAs participate in regulating molecular processes including gene regulation and may become dysregulated in disease conditions such as atherosclerosis. ncRNAs can be categorized into small (<200 nt) or long (>200 nt) ncRNAs (sncRNA or lncRNA, respectively) that have similar functions in regulating molecular processes (47). For example, sncRNAs and lncRNAs control gene expression via chromatin remodeling by recruiting chromatic remodeling complexes, transcriptional regulation via partial or complete complimentary sequences, post-transcriptional modifications, and interference with translational machinery(48, 49). lncRNAs and sncRNAs have also been identified as potential biomarkers for certain

diseases such as cancer and CVD (50-52). Thanks to the continual progress made towards RNA detection, we are now aware of the diverse sncRNA subtypes, which includes microRNA (miRNA), piwi-interacting RNA (piRNA), circular RNA (circRNA), and highly modifies sncRNA species tRNA-derived sncRNA (tsRNA) and rRNA-derived sncRNA (rsRNA). Importantly, many of these remain underexplored.

tsRNAs (also referred to as tDRs, tRFs, or tiRNAs) have been gaining much attention recently due, in part, to their evolutionary conserved sequences and roles in regulating gene expression, translation, apoptosis, histone modifications, cell-cell communication, and for their role in epigenetic regulation (53-56). However, tsRNA mechanisms of action are still being investigated. The first report investigating tsRNAs in atherosclerosis was a human study conducted by He et al in 2021, which involved plaque samples from healthy individuals and patients with atherosclerosis. In the atherosclerotic patients, 315 dysregulated tsRNAs were identified including tsRNA-Gly-GCC (referred to as tRF-Gly-GCC in the study). Further exploration revealed that tsRNA-Gly-GCC may regulate cell adhesion, proliferation, and migration in endothelial cells and VSMCs in vitro (57). Though this study demonstrates the potential role of tsRNAs in atherosclerosis development, more studies are needed to elucidate their roles and mechanisms.

1.2.1 Detection of highly modified sncRNAs

With the continual progress made towards RNA detection, we are now aware of the diverse sncRNA landscape, which includes the highly modified tsRNAs, rsRNAs, piRNAs, circRNAs, and others. However, RNA species such as tsRNAs and rsRNAs contain high levels of modifications (e.g., methylation and terminal modifications) that act as physical

barriers during cDNA construction and render it difficult to capture via traditional sequencing methods (58-60). For example, N1-methyladenosine (m1A), N3-methylcytidine (m3C), and N1-methylguanosine (m1G) are modifications found on tsRNAs which block reverse transcription during traditional cDNA construction (58, 59). As a result, methylated tsRNAs and other sncRNAs escape library construction and remain undetected. Additionally, several sncRNA species contain 3' terminal modifications including 3'-phosphate (3'-P) and 2'3'-cyclic phosphate (2'3'-cP) that block adaptor ligation which also escape traditional library construction (60). Although these modifications hinder our detection capacity of sncRNAs, they are essential for the stability and function of RNA in normal and pathological conditions (30, 43, 61).

To address this technical obstacle, we developed a new technique, called PANDORA-seq (Panoramic RNA Display by Overcoming RNA Modification Aborted Sequencing), to overcome the limitations in sncRNA discovery (Figure 1.2), which can detect more rsRNA and tsRNA than traditional-seq (59). Specifically, PANDORA-seq utilizes a pre-size-selection step and enzymatic treatments to overcome RNA fragmentation and modifications (Figure 1.2). The PANDORA-seq method has revealed distinct patterns of tsRNA and rsRNA expression profiles in a tissue and cell specific manner, which is not detected with traditional-seq (59). PANDORA-seq has also been previously used to detect dysregulated tsRNAs in sperm under certain conditions, such as chemical exposures (37, 62). By utilizing PANDORA-seq, we are now able to identify more tsRNA and rsRNA species that become dysregulated in diseased conditions.

1.2.2 sncRNAs as epigenetic regulators and carriers of diseased phenotypes

The epigenome refers to the genomic chemical imprints that do not involve changes in genetic sequences but can regulate gene expression patterns. This epigenetic information can be inherited from parent to offspring and is also responsible for determining cell fates (63). However, the epigenome is sensitive to environmental stimuli and may undergo epigenetic re-programming, which can lead to changes in gene expression causing phenotypic changes in the absence of genetic mutations. Epigenetic modifications and regulators such as DNA methylation, histone modifications, and sncRNAs have been proposed as the main mechanisms for the epigenetic transmission of disease risk across multiple generations (63).

SncRNAs like piRNAs and tsRNAs have been known to exert epigenetic regulation. piRNAs are a class of small noncoding RNAs that are mainly expressed in the germline and interact with PIWI proteins. The piRNA/PIWI complex recruits epigenetic modification factors to silence transposon elements, regulate chromatic remodeling via histone modification, and perform DNA methylation (64-66). Similarly, tsRNAs can also interact with PIWI proteins to exert similar epigenetic functions, such as histone modification (67, 68). Specifically, tsRNA-Glu can interact with PIWIL4 to recruit H3K9 histone methyltransferases to stimulate CDA1 promoter methylation (67). tsRNAs may also participate in posttranscriptional gene silencing by acting similarly to miRNAs and forming RISC complexes (69). tsRNAs have also been implicated in regulating histone assembly via downstream heterochromatin-mediated transcriptional repression (70).

Further studies are required to fully elucidate the mechanism behind tsRNA-mediated epigenetic regulation.

It has been discovered that mature mouse sperm carry a subset of tsRNAs and rsRNAs, which are the dominant form of small RNAs in mature sperm (31, 71, 72). These tsRNAs are also sensitive to expression and modification alterations with exposures to certain stimuli (i.e., HFD, low protein diet, and EDCs) (31, 72-75). In fact, it was discovered that the injection of highly modified sperm tsRNA/rsRNA-enriched RNA fractions (30-40nt) from HFD-diet fed male mice into normal zygotes induced metabolic disorders in the F1 offspring (30). It was further demonstrated that an RNA methyltransferase, Dnmt2, can regulate the biogenesis of both tsRNAs and rsRNAs, and alter secondary sncRNA structures and biological properties which underline sperm RNA's biological impact in epigenetic inheritance (31). These emerging data promote the concept that sperm RNAs and their RNA modifications form a sperm RNA code—a type of epigenetic information beyond the DNA sequence that induces offspring phenotypes mirroring paternal environmental stressors (32). Although the mechanism of tsRNA-mediated epigenetic regulation of metabolic disease is still being investigated, these studies set the stage to further examine a wider range of diseases, such as cardiovascular disease.

1.2.3 tsRNA biogenesis in the male reproductive system

The biogenesis of tsRNAs is driven by systematized tRNA cleavage to produce tRNA halves (~30 nt), shorter 3' and 5' tsRNA fragments, or internal fragments (~18-22 nt) (55, 56). tsRNA halves are generated by anticodon loop cleavage by angiogenin (ANG) (76-78), while the shorter fragments are generated by D-loop and T-loop Dicer-induced

cleavage (78). Likewise, other ribonucleases (i.e., RNase T2, RNase L, RNase P, etc.) are known to cleave tRNAs at various sites (55, 78). Modifications on mature tRNAs can also regulate tRNA cleavage by promoting or suppressing cleavage at certain sites. For example, DNMNT2 is a methyltransferase that initiates m^5C methylation on multiple tRNAs, which prevents cleavage at those sites. On the other hand, loss of m^5C methylation increases cleavage susceptibility (79). Together the expression of cleavage and modification enzymes (tsRNA-biogenesis genes) facilitate precise tsRNA biogenesis, which mediates biological processes in the cell.

External stimuli may alter the expression of tsRNA-biogenesis genes in the male reproductive system, resulting in changes in the tsRNA landscape in the sperm (30, 80). Notably, sperm are unable to synthesize their own tsRNAs because they are highly compacted and transcriptionally inactive. Instead, sncRNAs are trafficked from epididymal epithelial cells during post-testicular maturation via extracellular vesicles called epididysomes (81). Interestingly, it has been reported that sperm in the different compartments of the epididymis contain varying levels of sncRNA subtypes and become increasingly enriched with tsRNAs by the time sperm has reached the cauda epididymis (82). Therefore, changes in tsRNA-biogenesis genes in the epididymis in response to external stimuli can alter the tsRNA landscape that is eventually shuttled to the sperm, leading to downstream epigenetic changes.

1.3 IKKβ and NF-κB Signaling – an Overview

Chronic low-grade inflammation has been established as a major contributor to the development of atherosclerosis (7). Many inflammatory pathways that contribute to the cardiometabolic disease risk are regulated by the transcriptional factor NF-κB, a master regulator of the innate and adaptive immune responses (83, 84). In non-stimulated cells, NF-kB remains in the cytoplasm bound to specific inhibitory proteins – the inhibitors of NF-κB (IκBs). In response to various stimuli including proinflammatory cytokines, infectious agents, reactive oxygen species, and free fatty acids, membrane-bound receptors such as the tumor necrosis factor receptor family, interleukin-1 receptor, and toll-like receptors, become activated leading to the activation of the IKK complex (85, 86). The IKK complex is composed of two catalytic subunits (IKKα and IKKβ) and a regulatory subunit (IKKγ/NEMO). IKKβ and its serine-threonine kinase activity are essential for the phosphorylation and ubiquitination of IκB leading to free NF-κB that can then translocate to the nucleus and regulate the expression of many target genes (84, 87). In addition to regulating the NF-κB pathway, more new targets of IKKβ have also been identified, including b-catenin, x-box binding protein, and insulin receptor-1 (Figure 1.3). The known IKKβ substrates and their functions in tumorigenesis, inflammation, diabetes, hormone response, and cell survival have been discussed in detail in several comprehensive reviews (88, 89).

1.3.1 The Role of IKKβ in Atherosclerosis

For many years, the NF-κB pathway has been implicated in the pathogenesis of atherosclerosis (90). For example, NF-κB activation has been detected in atherosclerotic

plaques, including macrophages, endothelial cells, and smooth muscle cells in both human and animal models (91-94). Previous studies have implicated that NF-κB activation in human atherosclerosis was IKKβ-dependent and resulted in up-regulation of proinflammatory and prothrombotic mediators (95). However, recently studies have demonstrated that the functions of IKKβ in atherosclerosis are complex and that IKKβ in different tissues or cell types may have different impact on atherosclerosis development in animal models. As a significant player in atherosclerosis initiation and progression, studies have suggested that the inflammatory response in endothelial dysfunction can be driven by IKKβ/NF-κB signaling (4, 91, 96). Gareus et al. previously demonstrated that inhibition of NF-κB activity through the deletion of IKKγ, or expression of a dominant-negative IκBα decreases atherosclerosis in atherogenic prone mice (4). They also found that inhibition of NF-κB in endothelial cells reduced the expression of proinflammatory cytokines, chemokines, and adhesion molecules, leading to decreased monocyte recruitment into the plaque (4). Consistently, inhibition of IKKβ in human umbilical vein endothelial cells has been shown to block NF-κB activation, leading to decreased adhesion molecule gene expression including E-selectin, ICAM-1, and VCAM-1 (97). By contrast, constitutive activation of endothelial IKKβ in mice increased monocyte infiltration into the subintimal space, which contributed to exacerbating early and late-stage atherosclerosis (98). Indeed, the rise of age-associated endothelial dysfunction is correlated with increased IKK activation in arteries while pharmacological inhibition of IKK by salicylate has been shown to improve age-related endothelial dysfunction (99). Thus, targeting endothelial cell IKKβ may have beneficial effects against atherosclerosis development.

The M1, or proinflammatory, macrophage plays a key role in atherosclerosis development, while M2, or anti-inflammatory, macrophages enhance plaque regression and stability (100). Evidence suggests that IKKβ/NF-κB pathway activation polarizes macrophages to the M2, anti-inflammatory phenotype through negative crosstalk with STAT1 (101, 102). To study the role of macrophage IKKβ in atherosclerosis, Kanters et al. transplanted IKKβ-deficient bone marrow-derived macrophages into atherogenic prone low-density lipoprotein receptor-deficient ($LDLR^{-/-}$) mice. They found that the mice receiving IKKβ-deficient macrophages exhibited enhanced atherosclerotic lesion development and increased necrosis, which suggests a protective role of bone marrow-derived macrophage IKKβ against atherosclerosis development (103). However, the same group used a similar method to delete IκBα in myeloid cells, aimed to activate NF-κB signaling. Interestingly, those mice displayed increased atherosclerosis lesion size and leukocyte adhesion without significantly increasing NF-κB targeted genes (104), indicating pro-atherogenic effects of canonical NF-κB activation. Several other studies have also found that macrophage IKKβ/NF-κB pathway has pro-atherogenic effects (105, 106). For example, inhibition of NF-κB in macrophages through the overexpression of a trans-dominant and non-degradable form of IκBα can reduce macrophage foam cell formation *in vitro* (105). Further, myeloid-specific IKKβ deficiency decreased diet-induced atherosclerosis in $LDLR^{-/-}$ mice by diminishing macrophage inflammatory responses such as adhesion, migration, and lipid uptake in macrophages (106). Collectively, these results indicate the role of macrophage IKKβ/NF-κB in atherogenesis

is complex and more studies are needed to completely understand how IKKβ functions in myeloid cells to regulate atherosclerosis development.

In addition to endothelial and immune cells, VSMCs also play a key role in atherogenesis. In the early stages of atherosclerosis, VSMCs undergo a phenotypic switch from contractile to synthetic where they gain the ability to proliferate and migrate into the intimal layer. This provides a beneficial effect as these VSMCs proliferate and migrate to the cap of the plaque and reinforces its stability, lowering the risk for plaque rupture (107). An earlier study demonstrated that IKKα and IKKβ were activated in IL-1β-induced proliferative response of human saphenous vein smooth muscle cells (108). Notably, the proliferative ability of human VSMCs were diminished in IKKα and IKKβ mutant transfected cells (108). The role of VSMC IKKβ in atherosclerosis was also investigated in LDLR$^{-/-}$ mice (109). Deficiency of IKKβ in VSMCs driven by a SM22Cre-IKKβ-flox system protected LDLR$^{-/-}$ mice from diet-induced vascular inflammation and atherosclerosis development (109). These studies suggest that inhibiting IKKβ/NF-κB signaling in the vasculature has anti-atherogenic effects.

1.3.2 Non-canonical mechanisms of IKKβ

While deletion of IKKβ in VSMCs decreased atherosclerosis development in LDLR$^{-/-}$ mice (109), those mice were also protected from diet-induced obesity and insulin resistance. Interestingly, many adipocyte precursor cells express SMC markers and ablation of IKKβ blocked adipocyte differentiation in vitro and in vivo, suggesting that IKKβ functions in adipocyte precursor cells to regulate adiposity (109). Indeed, selective deletion of IKKβ in the white adipose lineage further elucidated the role of adipose

progenitor cell IKKβ signaling in regulating adiposity and metabolic function (109, 110). Deficiency of adipose progenitor IKKβ decreased high-fat feeding-induced adipogenesis and systemic inflammation, resulting in decreased adiposity and insulin resistance in those mice (109, 110). The function of IKKβ in the regulation of adipogenesis was further confirmed in mesenchymal stem cells (MSCs) (111). Mechanistic studies then revealed an important crosstalk between IKKβ and Wnt/β-catenin signaling (111). Interestingly, IKKβ is a β-catenin kinase that can directly phosphorylate the conserved degron motif of β-catenin to prime it for β-TrCP-mediated ubiquitination and degradation (85, 111). Wnt/β-catenin signaling has been well studied to inhibit adipocyte differentiation (112, 113) and the impact of IKKβ signaling on adipogenesis was abolished in β-catenin-deficient MSCs (85, 111). Thus, IKKβ-mediated β-catenin phosphorylation may play a critical role in regulating adipocyte differentiation and adiposity in obesity.

Insulin resistance is a very complex syndrome and IKKβ has been shown to regulate insulin resistance by directly interfering with the insulin signaling pathway (114). Once stimulated by its ligand, insulin, the insulin receptor (IR) becomes activated and phosphorylates IRS-1 on its tyrosine residues, leading to increased glucose uptake (115). As a serine kinase, IKKβ can ectopically phosphorylate IRS-1 on multiple serine residues, which prevents proper signaling (116). Several studies have demonstrated that treatment with glucose lowering drugs and molecules such as kaempferol (117), timosaponin B-II (TB-II) (118), rosiglitazone (119), and bovine α-lactalbumin hydrolysates (α-LAH) (120) can alleviate insulin resistance by decreasing or inhibiting IKKβ levels/activity resulting in a reduction of ectopic IRS-1 serine phosphorylation.

Inflammation is an important contributor of insulin resistance, and adipose tissue is one of the important tissues for this high-fat feeding-elicited inflammatory response (121). Adipose IKKβ signaling has been implicated in obesity-associated insulin resistance. For example, studies have found that IKKβ deficiency in adipocyte precursors or adipose lineage cells can protect mice from diet-induced obesity, systemic inflammation, and insulin resistance (109, 110). Several studies demonstrated that IKKβ deficiency and XBP1 overexpression attenuates FFA-induced inflammation and impairment of insulin signaling in cultured adipocytes (122, 123). While hepatic IKKβ increases nuclear translocation of XBP1 (124), adipocyte IKKβ is inhibited by XBP1 (123), indicating a more complex role of IKKβ/XBP1 interaction in cardiometabolic disease. Overexpression of IKKβ in adipocytes also led to increased adipose tissue inflammation in mice (125). Paradoxically, those mice were resistant to diet-induced obesity and insulin resistance, likely due to increased energy expenditure (125). Deletion of adipocyte IKKβ did not affect obesity in mice but resulted in elevated adipose tissue inflammation, increased macrophage infiltration and exacerbated insulin resistance (126, 127). With more new molecular targets of IKKβ being discovered, there will be more opportunities for fully understanding the complex function of IKKβ in cardiometabolic diseases and for developing new and effective therapeutic approaches.

1.4 Scope of Dissertation

1.4.1 Identification and characterization of transfer RNA-derived small RNAs associated with atherosclerosis development

The overall goal of this study is to utilize PANDORA-seq to identify previously undetected sncRNAs, such as tsRNAs and rsRNAs, in the intima and sperm of hypercholesterolemic LDLR$^{-/-}$ mice. Within this study we also investigate the intergenerational transmission of cardiometabolic disease in the offspring of hypercholesterolemic vs normocholesterolemic LDLR$^{-/-}$ mice.

Specific Aim 1: Identify and elucidate the role of tsRNAs associated with atherosclerosis development in male LDLR$^{-/-}$ mice using the PANDORA-seq method.

Specific Aim 2: Investigate the intergenerational effects of paternal hypercholesterolemia on offspring cardiometabolic health.

Specific Aim 3: Identify the sncRNA landscape in the sperm of HCD-fed LDLR$^{-/-}$ mice.

1.4.2 The role of fibroblast IKKβ in atherosclerosis development

The overall goal of this study is to reveal the role of adventitial fibroblast IKKβ on atherosclerosis plaque development and stability. Studies on atherosclerosis mainly focus on the inner layers of the vasculature, and not much is known about the role of the adventitia or adventitial fibroblasts in atherosclerosis development.

Specific Aim 1: Identify the role of fibroblast IKKβ on plaque development utilizing transgenic mouse models to delete IKKβ in fibroblasts.

Specific Aim 2: Evaluate the cellular heterogeneity and transcriptional features associated with fibroblast IKKβ-deficient mediated plaque instability.

1.5 Figures

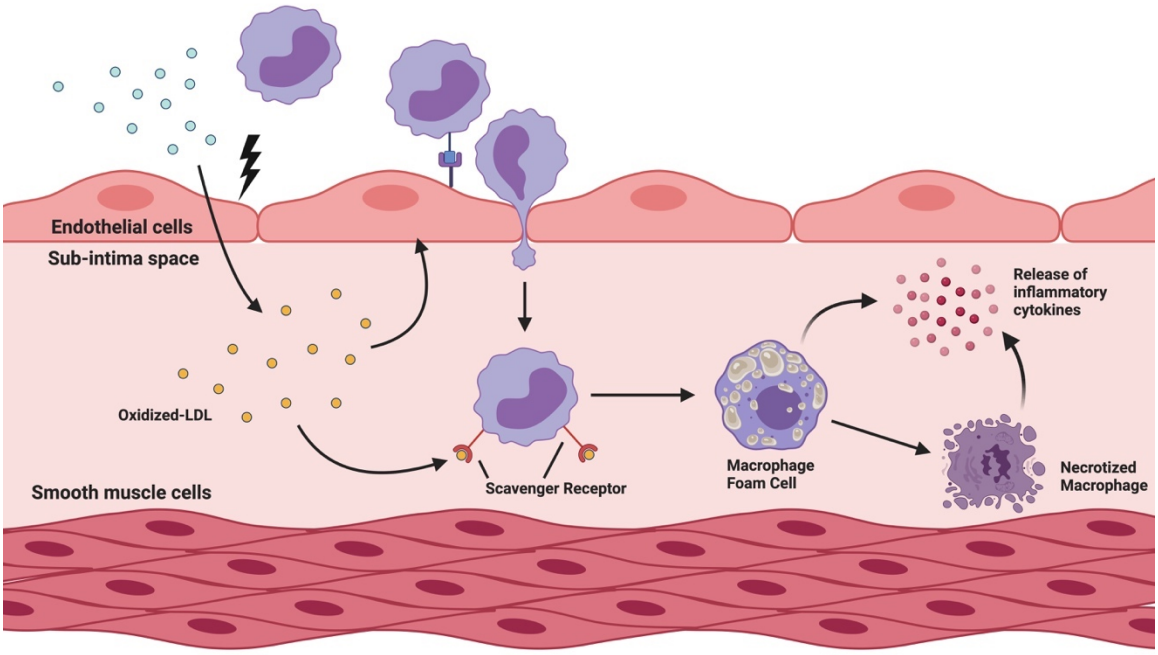

Figure 1.1 Schematic of atherosclerosis at the cellular level. The presence of risk factors injures the intimal layer of endothelial cells causing endothelial dysfunction. Circulating lipids, such as LDL, infiltrate the sub-intimal space and become oxidized (ox-LDL) due to the inflammatory environment and further contribute to chronic inflammation. Endothelial dysfunction increased chemokines and adhesion molecules that aid in monocyte recruitment and infiltration into the subintimal space. The monocytes, now macrophages, uptake ox-LDL with scavenger receptors and become macrophage foam cells. The foam cells then necrotize and/or further contribute to the release of inflammatory cytokines.

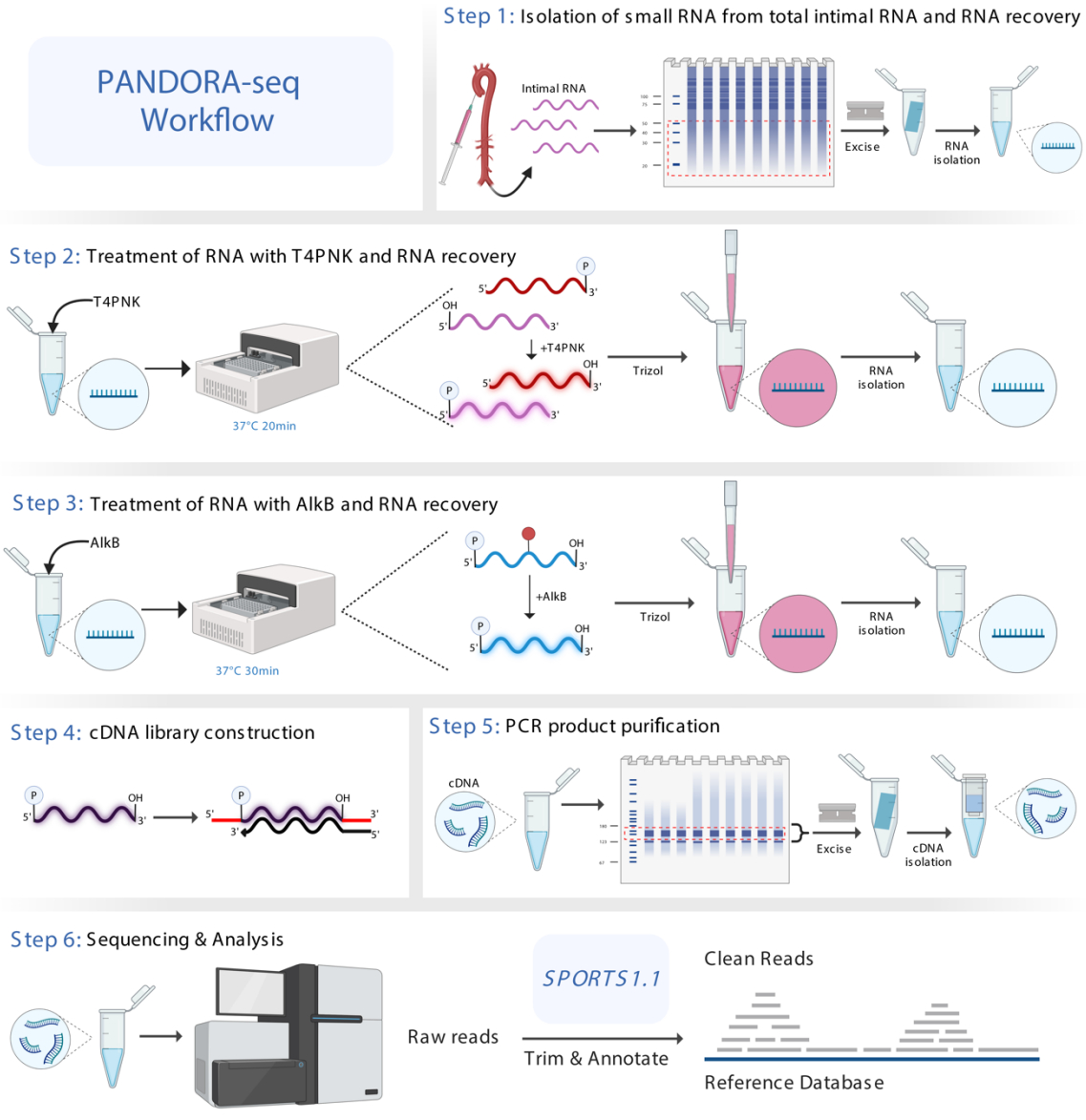
PANDORA-seq Workflow
Step 1: Isolation of small RNA from total intimal RNA and RNA recovery
Intimal RNA
Excise
RNA isolation
Step 2: Treatment of RNA with T4PNK and RNA recovery
T4PNK
37°C 20min
+T4PNK
Trizol
RNA isolation
Step 3: Treatment of RNA with AlkB and RNA recovery
AlkB
37°C 30min
+AlkB
Trizol
RNA isolation
Step 4: cDNA library construction
Step 5: PCR product purification
cDNA
Excise
cDNA isolation
Step 6: Sequencing & Analysis
Raw reads
SPORTS1.1
Trim & Annotate
Clean Reads
Reference Database

Figure 1.2 Schematic of PANDORA-seq workflow. Step 1: Small RNAs from intimal total RNAs were excised from PAGE gel. Step 2: Purified small RNAs were subjected to T4PNK treatment. Step 3: Purified small RNAs were subjected to Alkb treatment. Step 4: NEBNext Small RNA Library Prep Set for Illumina was used for cDNA library construction. Step 5: PCR products were purified with PAGE gel. Step 6: Final product was sequenced and annotated using the *SPORTS1.1* pipeline. A detailed protocol of PANDORA-seq is included in the Materials and Methods section. The image was created by using BioRender.com.

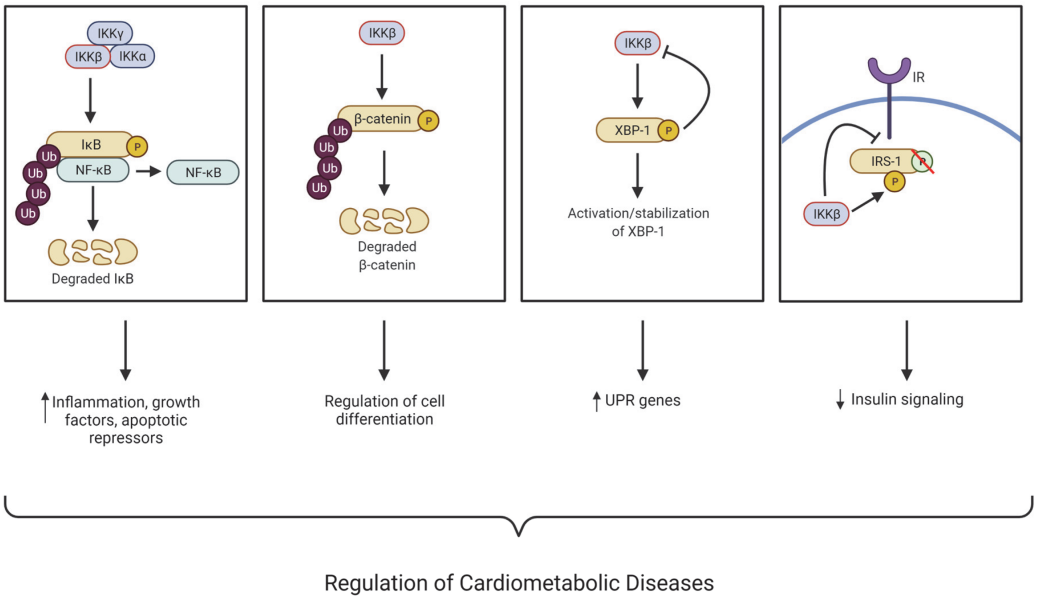

Figure 1.3: IKKβ regulates many cellular processes associated with the development of cardiometabolic diseases through NF-κB-dependent and -independent mechanisms. IκB kinase (IKK); Nuclear factor kappa B (NF-κB); X-box binding protein (XBP-1); Insulin receptor substate 1 (IRS-1); Insulin receptor (IR); Ubiquitination (Ub).

2. Chapter 2: PANDORA-seq unveils the hidden small noncoding RNA landscape in atherosclerosis of LDL receptor-deficient mice

2.1 Abstract

Small noncoding RNAs (sncRNAs) play diverse roles in numerous biological processes. While the widely used RNA sequencing (RNA-Seq) method has advanced sncRNA discovery, RNA modifications can interfere with the complementary DNA library construction process, preventing the discovery of highly modified sncRNAs including transfer RNA-derived small RNAs (tsRNAs) and ribosomal RNA-derived small RNAs (rsRNAs) that may have crucial functions in disease development. To address this technical obstacle, we recently developed a novel PANDORA-Seq (Panoramic RNA Display by Overcoming RNA Modification Aborted Sequencing) method to overcome RNA modification-elicited sequence interferences. To identify novel sncRNAs associated with atherosclerosis development, LDL receptor-deficient ($LDLR^{-/-}$) mice were fed a low-cholesterol diet or high-cholesterol diet (HCD) for 9 weeks. Total RNAs isolated from the intima were subjected to PANDORA-Seq and traditional RNA-Seq. By overcoming RNA modification-elicited limitations, PANDORA-Seq unveiled an rsRNA/tsRNA-enriched sncRNA landscape in the atherosclerotic intima of $LDLR^{-/-}$ mice, which was strikingly different from that detected by traditional RNA-Seq. While microRNAs were the dominant sncRNAs detected by traditional RNA-Seq, PANDORA-Seq substantially increased the reads of rsRNAs and tsRNAs. PANDORA-Seq also detected 1,383 differentially expressed sncRNAs induced by HCD feeding, including 1,160 rsRNAs and 195 tsRNAs. One of HCD-induced intimal tsRNAs, tsRNA-Arg-CCG, may contribute to atherosclerosis

development by regulating the proatherogenic gene expression in endothelial cells. Overall, PANDORA-Seq revealed a hidden rsRNA and tsRNA population associated with atherosclerosis development. These understudied tsRNAs and rsRNAs, which are much more abundant than microRNAs in the atherosclerotic intima of $LDLR^{-/-}$ mice, warrant further investigations.

2.2 Introduction

Atherosclerosis is a chronic inflammatory disease characterized by the accumulation of cholesterol, immune cells, and fibrous elements in the sub-intimal layer of the artery leading to plaque formation and cardiovascular events (5, 128-131). At the cellular level, the initial stages of atherosclerosis development involve endothelial dysfunction followed by macrophage infiltration, lipid accumulation, and vascular smooth muscle cell (SMC) migration in the intimal layer of the vasculature (128, 129, 132). While many cell types contribute to atherosclerosis (132-135), endothelial cells in the intimal layer are critical for atherosclerosis initiation and progression (132). Many genetic and environmental factors have been identified to contribute to atherosclerosis development and endothelial dysfunction (136), such as environmental pollutants (137-140) and diet (141). In addition to well-defined risk factors, numerous noncoding RNAs, such as long non-coding RNAs (lncRNAs) and small non-coding RNAs (sncRNAs), have been shown to play important roles in regulating atherosclerosis development (53, 142-145). For example, several lncRNAs including MALAT1 and VINAS have been demonstrated to regulate atherosclerosis development (53, 144, 145).

For sncRNAs, most studies in the atherosclerosis research field focus on the functions of microRNAs (miRNAs) in atherogenesis (53, 142, 143). In addition to miRNAs, there are many other sncRNA categories including transfer RNA-derived small RNAs (tsRNAs), ribosomal RNA-derived small RNA (rsRNAs), YRNA-derived small RNAs (ysRNAs), and piwi-interacting RNA (piRNAs) (146-150). However, the functions of these understudied sncRNAs in atherosclerosis and cardiovascular disease (CVD) are mostly unknown. As compared to miRNAs, many of these sncRNAs including tsRNAs and rsRNAs are highly modified since their precursors (e.g., tRNAs and rRNAs) bear various RNA modifications such as RNA methylations (e.g., m^1G, m^1A and m^3C) (146, 147, 151-153). In addition, terminal modifications (e.g., 3'-phosphate and 2',3'-cyclic phosphate) also commonly occur during tsRNA and rsRNA biogenesis (154-156). These modifications can interfere with the reverse transcription and adaptor ligation processes in the widely used cDNA library construction protocol for standard RNA sequencing (RNA-seq) analysis (147, 154, 157, 158), which prevents the detection of highly modified sncRNAs by the traditional RNA-seq method (146). To address this issue, we recently developed an innovative RNA-seq protocol, PANDORA-seq (Panoramic RNA Display by Overcoming RNA Modification Aborted Sequencing) which employs a combinatorial enzymatic treatment protocol to remove key RNA modifications that block adapter ligation and reverse transcription processes during cDNA library construction (147). PANDORA-seq has enabled us to detect the highly modified sncRNAs including tsRNAs and rsRNAs, resulting in the discovery of higher abundant levels of tsRNAs/rsRNAs in various tissues and cell types that were undetectable by traditional RNA-seq (37, 146, 147).

In the current study, we used PANDORA-seq to identify novel sncRNAs that are associated with atherosclerosis development in LDL receptor-deficient ($LDLR^{-/-}$) mice. By overcoming RNA modification-elicited limitations, PANDORA-seq unveiled a rsRNA- and tsRNA-enriched sncRNA landscape in the atherosclerotic intima of $LDLR^{-/-}$ mice, which was strikingly different from that detected by traditional RNA-seq. We also found that one of the tsRNAs, tsRNA-Arg-CCG was upregulated in the atherosclerotic intima of $LDLR^{-/-}$ mice. Interestingly, tsRNA-Arg-CCG can affect the expression of pro-atherogenic genes in human endothelial cells, which may contribute to atherosclerosis development.

2.3 Methods

2.3.1 Animals

3-week-old male C57BL/6 $LDLR^{-/-}$ mice (Jackson Laboratories) were fed ad libitum on a semisynthetic low-fat (4.2% fat) AIN76 diet containing either low cholesterol (LCD; 0.02% cholesterol; Research Diets) or high cholesterol (HCD; 0.5% cholesterol; Research Diets) for 9 weeks until they were euthanized at 12 weeks of age (138, 159-161). All animals were housed in pathogen-free microisolator cages in a temperature-controlled environment with a 12-h light-dark cycle. All experimental mice used in this study were male. However, studying a single sex has limitations since sex differences have been widely reported in mouse atherosclerosis studies (162). Body composition was measured by EchoMRI (Echo Medical System) (163-165), and intraperitoneal glucose tolerance test (IPGTT) was performed as previously described (160, 161). On the day of sacrifice, mice

were fasted for 6 h following the dark cycle (feeding cycle) and blood and major organs were collected as previously described (160, 164, 166). All animal studies were performed in compliance with the approved protocols by the Institutional Animal Care and Use Committee of the University of California, Riverside.

2.3.2 Blood Analysis

Serum total cholesterol and total triglyceride concentrations were measured using the Wako Cholesterol E enzymatic colorimetric assay (Wako, 999-02601) and the Wako L-type TG M assay (Wako, 994-02891) according to the manufacturer's instructions (FUJIFILM Medical Systems U.S.A., Inc., Richmond, VA, USA). The lipoprotein fractions were isolated in a Beckman Coulter XPN100-IVD ultracentrifuge as previously described (164, 167). Lipoprotein fractions were isolated by centrifuging 60 µL of serum at 40,000 RPM for 5 h at 4°C in a Beckman Coulter Type 42.2 Ti Rotor at its own density (1.006g/mL). The infranatant was then adjusted to a density of 1.063g/mL with solid potassium bromide to harvest the VLDL (<1.006g/mL), LDL ($1.006 \leq d \leq 1.063$g/mL), and HDL (d>1.063g/mL) fractions by spinning at 40000 RPM for 24 h at 4°C. The cholesterol content of the lipoprotein fractions was then measured enzymatically (Wako, cholesterol 999-02601).

2.3.3 Atherosclerotic Lesion Analysis

The atherosclerotic lesion sizes were quantified as previously described (135, 138, 168, 169). To quantify the plaque area at the aortic root, Optimal Cutting Temperature (OCT)-compound-embedded hearts were sectioned at a 12-µm thickness keeping all the three valves of the aortic root in the same plane, and stained with oil red O. To quantify

atherosclerotic plaque area at the brachiocephalic artery (BCA), the OCT-embedded brachiocephalic arteries were sectioned from distal to proximal at a thickness of 10μm. BCA atherosclerotic lesions from the 29base to the internal elastic lamina were quantified in three equidistant oil red O-stained sections at 200, 400, and 600μm proximal from the branching point of the brachiocephalic artery into the carotid and subclavian arteries. Images were taken and plaque size was quantified using a Nikon microscope (Nikon, Melville, NY, USA).

2.3.4 Immunohistochemistry

The aortic root of the mice freshly embedded in OCT and sectioned were first fixed in 4% PFA for 15 minutes and permeabilized with 0.1% Triton X-100 in PBS (PBST) for 15 min. The slides were then blocked with PBST containing 5% bovine serum albumin (BSA) (Sigma-Aldrich, A9647) for 1 h at room temperature. For immunostaining, slides were incubated with antibodies against CD68 (Bio-Rad AbD Serotec, MCA1957) and αSMA (Abcam, ab5694) at 4°C for 12 to 15 hours (131, 160, 168). The sections were rinsed with PBS and incubated with fluorescein-labeled secondary antibodies (Life Technologies). The nuclei were stained by mounting the slides with DAPI medium (Vector Laboratories). Samples were imaged and analyzed with a Nikon fluorescence microscope. Images were taken, and the positively labeled area was quantified using a Nikon microscope. For trichrome staining, the aortic root freshly embedded in OCT and sectioned were stained with a trichrome stain (Masson) kit (Sigma-Aldrich, HT15) according to the manufacturer's instructions with some modifications to accommodate for frozen tissue (131, 160, 170). Briefly, sections were fixed in 4% PFA for 30 min then stained with

Biebrich Scarlet-Acid Fuchsin Solution for 1 min to stain the fibers red. The samples were rinsed with ddH2O and placed in Working Phosphotungstic/Phosphomolybdic Acid Solution for 1 hr followed directly with Aniline Blue staining for 1 min. Lastly, samples were placed in 1% Glacial Acetic Acid for 2 min and mounted with Permount. Images were taken and collagen content was quantified using a Nikon microscope (Nikon, Melville, NY, USA).

2.3.5 Cell Culture and Transfection

Human endothelial cell line HMEC-1 was purchased from AATC (CRL-3243) (171). HMEC-1 cells passaged less than 20 times were used for transfection. Synthetic control Oligo and tsRNA-Arg-CCG Oligo (Sigma-Aldrich) was transfected into the cells with Lipofectamine RNAiMAX (Thermo Fisher, 13778100) (172) followed by RNA isolation after 24 hours. Total RNAs were isolated using TRIzol reagent (Sigma-Aldrich, T9424) as previously described (37, 169).

2.3.6 Northern Blot

Northern blot was performed as we previously described (147). Total RNAs isolated from HMEC-1 cells were separated by a 10% urea-PAGE gel followed by SYBR gold staining of nucleic acids (Thermo Fischer, S11494) and immediately imaged. The RNA was then transferred to a positively charged nylon membrane (Roche, 11417240001) and ultraviolet crosslinked with 0.12J of energy. Membranes were hybridized with PerfectHyb Plus Hybridization Buffer (Sigma-Aldrich, H7033) for 1 hour at 42˚C. To detect tsRNA-Arg-CCG, membranes were incubated overnight in 42˚C with a DIG-labeled oligonucleotide probe (5’DIG- CGAACCCACAATCCCCAGCT-3’).

2.3.7 Intimal RNA Isolation

The aortas of LDLR$^{-/-}$ mice were isolated and flushed with PBS followed by intimal peeling using TRIzol reagent (Sigma-Aldrich, T9424) (145). A total of ~300-400 μL of Trizol was flushed into the aorta for 10 seconds (~100μL) followed by a 10-second pause and repeated 3 times, as previously described (145, 173). The flowthrough was collected in a 1.5mL Eppendorf tube followed by RNA extraction as previously described (147, 164, 166). Total RNAs from the remaining aorta (media and adventitia) were also isolated using TRIzol for gene expression analyses. Intimal RNA integrity and concentrations were confirmed using an Agilent 2100 Bioanalyzer and Aligent RNA 6000 Nano Kit (Agilent Technologies Inc, 5067-1511) (147).

2.3.8 Quantitative Real-Time PCR Analysis

Quantitative Real-Time PCR (QPCR) were performed by using gene-specific primers and SYBR Green PCR kit (Bio-Rad Laboratories) on a Bio-Rad CFX Real-Time-PCR Machine as previously described (37, 138, 164). The sequences of primers used in this study are listed in Table 2.1.

2.3.9 PANDORA-seq of intimal small RNAs

PANDORA-seq protocol has been recently described in our recent report (147). Here we provided detailed information for PANDORA-seq of intimal small RNAs.

Isolation of specified size RNA from total RNAs

The RNA sample from the intima was mixed with an equal volume of 2× RNA loading dye (New England Biolabs, B0363S) and incubated at 75 °C for 5 min. The mixture

was loaded into 15% (wt/vol) urea polyacrylamide gel (10 ml mixture containing 7 M urea (Invitrogen, AM9902), 3.75 ml Acrylamide/Bis 19:1, 40% (Ambion, AM9022), 1 ml 10× TBE (Invitrogen, AM9863), 1 g l^{-1} ammonium persulfate (Sigma–Aldrich, A3678-25G) and 1 ml l^{-1} TEMED (Thermo Fisher Scientific, BP150-100) and run in a 1× TBE running buffer at 200 V until the bromophenol blue reached ~1cm from the bottom of the gel. Small RNA of 15-50 nucleotides was visualized with SYBR Gold solution (Invitrogen, S11494) and excised based on a small RNA ladder (New England Biolabs, N0364S) (147). The RNA was eluted in 0.3 M sodium acetate (Invitrogen, AM9740) and 100 U ml^{-1} RNase inhibitor (New England Biolabs, M0314L) overnight at 4 °C. The samples were then centrifuged for 10 min at 12,000x g at 4°C. The aqueous phase was mixed with pure ethanol, 3 M sodium acetate and linear acrylamide (Invitrogen, AM9520) at a ratio of 3:9:0.3:0.01 and incubated at -20 °C for 2 hrs and centrifuged for 25 min at 12,000 x g at 4°C (147). After removing the supernatant, the precipitate was resuspended in nuclease-free water.

Treatment of RNA with AlkB

The intimal RNA was incubated in a 50 µL reaction mixture containing 50 mM HEPES (Fisher Scientific, 15630080), 75 µM ferrous ammonium sulfate, 1 mM α-ketoglutaric acid (Sigma–Aldrich; K1128), 2 mM sodium ascorbate, 50 mg l^{-1} bovine serum albumin (Sigma-Aldrich, A9647), 4 µg mL^{-1} AlkB, 2,000 U ml^{-1} RNase inhibitor and RNA at 37°C for 30 min (147). Then, the mixture was added into 500 µL TRIzol reagent for RNA isolation.

Treatment of RNA with T4PNK

The intimal RNA was incubated in 50μL reaction mixture containing 5μL 10× PNK buffer (New England Biolabs, B0201S), 1 mM ATP (New England Biolabs, P0756S), 10 U T4PNK (New England Biolabs, M0201L) and RNA at 37°C for 20 min (147). Then, the mixture was added into 500μL TRIzol reagent for RNA isolation.

Small RNA library construction and deep sequencing

The adapters were obtained from the NEBNext Small RNA Library Prep Set for Illumina (New England Biolabs, E7330S) and ligated sequentially. First, we added a 3' adapter system under the following reaction conditions: 70°C for 2 min and 16°C for 18 h. Second, we added a reverse transcription primer under the following reaction conditions: 75°C for 5 min, 37°C for 15 min and 15°C for 15 min. Third, we added a 5' adapter mix system under the following reaction conditions: 70°C for 2 min and 25°C for 1 h. First-strand cDNA synthesis was performed under the following reaction conditions: 70°C for 2 min and 50°C for 1 h. PCR amplification with PCR Primer Cocktail and PCR Master Mix was performed to enrich the cDNA fragments under the following conditions: 94°C for 30 s; 17 cycles of 94°C for 15 s, 62°C for 30 s and 70°C for 15 s; 70°C for 5 min; and hold at 4°C. Then, the PCR product was purified from PAGE gel.

Small RNA annotation and analyses for PANDORA-seq data

Small RNA sequences were annotated using the software SPORTS1.1 with one mismatch tolerance (SPORTS1.1 parameter setting: -M 1). Reads were mapped to the following individual non-coding RNA databases sequentially: (1) the miRNA database

34iRbase 21; (2) the genomic tRNA database GtRNAdb; (3) the mitochondrial tRNA database mitotRNAdb; (4) the rRNA and YRNA databases assembled from the National Center for Biotechnology Information nucleotide and gene database; (5) the piRNA databases, including piRBase and piRNABank; and (6) the non-coding RNAs defined by Ensembl and Rfam 12.3. The tsRNAs were annotated based on both pre-tRNA and mature tRNA sequences. Mature tRNA sequences were derived from the GtRNAdb and mitotRNAdb sequences using the following procedures: (1) predicted introns were removed; (2) a CCA sequence was added to the 3′ ends of all tRNAs; and (3) a G nucleotide was added to the 5′ ends of histidine tRNAs. The tsRNAs were categorized into four types based on the origin of the tRNA loci: 5′ tsRNA (derived from the 5′ end of pre-/mature tRNA); 3′ tsRNA (derived from the 3′ end of pre-tRNA); 3′ tsRNA-CCA end (derived from the 3′ end of mature tRNA); and internal tsRNAs (not derived from 3′ or 5′ loci of tRNA). For the rsRNA annotation, we mapped the small RNAs to the parent rRNAs in an ascending order of rRNA sequence length to ensure a unique annotation of each rsRNA (for example, the rsRNAs mapped to 5.8S rRNA would not be further mapped to the genomic region overlapped by 5.8S and 45S rRNAs). We then employed the edgeR algorithm (174) to perform the comparison of sncRNA expression patterns between groups. We applied the TMM algorithm to perform reads count normalization and effective library size estimation and the likelihood ratio test to identify the differentially expressed sncRNA species. The sncRNA species with a false discovery rate (FDR)< 0.1 and fold change (FC) > 2 were deemed differentially expressed.

2.3.10 Intimal Transcriptome Analysis

The creation of cDNA libraries and sequencing were performed using the Illumina standard operation pipeline as previously described (160, 166, 169, 175, 176). For data analysis, we applied the Salmon tool to quantify the mRNA expression from the raw sequencing data with the default setting, based on the Ensembl mouse cDNA annotation (GRCm38). We then employed the edgeR algorithm (174) to perform the comparison in transcriptomic pattern between groups, using the TMM algorithm to perform read count normalization and effective library size estimation and the likelihood ratio test to identify the DEGs. The genes with FDR <0.1 and FC >2 was deemed differentially expressed. We further performed pathway analysis upon the differentially expressed genes using the definition from Kyoto Encyclopedia of Genes and Genomes (KEGG) project. For each KEGG pathway, we computed a geneset score, using the Functional Analysis of Individual Microarray Expression (FAIME) algorithm (177). A higher FAIME score suggests a higher overall expression of a given pathway. All the RNA-seq datasets have been deposited in the Gene Expression Omnibus (GSE213305).

2.3.11 Statistical Analysis

All data except the high-throughput sequencing data are presented as the mean ± SEM. Individual pairwise comparisons were analyzed by two-sample, two-tailed Student's t-test unless otherwise noted, with $P<0.05$ was regarded as significant using GraphPad Prism. One-way analysis of variance (ANOVA) with uncorrected Fisher's LSD test was used for analyzing different origins of the tsRNA/miRNA expression ratio under different treatments. N numbers are listed in figure legends.

2.4 Results

2.4.1 Feeding LDLR−/− mice a low-fat, high-cholesterol diet promotes hypercholesterolemia without affecting adiposity and metabolic phenotypes

To investigate sncRNAs associated with atherosclerosis development, male $LDLR^{-/-}$ mice were fed a low-fat (4.3% fat) AIN76 diet containing 0.02% or 0.5% cholesterol for 9 weeks (159). We and others have successfully used this diet to induce atherosclerosis development without eliciting obesity and associated metabolic disorders in $LDLR^{-/-}$ or $ApoE^{-/-}$ mice (159-161, 169, 178, 179). Consistently, we found that $LDLR^{-/-}$ mice fed the relatively high-cholesterol diet (HCD, 0.5% cholesterol) had similar body weight and growth curve as mice fed the low-cholesterol diet (LCD, 0.02% cholesterol) (Figure 2.1A). HCD- and LCD-fed mice also had similar body composition, including fat mass and lean mass (Figure 2.1B). Glucose tolerance tests also demonstrated that exposure to these diets did not alter glucose tolerance in $LDLR^{-/-}$ mice (Figure 2.1C). Consistent with previous results (159, 178), HCD feeding led to elevated serum total cholesterol levels without affecting triglyceride levels (Figure 2.1D). Lipoprotein fraction analysis was then performed, and mice fed HCD had significantly higher atherogenic LDL and VLDL cholesterol levels, but similar HDL cholesterol levels as compared with LCD-fed mice (Figure 2.1E). Thus, the low-fat HCD can promote hypercholesterolemia without inducing obesity or metabolic disorders in $LDLR^{-/-}$ mice.

2.4.2 High-cholesterol diet feeding effectively induces atherosclerosis development in lean LDLR−/− mice

Atherosclerotic lesion areas were then analyzed in the aortic root and brachiocephalic artery (BCA) of LCD or HCD-fed LDLR$^{-/-}$ mice. We found that HCD feeding significantly increased atherosclerotic lesion areas in the aortic root of LDLR$^{-/-}$ mice as compared with LCD-fed mice (183,487.7 ± 48,193.4 mm^2 vs. 8,378.9 ± 4,142.7 mm^2) (Figure 2.1F). Short-term LCD feeding did not induce observable atherosclerosis development in BCA of LDLR$^{-/-}$ mice (Figure 2.1G). However, exposure to HCD significantly increased the atherosclerotic lesion areas in the BCA of LDLR$^{-/-}$ mice (8,559.8 ± 3,652.6 mm^2 vs. 0 ± 0 mm^2) (Figure 2.1G).

In addition to lesion size, we characterized multiple factors that are associated with atherosclerosis development, including macrophage infiltration, SMC migration, and collagen production. As expected, immunostaining for macrophage and SMC markers showed increased macrophage contents and SMC migration in the atherosclerotic plaque of HCD-fed LDLR$^{-/-}$ mice (Figure 2.2, A-C). Furthermore, Masson's Trichrome staining also demonstrated that HCD feeding led to increased collagen content in the atherosclerotic lesions of LDLR$^{-/-}$ mice as compared to LCD-fed mice (Figure 2.2D). Collectively, these results demonstrate that the low-fat HCD feeding can effectively induce atherosclerosis development in lean LDLR$^{-/-}$ mice.

2.4.3 Transcriptome analysis reveals altered atherosclerosis-related gene expression in the intima of HCD-fed LDLR−/− mice

We next isolated intimal RNAs for regular RNA sequencing (RNA-seq) analysis to understand the transcriptomic changes in the intima of $LDLR^{-/-}$ mice. Total RNAs isolated from the intima and remaining aortic fraction were first characterized by endothelial marker (e.g., VE-Cadherin and Tie2) and SMC marker (Myh11 and α-smooth muscle actin) expression. Consistent with previous studies (145), our results confirmed the enrichment of endothelial markers and the low expression levels of SMC markers in the intima as compared with that of media/adventitia (Figure 2.3). By contrast, the media/adventitial fraction has the high expression levels of SMC markers but low expression levels of endothelial cell markers (Figure 2.3).

RNA-seq analysis of the intima uncovered 1,313 differentially expressed genes (DEGs) in the intima of HCD-fed $LDLR^{-/-}$ mice as compared with LCD-fed mice with a false discovery rate (FDR) of < 0.1 and fold change (FC) > 2 as the cut-off threshold (180) (Figure 2.4A). Kyoto Encyclopedia of Genes and Genomes (KEGG) analysis then revealed that many upregulated DEGs were enriched in several biological processes that contribute to atherosclerosis development including "cytokine-cytokine receptor interaction," "chemokine signaling pathway," and "cell adhesion molecules" (Figure 2.4B). In addition, some DEGs were also enriched in lysosome and phagosome associated pathways that are also important for atherosclerosis development (Figure 2.4B). By using the Functional Analysis of Individual Microarray Expression (FAIME) algorithm, we verified the geneset scores of these pathways were significantly increased in HCD-fed $LDLR^{-/-}$ mice as

compared with LCD-fed mice (Figure 2.4C). The genes associated with these pathways were also upregulated in HCD-fed LDLR$^{-/-}$ mice (Figure 2.4D). Taken together, intimal RNA-seq analysis confirmed the altered atherosclerosis-related genes and pathways that are associated with the increased atherosclerosis in HCD-fed LDLR$^{-/-}$ mice.

2.4.4 PANDORA-seq but not traditional RNA-seq unveils a rsRNA- and tsRNA-enriched sncRNA landscape in the atherosclerotic intima of LDLR−/− mice

Many sncRNAs bear specific modifications, which can prevent the detection of sncRNAs in widely used traditional RNA-seq methods (146). To overcome this obstacle, we recently developed a novel small RNA sequencing method, PANDORA-seq, to eliminate the RNA modification-elicited sequence interferences (147). To determine whether PANDORA-seq can detect novel sncRNAs associated with atherosclerosis development, intimal RNA was collected and processed through both traditional small RNA-seq and PANDORA-seq followed by SPORTS1.1 bioinformatics analysis (147, 181). Since miRNAs are not as highly modified as other sncRNAs such as rsRNAs/tsRNAs, they can be readily detected by traditional-seq (146, 147). Indeed, traditional-seq detected a miRNA-enriched sncRNA landscape in the intima of both LCD (47.9%) and HCD (55.9%)-fed LDLR$^{-/-}$ mice (Figure 2.5A). However, PANDORA-seq revealed a totally different sncRNA landscape in which rsRNAs and tsRNAs account for 83.1% (LCD) and 82.4% (HCD) of total detected sncRNAs in the intima of LDLR$^{-/-}$ mice (Figure 2.5A).

As rsRNA reads were dominant in PANDORA-seq results which consumed the relative reads of other sncRNAs (Figure 2.5A), we filtered out rsRNAs from the total

sncRNA reads and found that PANDORA-seq but not traditional RNA-seq detected an increased tsRNA:miRNA ratios in both LCD- and HCD-fed mice (Figure 2.5B). The origins, from which the tsRNAs are derived (5'tsRNAs, 3'tsRNAs, 3'tsRNAs with a CCA end, and internal tsRNAs), were also analyzed. PANDORA-seq revealed an increased relative expression of specific tsRNA origins as compared to traditional RNA-seq (Figure 2.5C). Consistent with previous studies, a majority of tsRNAs are derived from the 5' end of mature tRNAs (147). Specific rRNA loci, where rsRNA are derived, were also evaluated, and the data demonstrate increased rsRNA detection by PANDORA-seq (Figure 2.6). These results suggest that PANDORA-seq can detect highly modified sncRNAs such as tsRNAs and rsRNAs in the atherosclerotic intima of $LDLR^{-/-}$ mice that were otherwise undetectable by the traditional RNA-seq method.

2.4.5 PANDORA-seq detects more differentially expressed sncRNAs associated with atherosclerosis development in the intima of HCD-fed LDLR−/− mice

We further analyzed both PANDORA-seq and traditional RNA-seq results to determine how HCD feeding alters the expression levels of sncRNAs in the intima of $LDLR^{-/-}$ mice. While traditional RNA-seq only detected a small number of differentially regulated sncRNAs, including only 16 rsRNAs and tsRNAs, PANDORA-seq detected a total of 1,383 differentially regulated sncRNAs (FC >2 and FDR <0.1), including 1160 rsRNAs and 195 tsRNAs (180) (Figure 2.7A). PANDORA-seq also detected 28 differentially regulated miRNAs in the intima of HCD-fed $LDLR^{-/-}$ mice (180) (Figure 2.7B). Many of those miRNAs are consistent with previous reports such as miR-146b,

miR-155, and miR-125a, though the functions of these miRNAs on atherogenesis have not been completely understood (142, 143).

Next, we compared rsRNA expression patterns between LCD and HCD-fed LDLR$^{-/-}$ mice from individual ribosomal RNA (e.g., 5S, 12S, and 28S) by analyzing the specific loci where rsRNAs were derived (Figure 2.7C and Figure 2.6). The mapping of rsRNAs from 5S, 12S, and 28S, used as examples, showed dynamic expression patterns in response to HCD feeding detected by PANDORA-seq (Figure 2.7C). We also generated a heatmap to compare the 195 significantly altered intimal tsRNAs between HCD- and LCD-fed mice detected by PANDORA-seq (180) (Figure 2.7D). Further, mapping of tsRNA expression patterns on individual tRNA length scales (tRNA-Trp, tRNA-Arg, tRNA-Ser, tRNA-Leu, and tRNA-Asp used as examples) revealed that those tsRNAs also contain distinct dynamic responses to HCD feeding (Figure 2.7E). The functions of those tsRNAs are mostly unknown and more studies are required to investigate the role of those tsRNAs in atherogenesis.

2.4.6 High-cholesterol diet-induced tsRNA-Arg-CCG affects pro-atherogenic gene expression in endothelial cells in vitro

Endothelial cells play an essential role in regulating vascular inflammation and the initiation and progression of atherosclerosis (133). To investigate the potential function of tsRNAs identified by PANDORA-seq in atherosclerosis, we selected one of the HCD-induced tsRNAs, tsRNA-Arg-CCG for in vitro analysis. tsRNA precursors, tRNAs, are a highly conserved RNA species (55), and human and murine tRNA-Arg-CCG also shared the same sequence (Figure 2.8A). We transfected synthetic tsRNA-Arg-CCG

oligonucleotides into human endothelial cells, HMEC-1 cells (171). Northern blot was then performed to confirm the successful overexpression of tsRNA-Arg-CCG in HMEC-1 cells (Figure 2.8B). Interestingly, we found that overexpression of synthetic tsRNA-Arg-CCG led to increased expression of several pro-atherogenic genes including IL-6, IL-1α, ICAM-1, VCAM-1, and MCP-1 in HMEC-1 cells (Figure 2.8C). Therefore, tsRNA-Arg-CCG may have pro-atherogenic properties in vivo, which warrants further investigation.

2.5 Discussion

sncRNAs are a major family of non-coding RNAs that play critical roles in numerous biological processes. Certain small RNA populations such as miRNAs and piRNAs have been extensively studied and have also been implicated in atherosclerosis (182, 183). In addition to those well characterized sncRNAs, recent studies have revealed the wide existence and unexpected functions of new classes of sncRNAs including tsRNAs and rsRNAs (153, 181, 184, 185). However, the functions of those non-canonical sncRNAs in atherosclerosis or CVD are mostly unknown. A major obstacle in discovering and studying these sncRNA is that the currently widely used RNA-seq protocol generates biased sequencing results and often fails to detect these species (146, 147). Many sncRNAs including tsRNAs and rsRNAs bear RNA modifications that interfere with adapter ligation and reverse transcription processes during cDNA library construction process, leading to unsuccessful detection of tsRNAs and rsRNAs in various tissues and cells (146, 147). For example, tsRNAs contain N^1-methyladenosine (m^1A), N^3-methylcytidine (m^3C), and N^1-methylguanosine (m^1G) modifications that hinder reverse transcription process during

traditional cDNA construction (58, 147). Additionally, some sncRNA species, including tsRNAs and rsRNAs, contain 3' terminal modifications such as 5'-phosphate and 2'3'-cyclic phosphate that block adaptor ligation and escape traditional library construction (60). Therefore, the modified tsRNAs, rsRNAs, and other sncRNAs may escape library construction and remain undetected by traditional RNA-seq. To overcome this obstacle, we recently developed PANDORA-seq based on a combination of enzymatic treatments (e.g., T4PNK and AlkB treatments) with optimized protocols that improv both RNA 3' and 5' adapter ligation and reverse transcription during cDNA library construction (147). PANDORA-seq has major advantages over previous methods designed to target either adapter ligation or reverse transcription processes alone, leading to the identification of abundant modified tsRNAs and rsRNAs in various tissues and cells (37, 146, 147). In the current study, PANDORA-seq unveiled a rsRNA- and tsRNA-enriched sncRNA landscape in the atherosclerotic intima of $LDLR^{-/-}$ mice which was strikingly different from that detected by traditional RNA-seq. While miRNAs were the dominant sncRNAs detected by traditional RNA-seq (e.g., ~56% of total sncRNAs in HCD-fed mice), PANDORA-seq detected a substantially different sncRNA population with rsRNAs and tsRNAs accounting for >82% of total sncRNAs. In addition, traditional RNA-seq only detected a few differentially expressed rsRNAs and tsRNAs induced by HCD feeding but PANDORA-seq detected more than 1,300 differentially expressed rsRNAs and tsRNAs. Thus, by overcoming RNA modification-elicited limitations, PANDORA-seq revealed the hidden rsRNAs and tsRNAs population associated with atherosclerosis development undetected by traditional RNA-seq.

To identify novel sncRNAs associated with atherosclerosis development, we fed LDLR$^{-/-}$ mice a low-fat LCD or HCD for 9 weeks. As expected, HCD feeding resulted in severe hypercholesterolemia and large atherosclerotic lesions in LDLR$^{-/-}$ mice. The atherosclerotic lesions of LCD-fed mice were quite small, partially due to the relatively short feeding period (9 weeks) and young age of the mice (12 weeks old) at the time of euthanasia. Previous studies using the same LCD but longer feeding period resulted in larger atherosclerotic lesions (159, 169). However, the relatively big difference of atherosclerotic lesion sizes between LCD and HCD-fed mice is ideal for the current study. Aiming to identify genes and sncRNAs associated with atherosclerosis development, we also focused on the intima of hypercholesterolemic LDLR$^{-/-}$ mice and performed transcriptome and sncRNA analyses via high-throughput RNA-seq and PANDORA-seq. Previous studies have used whole aortic tissues for traditional RNA-seq (57, 186-188). Since intima is the main site for atherosclerotic plaque initiation and development, we chose to isolate RNAs from the intimal for further analyses. As expected, transcriptomic analysis revealed enriched pathways for inflammatory and immune responses, which is consistent with previous studies on whole atherosclerotic arteries and the well-established role of the immune response in atherosclerosis (5, 186, 189). For example, the C-C motif chemokine ligand family (CCL2, CCL3, CCL4 and CCL5) associated with increased inflammatory responses in atherosclerosis (190), were upregulated in the intima of HCD-fed LDLR$^{-/-}$ mice. Our transcriptomic results are consistent with known functions of the genes and pathways in atherogenesis based on previous human and rodent studies (186, 187, 191-193), which validated our experimental approach using intimal samples.

Previous sncRNA studies in the atherosclerosis research field have mainly focused on the function of miRNAs (53, 142, 143). Our PANDORA-seq results also revealed differentially expressed miRNAs that are consistent with traditional-seq results and previous reports. For example, miRNA-146, which targets the 3'UTR region of TRAF6 to regulate NF-κB activation, has been shown to be associated with atherosclerosis development or CVD in humans (194, 195). Consistently, we found miRNA-146b was upregulated in the intima of HCD-fed LDLR$^{-/-}$ mice as compared with LCD-fed mice. In addition, we also found that miRNA-31 was upregulated in atherosclerotic intima of HCD-fed LDLR$^{-/-}$ mice. miRNA-31 is expressed in both endothelial cells (196) and macrophages (197), which targets the 3'UTR region of adhesion molecule E-selection and may also contribute to atherosclerosis development (196-198).

Since miRNAs are not as highly modified as other sncRNAs such as rsRNAs or tsRNAs (146, 147), miRNAs can then be readily detected by traditional-seq and becomes the major small RNA species in traditional-seq results. However, these results are misleading as traditional-seq failed to detect sncRNAs with extensive terminal/internal modifications (146, 147). We have recently comprehensively compared the strengths of PANDORA-seq to that of traditional-seq (146, 147), and demonstrated the advantages of PANDORA-seq enabled by overcoming RNA modifications which generate sequencing bias in the traditional-seq method. In addition to miRNAs, PANDORA-seq can detect other highly modified rsRNAs and tsRNAs which were not detected by traditional-seq (146, 147). Our PANDORA-seq results showed that percentage of miRNA reads is very small (~0.4-0.6%) but rsRNAs and tsRNAs are much more abundant as compared to miRNA

reads, which is consistent with our recent studies (37, 147). However, these results do not mean that PANDORA-seq failed to detect miRNAs, but rather more objectively represent the true compositions of sncRNA population in the intima.

As compared to miRNAs, little is known about the function of tsRNAs and rsRNAs in CVD or atherosclerosis (53). These noncanonical sncRNAs have distinguishable features on evolutionary origin, abundance, biogenesis, and functions (146). Recent studies started to reveal the wide existence and functions of these new classes of sncRNAs (146, 153, 184, 185, 199). For example, tsRNAs are among the most ancient small RNAs in a wide range of species across all domains of life (55) and have received much attention due to their evolutionary conserved sequence and their roles in fundamental biological processes (54-56, 199). The functions of tsRNAs in other disease models, including cancer and metabolic disease, have been described (31, 55, 72, 200, 201). However, the role of the tsRNAs in atherosclerosis or CVD are mostly unknown. In the current study, PANDORA-seq but not traditional-seq identified many tsRNAs affected by HCD feeding in the intima of $LDLR^{-/-}$ mice. We found that one of HCD-induced intimal tsRNAs, tsRNA-Arg-CCG may play a role in regulating pro-atherogenic gene expression in endothelial cells in vitro. It is also important to note that tsRNA modifications can affect their secondary structure and function (31, 61, 72, 146). Although we demonstrated the pro-atherogenic properties of synthetic unmodified tsRNA-Arg-CCG in vitro, endogenous tsRNA-Arg-CCG with modifications may exert stronger or different phenotypes in vivo. Future studies are required to understand the functions of those tsRNAs in endothelial cell function and atherosclerosis and CVD.

As a low-input and high-throughput method, PANDORA-seq allows us to detect a vast amount of small RNAs from a low amount of RNA input from the intima. Nevertheless, a potential limitation of PANDORA-seq is the loss of RNA products during multiple RNA purification steps, which make it difficult to reach the level of single-cell library preparation. To address this limitation in the future, one potential solution is to improve the enzymes used in PANDORA-seq, which allows the library construction process to be performed in a one-pot reaction, thereby reducing the number of RNA purification steps and minimizing RNA loss. Combining the improved PANDORA-seq method with fluorescence-activated cell sorting would enable investigators to perform single-cell analysis for detecting cell type-specific highly modified sncRNAs. Future studies using single-cell PANDORA-seq would increase our understanding of the cell-type specific role of understudied sncRNAs in atherosclerosis.

In summary, we used a novel PANDORA-seq to identify sncRNAs associated with atherosclerosis development in LDLR$^{-/-}$ mice. By overcoming RNA modification-elicited limitations, PANDORA-seq substantially increased the reads of rsRNAs and tsRNAs, and revealed a rsRNA- and tsRNA-enriched sncRNA landscape in the atherosclerotic intima of LDLR$^{-/-}$ mice. We also found that one of HCD-induced intimal tsRNA-Arg-CCG has pro-atherogenic properties and may contribute to endothelial cell dysfunction and atherosclerosis development. To our knowledge, this is the first study to utilize PANDORA-seq to investigate sncRNAs in atherosclerosis or CVD. Our results suggest that the understudied rsRNAs and tsRNAs are much more abundant than miRNAs in atherosclerosis-prone tissues. Findings from our studies will hopefully stimulate further

investigations of the functions of these previously underexplored sncRNAs in atherosclerosis or CVD.

2.6 Figures and Tables

Table 2.1 Primer Sequences used for qPCR

Genes	Primer sequences	Genes	Primer sequences
hGAPDH	5'- AACTTTGGCATTGTGGAAGG -3'	hIL-6	5'- TAGTCCTTCCTACCCCAATTTCC -3'
	5'- GGATGCAGGGATGATGTTCT -3'		5'- TTGGTCCTTAGCCACTCCTTC -3'
hVE-Cadherin	5'- ATTGAGACAGACCCCAAACG -3'	hIL-1α	5'- GCACCTTACACCTACCAGAGT -3'
	5'-TTCTGGTTTTCTGGCAGCTT -3'		5'- TGCAGGTCATTTAACCAAGTGG -3'
hTie2	5'- AAGACATACGTGAACACCAC -3'	hIL-1β	5'- GCAACTGTTCCTGAACTCAACT -3'
	5'- AGTCAGAACACACTGCAGAT -3'		5'- ATCTTTTGGGGTCCGTCAACT -3'
hMyh11	5'-AAGGAAACACCAAGGTCAAGCAGC -3'	hICAM-1	5'- GTGATCCCTGGGCCTGGTG -3'
	5'- TCATTGCTCTCTGTGGCCTCATCT -3'		5'- GGAAACGAATACACGGTGATGG -3'
hαSMA	5'- CGCTGTCAGGAACCCTGAGA -3'	hVCAM-1	5'- TACCAGCTCCCAAAATCCTG -3'
	5'- CGAAGCCGGCCTTACAGA -3'		5'- TCTGCTAATTCCAGCCTCGT -3'
hMCP-1	5'- TTAAAAACCTGGATCGGAACCAA -3'		
	5'- GCATTAGCTTCAGATTTACGGGT -3'		

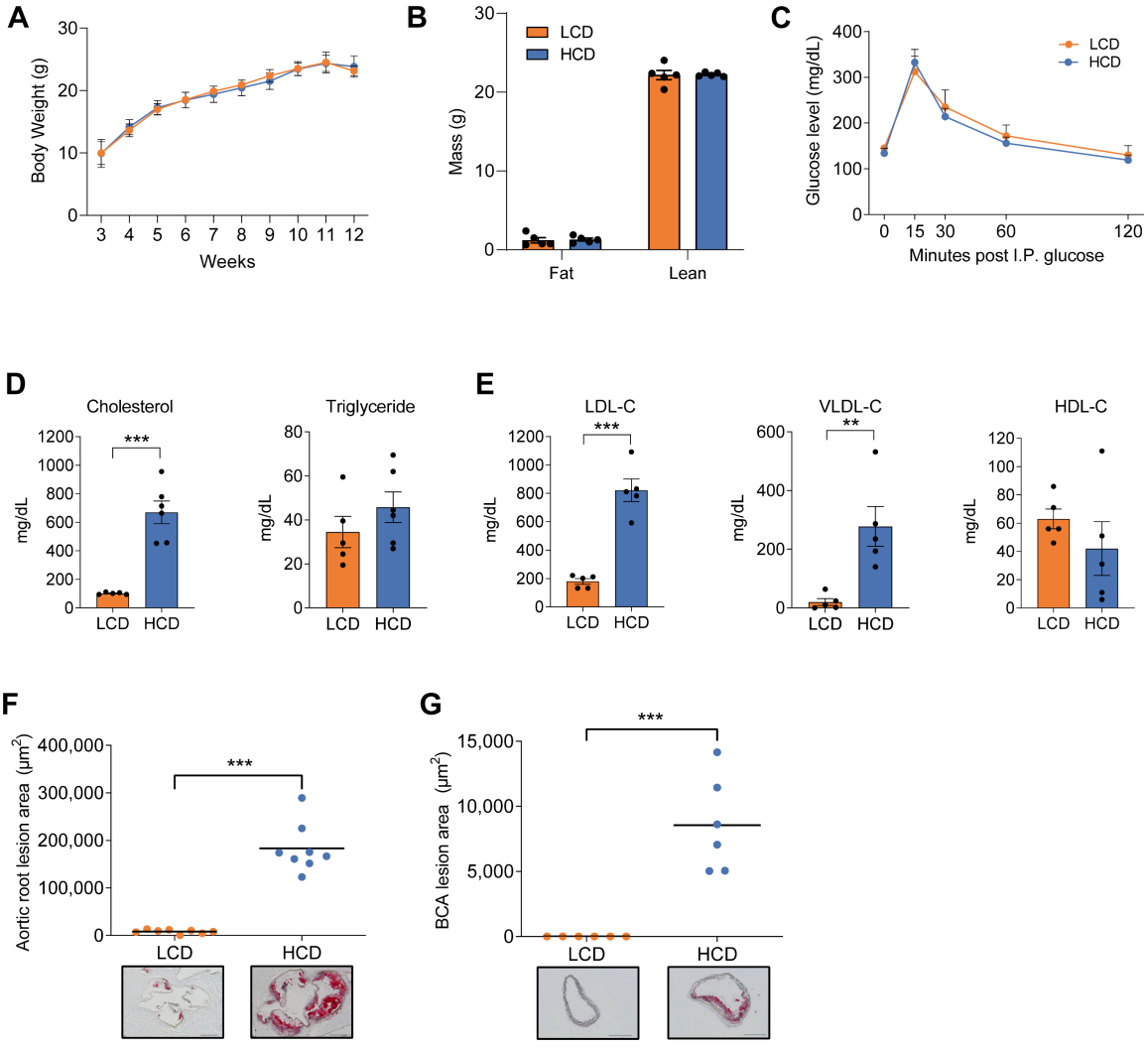
A
Body Weight (g)
Weeks
B
LCD
HCD
Mass (g)
Fat
Lean
C
Glucose level (mg/dL)
Minutes post I.P. glucose
D
Cholesterol
Triglyceride
mg/dL
E
LDL-C
VLDL-C
HDL-C
F
Aortic root lesion area (μm²)
G
BCA lesion area (μm²)

Figure 2.1. A low-fat, high-cholesterol diet effectively promotes hypercholesterolemia and atherosclerosis without inducing obesity and insulin resistance in LDL receptor-deficient mice.

Three-week-old male C57BL/6 $LDLR^{-/-}$ mice were fed a low-cholesterol diet (LCD, 0.02% cholesterol) or high-cholesterol diet (HCD, 0.5% cholesterol) for 9 weeks until euthanasia at 12 weeks of age. (A-C) Growth curves (A), body composition (B) and intraperitoneal glucose tolerance test (C) of LCD- and HCD-fed $LDLR^{-/-}$ mice. (D) Serum total cholesterol and triglyceride levels were measured. (E) Lipoprotein fractions (VLDL-C, LDL-C, and HDL-C) were isolated, and the cholesterol levels of each fraction were measured. (F) Quantitative analysis of the lesion area in the aortic root. Representative oil red O-stained aortic root sections displayed below the quantification data (scale bar = 200μm). (G) Quantitative analysis of the lesion area in the brachiocephalic artery (BCA). Representative oil red O-stained BCA sections displayed below quantification data (scale bar = 200μm). LCD, low-cholesterol diet; HCD, high-cholesterol diet; VLDL-C, very low-density lipoprotein cholesterol; LDL-C, low density lipoprotein cholesterol; HDL-C, high density lipoprotein cholesterol. All data are plotted as means ± S.E.M. (n=5-8 each group; *P<0.05; **P<0.01; ***P<0.001).

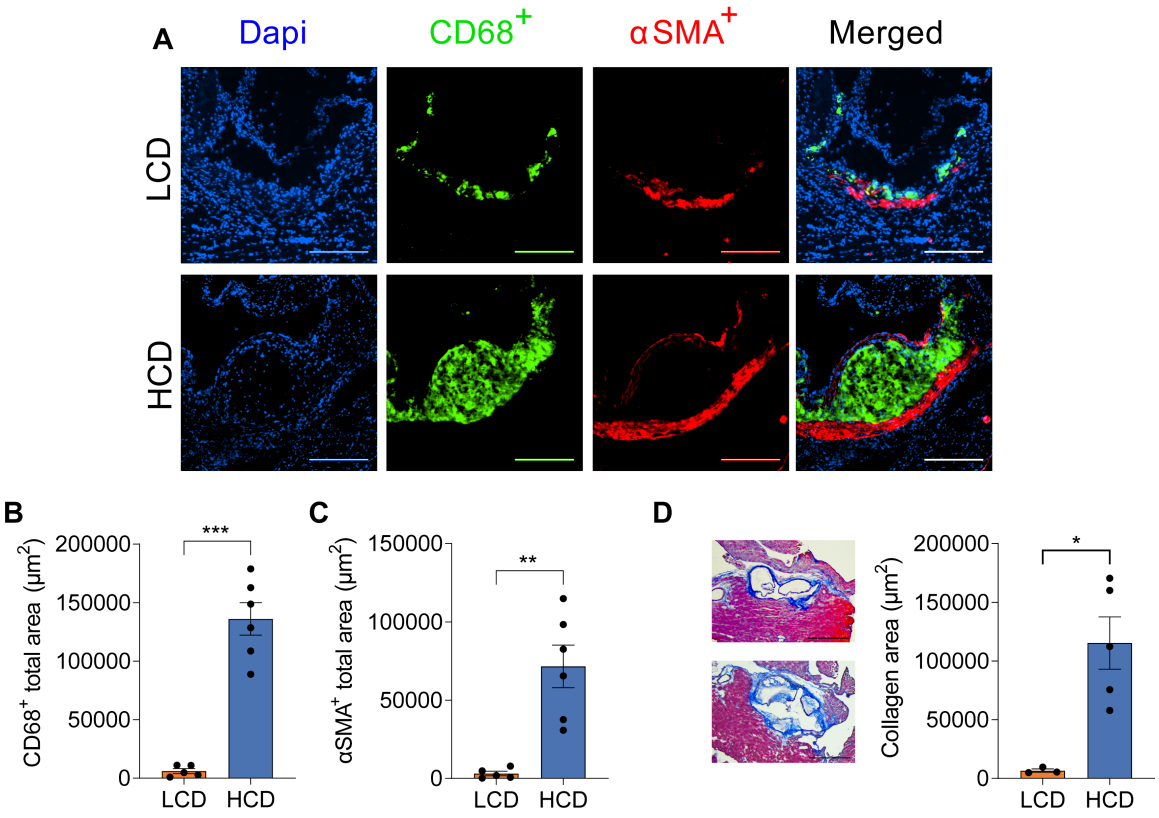
A
Dapi
CD68+
αSMA+
Merged
LCD
HCD
B
CD68+ total area (μm2)
200000
150000
100000
50000
0
***
LCD
HCD
C
αSMA+ total area (μm2)
150000
100000
50000
0
**
LCD
HCD
D
Collagen area (μm2)
200000
150000
100000
50000
0
*
LCD
HCD

Figure 2.2. High-cholesterol diet feeding induces atherosclerosis development in lean LDLR$^{-/-}$ mice.

Three-week-old male LDLR$^{-/-}$ mice were fed a low-cholesterol diet (LCD, 0.02% cholesterol) or high-cholesterol diet (HCD, 0.5% cholesterol) for 9 weeks until euthanasia at 12 weeks of age. (A) Representative images (scale bar=200μm) of immunofluorescence staining for CD68 (green), and αSMA (red) at the aortic root of LCD and HCD-fed LDLR$^{-/-}$ mice. The nuclei were stained with DAPI (blue). (B and C) Quantitative analysis of total CD68^{+} area (B) and total αSMA^{+} area (C) in atherosclerotic lesions of LCD and HCD-fed LDLR$^{-/-}$ mice. (D) Representative images (scale bar=500μm) and quantification data of Masson's Trichrome staining at the aortic root to examine the collagen contents. All data are plotted as means ± SEM (n=3-6 each group; *P<0.05; **P<0.01; ***P<0.001).

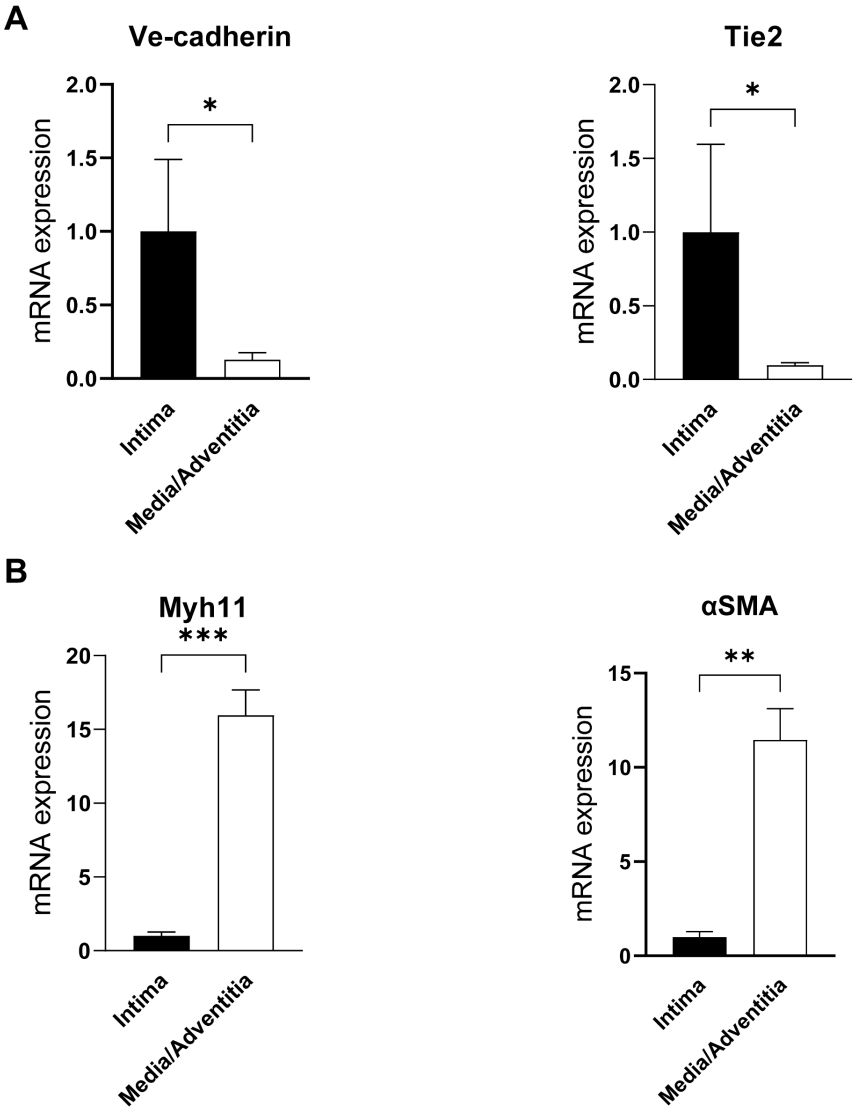
A
Ve-cadherin
mRNA expression
2.0
1.5
1.0
0.5
0.0
*
Intima
Media/Adventitia
Tie2
mRNA expression
2.0
1.5
1.0
0.5
0.0
*
Intima
Media/Adventitia
B
Myh11
***
mRNA expression
20
15
10
5
0
Intima
Media/Adventitia
αSMA
**
mRNA expression
15
10
5
0
Intima
Media/Adventitia

Figure 2.3. QPCR analysis of endothelia cell and smooth muscle cell markers in isolated aortic RNAs.

Three-week-old male LDLR$^{-/-}$ mice were fed an LCD for 9 weeks until euthanasia at 12 weeks of age. Total RNAs were isolated from the intima and remaining aorta (media/adventitia) and were used for QPCR analysis of the indicated endothelial cell markers (A) and smooth muscle cell markers (B). All data are plotted as means ± SEM (n=3-7 each group; *P<0.05; **P<0.01; ***P<0.001).

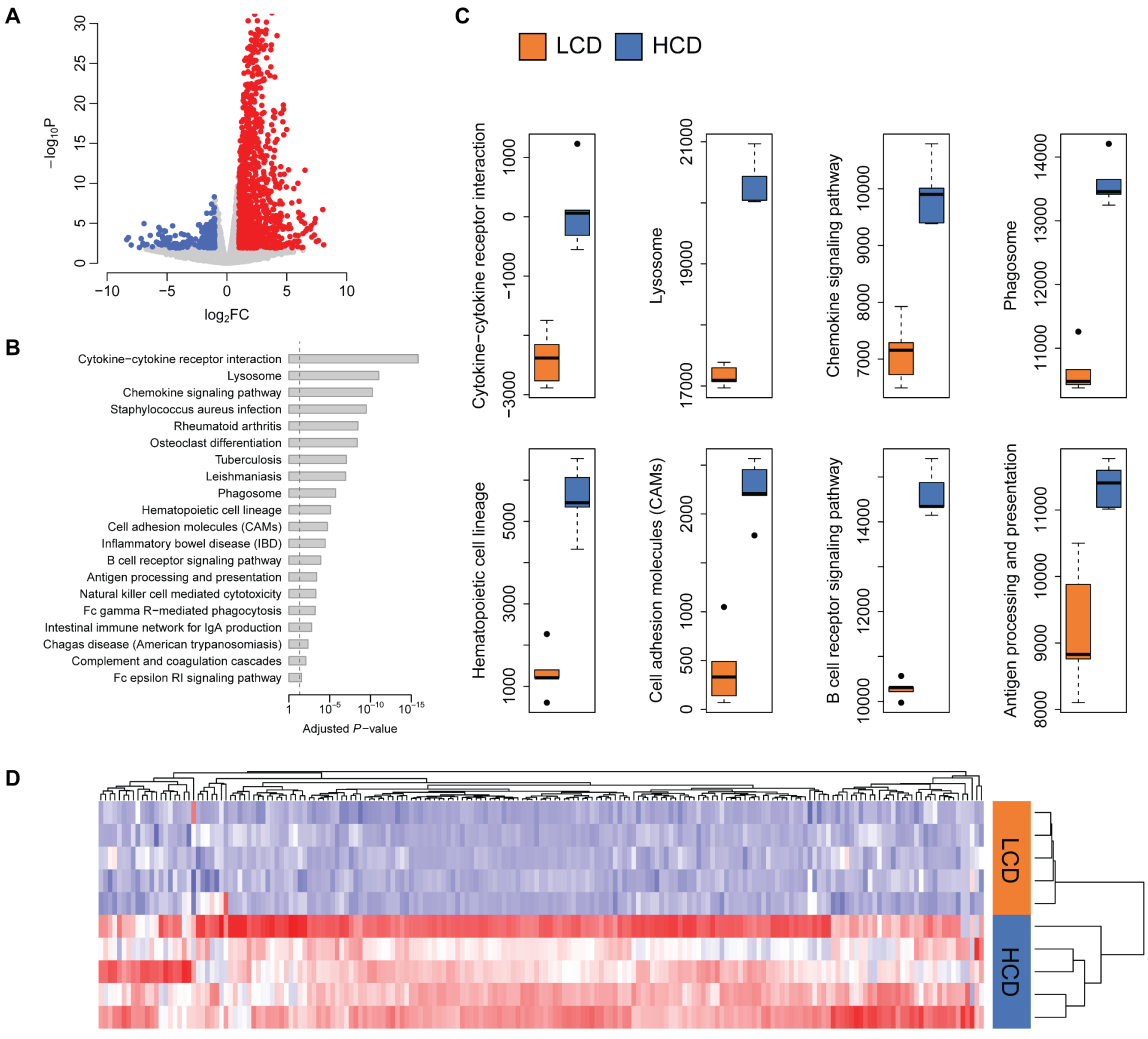
A
−log10P
log2FC
B
Cytokine−cytokine receptor interaction
Lysosome
Chemokine signaling pathway
Staphylococcus aureus infection
Rheumatoid arthritis
Osteoclast differentiation
Tuberculosis
Leishmaniasis
Phagosome
Hematopoietic cell lineage
Cell adhesion molecules (CAMs)
Inflammatory bowel disease (IBD)
B cell receptor signaling pathway
Antigen processing and presentation
Natural killer cell mediated cytotoxicity
Fc gamma R−mediated phagocytosis
Intestinal immune network for IgA production
Chagas disease (American trypanosomiasis)
Complement and coagulation cascades
Fc epsilon RI signaling pathway
Adjusted P−value
C
LCD
HCD
Cytokine−cytokine receptor interaction
Lysosome
Chemokine signaling pathway
Phagosome
Hematopoietic cell lineage
Cell adhesion molecules (CAMs)
B cell receptor signaling pathway
Antigen processing and presentation
D
LCD
HCD

Figure 2.4. High-cholesterol diet feeding affects many atherosclerosis-related gene expression in the intima of LDL receptor-deficient mice.

Three-week-old male LDLR$^{-/-}$ mice were fed an LCD or HCD for 9 weeks. Total RNA was isolated from the intima and used for RNA-seq analysis. (A) Volcano plot of differential expressed genes (DEGs) in the intima of HCD-fed LDLR$^{-/-}$ mice as compared with LCD-fed mice. Colored dots represent the enriched (red dots) or depleted (blue dots) DEGs with a false discovery rate (*FDR*) of < 0.1 and fold change (*FC*) > 2 as a cut-off threshold. (B) KEGG pathways significantly associated with upregulated DEGs in intimal of HCD-fed LDLR$^{-/-}$ mice. The *P*-values were computed by *Fisher*'s exact test. The vertical dash line indicates the significance level of $\alpha = 0.05$. The y-axis displays the KEGG pathways while the x-axis displays the adjusted *P*-values. (C) Geneset scores of the prioritized KEGG pathways. The geneset score was calculated using the FAIME algorithm. (D) Heatmap representation of DEGs involved in the pathways of "Cytokine-cytokine receptor interaction," "Chemokine signaling pathway," and "Cell adhesion molecules" "Lysosome," "Phagosome," "Hematopoietic cell lineage," "B cell receptor signaling pathway," and "Antigen processing and presentation." Each column shows one individual gene, and each row shows a biological replicate of mouse. Red represents relatively increased gene expression while blue denotes downregulation (n=5 each group).

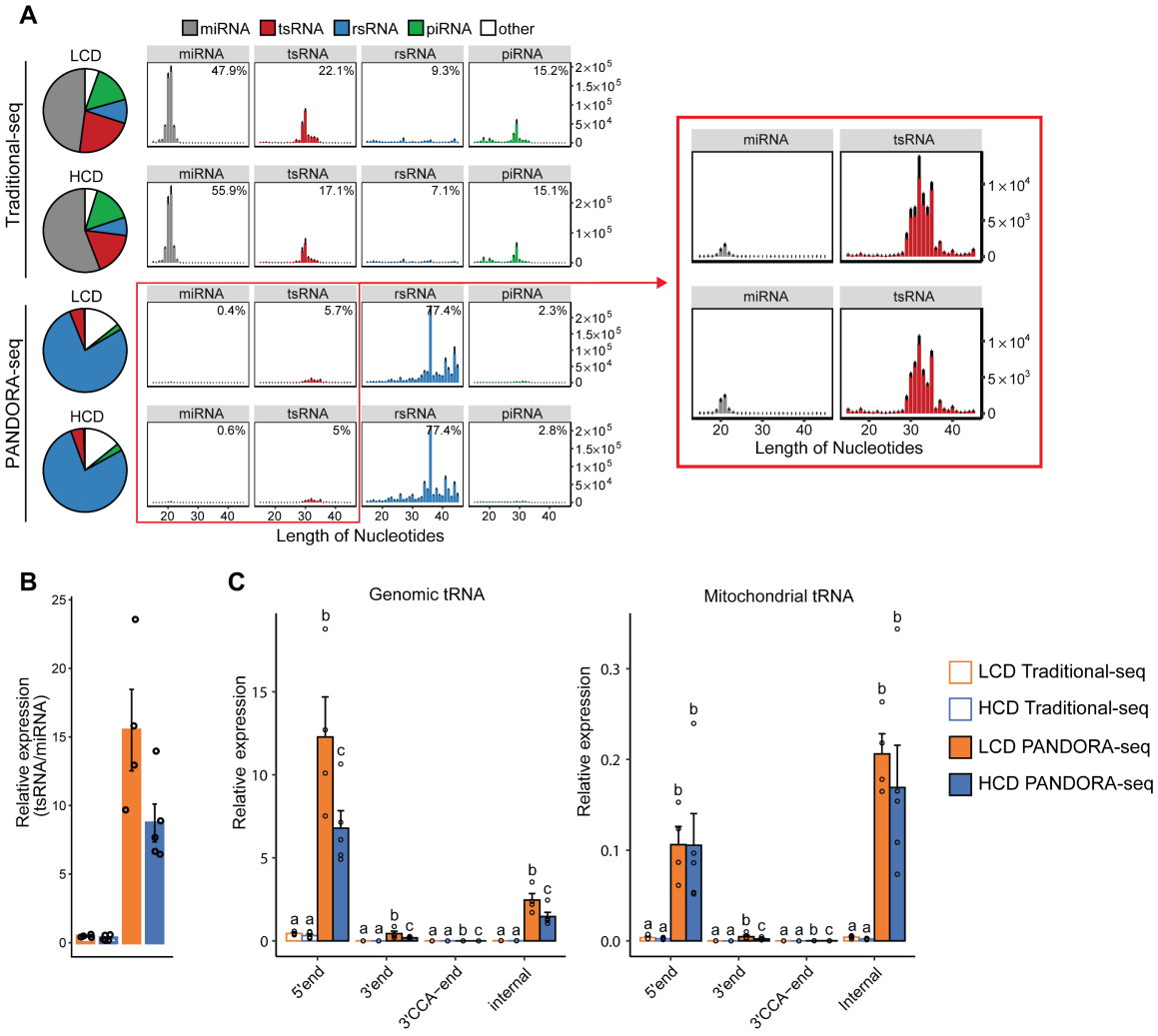
A
miRNA tsRNA rsRNA piRNA other
Traditional-seq
PANDORA-seq
LCD
HCD
47.9%
22.1%
9.3%
15.2%
55.9%
17.1%
7.1%
15.1%
0.4%
5.7%
77.4%
2.3%
0.6%
5%
77.4%
2.8%
Length of Nucleotides
B
Relative expression (tsRNA/miRNA)
C
Genomic tRNA
Mitochondrial tRNA
Relative expression
5'end
3'end
3'CCA-end
Internal
LCD Traditional-seq
HCD Traditional-seq
LCD PANDORA-seq
HCD PANDORA-seq

Figure 2.5. Read summaries and length distributions of different sncRNA categories in the intima of LDL receptor-deficient mice under traditional RNA-seq and PANDORA-seq.

Three-week-old male $LDLR^{-/-}$ mice were fed an LCD or HCD for 9 weeks. Total RNA was isolated from the intima and used for PANDORA-seq or traditional small RNA sequencing. (A) Dynamic landscapes of intimal sncRNAs including miRNAs, tsRNAs, rsRNAs, and piRNAs detected by traditional-seq and PANDORA-seq protocols. Zoomed panels of miRNAs and tsRNAs detected by PANDORA-seq are shown on the right. (B) Relative tsRNA/miRNA ratios under traditional-seq and PANDORA-seq protocols. (C) tsRNA responses to traditional-seq and PANDORA-seq in regard to different origins (5′ tsRNA, 3′ tsRNA, 3′ tsRNA-CCA end, and internal tsRNAs). The y axes represent the relative expression levels compared with total reads of miRNA. Different letters above the bars indicate statistically significant differences ($P < 0.05$). Same letters indicate $P > 0.05$. Statistical significance was determined by two-sided one-way ANOVA with uncorrected Fisher's LSD test. All data are plotted as means ± S.E.M. (n=4-5 in each group).

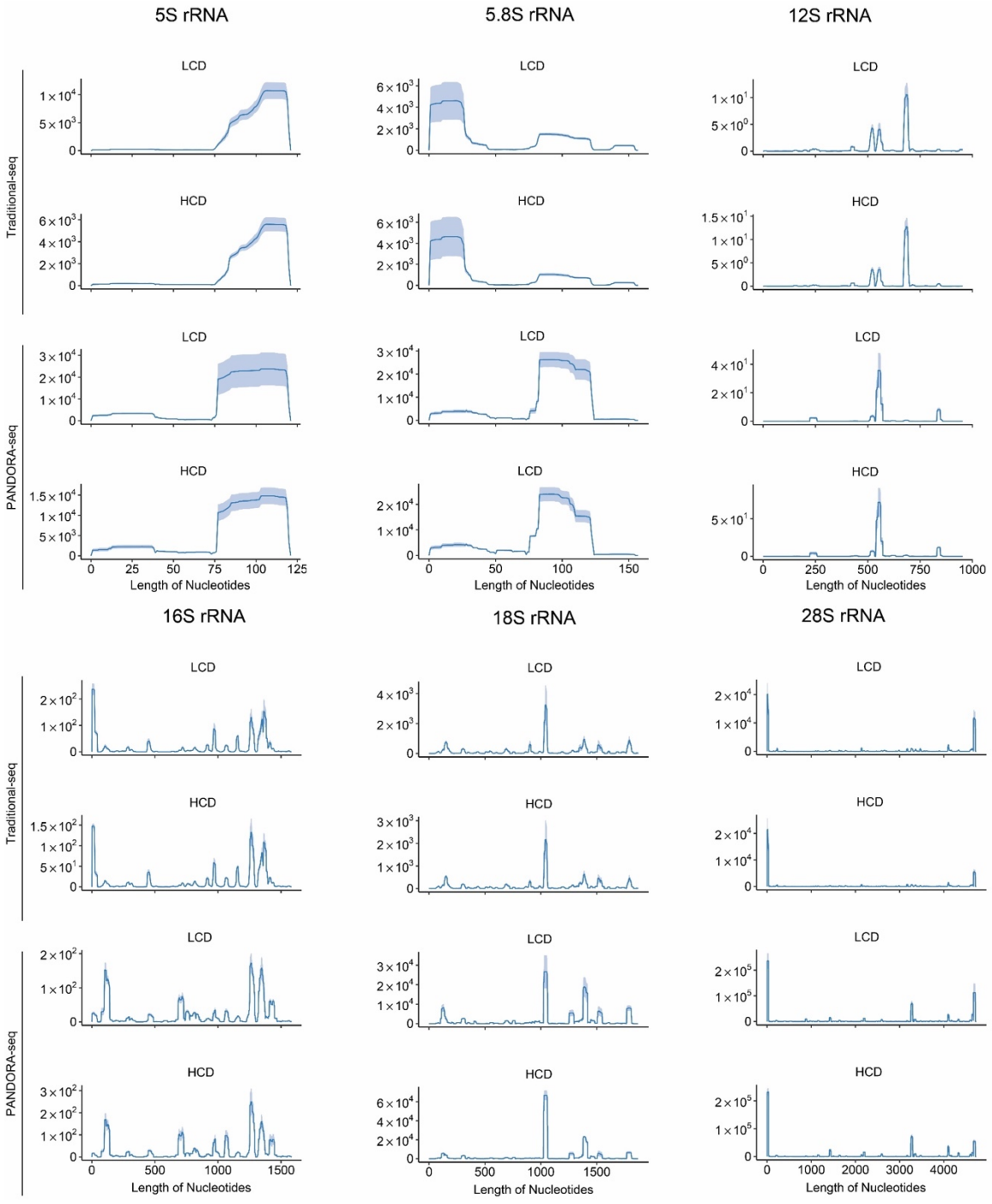
5S rRNA
5.8S rRNA
12S rRNA
16S rRNA
18S rRNA
28S rRNA
Traditional-seq
PANDORA-seq
LCD
HCD
Length of Nucleotides

Figure 2.6. Comparison of rsRNA-generating loci by rsRNA mapping data detected by PANDORA-seq and traditional RNA-seq. Three-week-old male LDLR$^{-/-}$ mice were fed an LCD or HCD for 9 weeks. Total RNA was isolated from the intima and used for PANDORA- seq or traditional RNA sequencing. Comparison of rsRNA-generating loci by rsRNA mapping data on 5S rRNA, 5.8S rRNA, 18S rRNA, 28S rRNA, 12S rRNA, and 16S rRNA detected by traditional RNA-seq and PANDORA-seq (n=4-5 in each group).

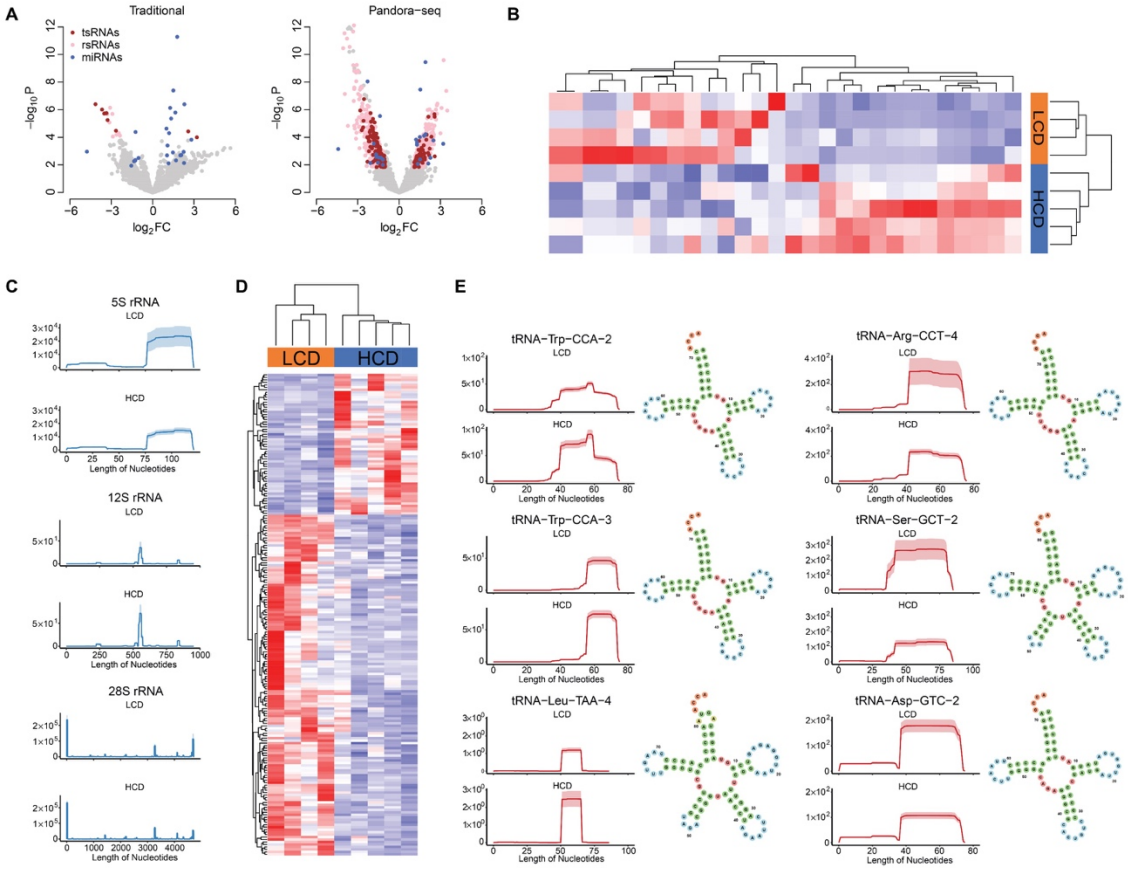
A
Traditional
Pandora-seq
tsRNAs
rsRNAs
miRNAs
−log10 P
log2FC
B
LCD
HCD
C
5S rRNA
12S rRNA
28S rRNA
LCD
HCD
Length of Nucleotides
D
LCD
HCD
E
tRNA-Trp-CCA-2
tRNA-Arg-CCT-4
tRNA-Trp-CCA-3
tRNA-Ser-GCT-2
tRNA-Leu-TAA-4
tRNA-Asp-GTC-2

Figure 2.7. Identification of significantly altered intimal sncRNAs associated with atherosclerosis development in LDL receptor-deficient mice by PANDORA-seq and traditional RNA-seq.

Three-week-old male LDLR$^{-/-}$ mice were fed an LCD or HCD for 9 weeks. Total RNA was isolated from the intima and used for PANDORA-seq or traditional small RNA sequencing. (A) Volcano plot of differentially expressed intimal sncRNAs identified by Traditional (left) and PANDORA-seq methods (right). Colored dots represent the differentially expressed tsRNAs (red dots), rsRNAs (pink dots), or miRNAs (blue dots) with a false discovery rate (*FDR*) < 0.1 and fold change (*FC*) > 2 as the cut-off threshold. (B) Heatmap representation of differentially expressed intimal miRNAs detected by PANDORA-seq. (C) Comparison of rsRNA-generating loci by rsRNA mapping data on 5S rRNA, 12S rRNA, and 28S rRNA detected by PANDORA-seq. (D) Heatmap representation of differentially expressed intimal tsRNAs detected by PANDORA-seq. (E) Dynamic responses to LCD or HCD of representative individual tsRNAs (pictured right). Biological replicates are represented in each row (B) or column (D). Red represents relatively increased expression while blue represents decreased expression with an *FDR* < 0.1 and *FC* >2 as the cut-off threshold (n=4-5 each group).

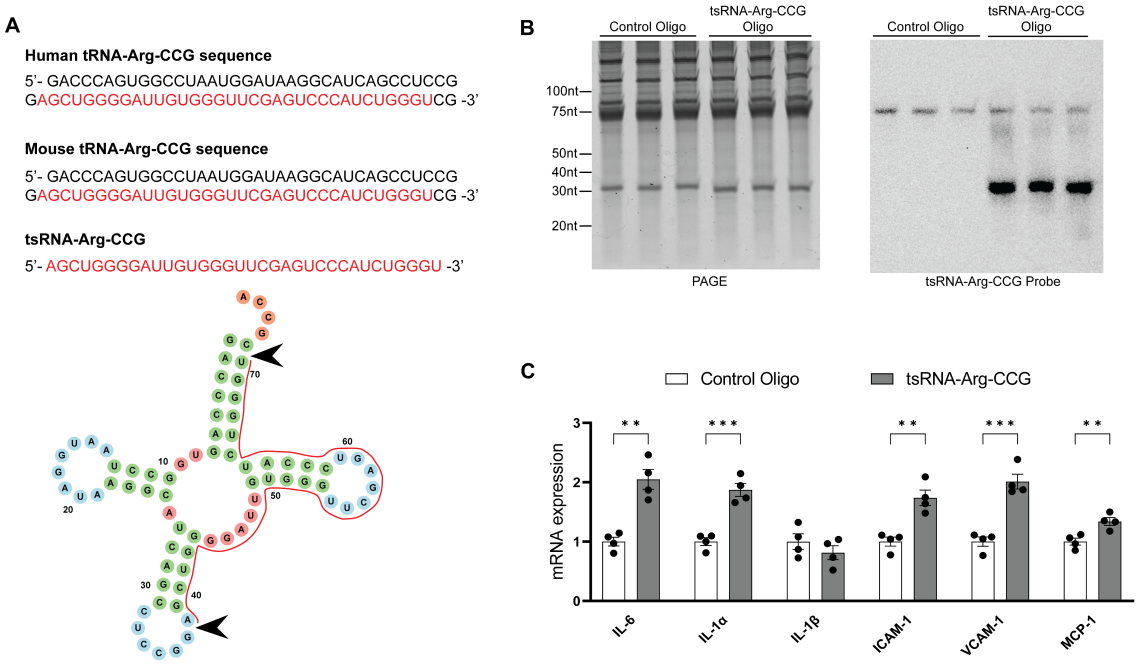

Figure 2.8. tsRNA-Arg-CCG affects pro-atherogenic gene expression in human endothelial cells in vitro.

(A) Sequences of human and murine tRNA-Arg-CCG and tsRNA-Arg-CCG (top), and representative figure of tRNA-Arg and tsRNA-Arg-CCG indicated with a red line (bottom; black arrowheads indicating cleavage site). (B and C) Human endothelia cells, HMEC-1 cells were transfected with synthetic tsRNA-Arg-CCG oligo. The expression levels of tsRNA-Arg-CCG after transfection was assessed with Northern blot (B). Expression levels of indicated genes were analyzed by QPCR (C) (n=4; **P<0.01; ***P<0.001).

3. Chapter 3: Paternal hypercholesterolemia elicits sex-specific exacerbation of atherosclerosis in adult offspring of LDL receptor-deficient mice

3.1 Abstract

Emerging studies suggest that various parental exposures affect offspring cardiovascular health, yet the specific mechanisms, particularly the influence of paternal cardiovascular disease (CVD) risk factors on offspring cardiovascular health, remain elusive. The present study explored how paternal hypercholesterolemia affects offspring atherosclerosis development using the LDL receptor-deficient ($LDLR^{-/-}$) mouse model. We found that paternal high-cholesterol diet feeding led to significantly increased atherosclerosis in F1 female, but not male, $LDLR^{-/-}$ offspring. Transcriptomic analysis highlighted that paternal hypercholesterolemia stimulated pro-atherogenic genes, including *Ccn1* and *Ccn2*, in the intima of female offspring. Sperm small non-coding RNAs (sncRNAs), particularly tRNA-derived small RNAs (tsRNAs) and rRNA-derived small RNAs (rsRNAs) contribute to the intergenerational transmission of paternally acquired metabolic phenotypes. Using a newly developed PANDORA-seq method, we identified high-cholesterol feeding elicited changes in sperm tsRNA/rsRNA profiles that were undetectable by traditional RNA-seq, potentially key factors mediating paternal hypercholesterolemia-elicited atherogenesis in offspring. Interestingly, high-cholesterol feeding altered sncRNA biogenesis-related gene expression in the epididymis but not testis of $LDLR^{-/-}$ sires, which may have led to the modified sperm sncRNA landscape. Our results underscore the sex-specific intergenerational impact of paternal

hypercholesterolemia on offspring cardiovascular health and contribute to the understanding of chronic disease etiology originating from parental exposures.

3.1 Introduction

Atherosclerosis is a complex disease characterized by the accumulation of cholesterol in large arteries, leading to plaque development in the intimal layer of the artery (136, 202, 203). Despite major advances in diagnoses and treatments, atherosclerotic cardiovascular disease (CVD) is still the leading cause of mortality and morbidity worldwide (204, 205). While many modifiable risk factors such as smoking, diet, and obesity have been well-established to contribute to atherosclerosis, there are also genetic and epigenetic factors that can increase the risk of developing atherosclerotic CVD (139), which may reduce the effectiveness of lifestyle interventions and current therapeutic interventions. Therefore, it is critical to identify these genetic and epigenetic factors and understand their mechanisms in atherosclerosis development to enhance patient preventative care through early detection methods.

In addition to the well-known traditional risk factors, strong evidence has suggested that parental environmental influences can impact the health of future generations (21, 22, 30, 31, 33-36, 206-210). Several large-scale clinical studies including the Framingham Heart Study, the Physicians' Health study, and the Women's Health Study have demonstrated the impact of parental CVD on offspring cardiometabolic health and revealed that offspring of parents with a history of early-onset CVD have a higher risk of developing CVD, even after adjusting for other risk factors (21-23). A few other human and animal

studies have also demonstrated that maternal or in utero exposure to certain CVD risk factors can elicit increased CVD risk in offspring. For example, hypercholesterolemia in mothers during pregnancy can significantly increase the number and size of fatty streaks in fetal aortas (24, 211). The Fate of Early Lesions in Children (FELIC) study demonstrated that aortic lesions in children of hypercholesterolemic mothers progressed much faster than that of children of normocholesterolemic mothers (25, 212). Animal studies also demonstrated that maternal or perinatal hypercholesterolemia can cause increased cardiovascular dysfunction or atherosclerosis development in the offspring (29, 213, 214). We also reported that maternal exposure to an atherogenic endocrine disrupting chemical (EDC), bisphenol A, led to exacerbated atherosclerosis in the adult offspring in mice (215).

While most studies have focused on the effects of maternal factors on offspring health, emerging evidence suggests that paternal exposures can also affect offspring's cardiometabolic heath (30-36, 45, 209, 210, 216, 217). For example, we previously demonstrated that paternal high-fat diet (HFD) feeding in mice can induce metabolic disorders in the offspring (30-32). Several other studies also found that exposure of male rats or mice to HFD can lead to increased diabetic phenotypes or metabolic disfunctions in offspring (45, 209). Paternal exposure to low-protein diets caused impaired vascular function and metabolic disorders in mouse offspring (33-36). In addition to dietary exposure, we and others reported that paternal exposure to a range of environmental toxicants can have inter- and trans-generational adverse effects on the metabolic health of their offspring (37-40). While various sperm epigenetic factors have been proposed to

contribute to intergenerational inheritance of environment-induced phenotypes in mammals (42), sperm small non-coding RNAs (sncRNAs) especially tRNA-derived small RNAs (tsRNAs) and rRNA-derived small RNAs (rsRNAs) can significantly contribute to the intergenerational transmission of paternally acquired metabolic phenotypes (32, 43-45).

While previous studies suggested that paternal factors affect offspring metabolic health, there are no animal studies investigating the impact of paternal exposures to unhealthy diets on atherosclerosis development of offspring. In the current study, we investigated the impact of paternal hypercholesterolemia on offspring atherosclerosis development in LDL Receptor-deficient ($LDLR^{-/-}$) mice. We reported here that paternal high-cholesterol diet (HCD) feeding led to significantly increased atherosclerosis in F1 female $LDLR^{-/-}$ offspring. We then used an innovative small RNA-seq method, PANDORA-seq (59, 146) to unveil the paternal hypercholesterolemia-elicited sperm sncRNA changes that may contribute to paternally acquired atherosclerosis in offspring.

3.2 Methods

3.2.1 Sex as a biological variant

Our study examined both male and female $LDLR^{-/-}$ mice and we found there were sex-dimorphic effects for atherosclerosis development in F1 offspring. For F0 mice, only male $LDLR^{-/-}$ mice were exposed to different diets since the study was designed to investigate the impact of paternal exposures on offspring atherosclerosis development.

3.2.2 Animals

3-week-old littermate male LDLR$^{-/-}$ mice (The Jackson Laboratories) were fed ad libitum on a semisynthetic low-fat (4.2% fat) AIN76 diet containing low cholesterol (LCD; 0.02% cholesterol; Research Diets) or high cholesterol (HCD; 0.5% cholesterol; Research Diets) for 8 weeks before mating with age-matched LCD-fed female LDLR$^{-/-}$ mice (C57BL/6 strain, Jackson Laboratories) (159, 160, 178-180). Male mice were housed with female mice with free access to LCD during the light cycle. Male mice were returned to their cages overnight with their assigned LCD or HCD, and female mice were maintained on LCD during mating, gestation, and lactation. Female mice were never exposed to HCD. After copulation was confirmed by vaginal plug detection, the male mice were removed from the mating cage and humanely euthanized. These initial mouse pairs are designated F0. The F1 offspring were weaned at 3 weeks of old and were given an LCD until euthanasia at 19 weeks old. To ensure the atherosclerotic phenotype we observed was not batch specific, 7 LCD-fed sires were mated with 8 control females and 6 HCD-fed sires were mated with 7 control females. Eight litters were generated from LCD-fed sires and 7 litters were generated from HCD-fed sires. At least one mouse from each litter was used for the study. All animals were housed in pathogen-free microisolator cages in a temperature controlled (~21°C) environment with a 12 hr light-dark cycle. On the day of euthanasia, mice were fasted for 6 hr following the dark cycle (feeding cycle). Mice were anesthetized with ketamine/xylazine (100/10 mg/kg BW) by intraperitoneal (IP) injection. The peritoneum and chest cavity of the mouse was opened to expose the heart. Blood was collected from the right ventricle of the heart using a 23G needle and 1mL syringe.

Following blood collection, the right atrium was nicked and 10mL of saline was injected into the left ventricle to perfuse the circulatory system, which also killed the mouse by exsanguination. The major tissues and organs were collected and weighed as previously described (160, 163, 166, 180). All animal studies were performed in compliance with the approved protocols by the Institutional Animal Care and Use Committee of the University of California, Riverside.

3.2.3 Metabolic phenotype analysis

Body weights (BW) were measured weekly. Body lean and fat mass was measured by NMR spectroscopy (EchoMRI, Echo Medical System). Intraperitoneal glucose tolerance test (IPGTT) was performed as previously described one week before sacrifice (37, 160).

3.2.4 Sperm isolation

Sperm from F0 mice were collected as previously described (59, 138). Mature sperm was released from the cauda epididymis and incubated in 5 mL of PBS at 37˚C for 15 min. Afterwards, the sperm were filtered through a 40μm cell strainer to remove any residual tissue debris. Sperm were then incubated in somatic cell lysis buffer (0.1% SDS and 0.5% Triton X-100) for 40 min on ice to remove somatic cells. Sperm was pelleted and collected in 1 ml of Trizol (Sigma-Aldrich, T9424) for RNA isolation.

3.2.5 Blood analysis

Blood samples were collected from the right ventricle and centrifuged at 1500x *g* for 15 min at 4°C. The upper clear phase (serum) was collected for lipid analysis. Serum total cholesterol and total triglyceride concentrations were measured using the Wako

Cholesterol E enzymatic colorimetric assay (Wako, 999-02601) and the Wako L-type TG M assay (Wako, 994-02891) according to the manufacturer's instructions (FUJIFILM Medical Systems U.S.A., Inc., Richmond, VA, USA). The lipoprotein fractions were isolated in a Beckman Coulter XPN100-IVD ultracentrifuge as previously described (161, 180, 218).

3.2.6 RNA isolation

Total RNAs were collected from F0 mouse sperm, testis, caput, and cauda epididymis, F1 mouse intima, and cultured cells as previously described (37, 59, 164, 180). For the intimal RNA isolation, aortas of F1 mice were isolated and flushed with PBS followed by intimal peeling using TRIzol reagent (Sigma-Aldrich, T9424). A total of ~300-400μL of Trizol was flushed into the aorta for 10 seconds (~100μL) followed by a 10 second pause for 3 times as previously described (180). The flowthrough was collected in a 1.5mL Eppendorf tube followed by RNA extraction.

3.2.7 Atherosclerotic lesion analysis

The atherosclerotic plaque sizes were quantified as previously described (138, 168, 169). To quantify the plaque area at the aortic root, Optimal Cutting Temperature (OCT)-compound-embedded hearts were sectioned at a 12μm thickness keeping all the three valves of the aortic root in the same plane, and stained with oil red O. To quantify atherosclerotic plaque area at the BCA, the OCT-embedded brachiocephalic arteries were sectioned from distal to proximal at a thickness of 10μm. BCA atherosclerotic lesions from the lumenal to the internal elastic lamina were quantified in three equidistant oil red O-stained sections at 200, 400, and 600μm proximal from the branching point of the

brachiocephalic artery into the carotid and subclavian arteries. Images were taken and plaque size was quantified using a Nikon microscope (Nikon, Melville, NY, USA).

3.2.8 Cell culture

Human endothelial cell line HMEC-1 was purchased from ATCC (catalog no.: CRL-3243) (180). Cells were treated with 1mg/ml CCN1 or CCN2 for 1, 3, or 4 hours and then used for the indicated QPCR and Wester blotting experiments. For macrophage adhesion assay, HMEC-1 cells were pretreated with 10ng/mL TNFα, 1mg/mL CCN1 or CCN2 for 24 hours. $LDLR^{-/-}$ mice were injected with 1mL of thioglycolate for 3 days to stimulate macrophage production. Isolated peritoneal macrophages were stained with calcein acetoxymethyl and incubated with HMEC-1's for 4 hours. The attached macrophages were fixed and counted under a fluorescence microscope. mESCs containing an Oct4-GFP reporter was kindly provided by Dr. Sihem Cheloufi (University of California, Riverside, CA). mESCs were maintained in stem cell media and passaged every two days in gelatin coated dishes as we previously described (59).

3.2.9 mESC transfection and embryoid body formation assay

mESC transfection and embryoid body formation assays were performed as we previously described (59). mESCs were transfected with vehicle, control oligos, and tsRNA/rsRNA pool oligos for EB differentiation assay. After 24 hours, the EBs were collected and total RNAs were extracted for further analysis. For each transfection, three independent replicates were performed. Vehicle and control oligos were used as controls. The tsRNA/rsRNA pool oligo contained the following RNAs: tsRNA-Glu-CTC/TTC (5'-ACCGCCGCGGCCCGGGTTCGTTTCCCGGTCAGGGAAC-3'),

mt-tsRNA-His-GTG

(5’-GGTGAATATAGTTTACAAAAAACATTAGACTGTGAATCTGACAA-3’),

rsRNA-18S (5’-TGGATCTTGGGAGCGGGCGGGCGGTCCGCCGCGAGGCGA-3’),

and

rsRNA-28S

(5’-CGCGACCTCAGATCAGACGTGGCGACCCGCTGAATTTAAGCAT-3’

and 5’-TCCTTCTGATCGAGGCCCAGCCCGTGGACGGTGTGAGGCCG-3’).

3.2.10 Quantitative Real-Time PCR

We measured the relative mRNA expression levels by Quantitative Real-Time PCR with the SYBR Green (Bio-Rad, 170–8886) kit using a Bio-Rad CFX Real-Time-PCR Machine (Bio-Rad, 184–5096) (37, 164, 180). The primer sequences are included in Table 3.1.

3.2.11 Western Blotting

Western blotting experiments were performed as previously described (37, 163, 218). Primary antibodies including anti-Actin (1:5000 dilution, Millipore Sigma A2066), anti-p65 (1:1000 dilution, Cell Signaling, 3034), and anti-Phospho-p65 (Ser 536) (1:1000 dilution, Cell Signaling, 93H1) and anti-rabbit secondary antibodies (1:5000 dilution, Millipore Sigma 12–348) were used for these experiments.

3.2.12 Immunofluorescence staining

The cryo-sections of mouse aortic root and cultured human HMEC-1 cells were used for immunofluorescence staining as previously described (168, 180). For immunostaining, samples were incubated with antibodies against MOMA2 (Bio-Rad,

MCA519a), MCP-1 (Abcam, ab7202), IL-6 (Bio-Rad AbD Serotec, MCA1490), α-SMA (Abcam, ab5694), CCN1 (R&D, 4055CR050), CCN2 (R&D, 9190CC050), or p65 (Santa Cruz Biotechnology, sc-372) at 4°C for 12 to 15 hours. The sections were rinsed with PBS and incubated with fluorescein-labeled secondary antibodies (Life Technologies). The nuclei were stained by mounting the slides with DAPI medium (Vector Laboratories).

3.2.13 RNA sequencing and transcriptomic data analysis

The creation of cDNA libraries and sequencing were performed using the Illumina standard operation pipeline as previously described (37, 166, 175, 176). For data analysis, we applied the *Salmon* tool to quantify the mRNA expression from the raw sequencing data with the default setting, based on the Ensembl mouse cDNA annotation (GRCm38). We then employed the *edgeR* algorithm (174) to perform the groupwise comparison in transcriptomic pattern, using the *TMM* algorithm to perform reads count normalization and effective library size estimation and the likelihood ratio test to identify the DEGs. The genes with a false discovery rate (FDR) <0.1 and a fold change (FC) >1.5 was deemed differentially expressed. We further performed gene ontology analysis upon the differentially expressed genes using the definition from GO project. The DAVID bioinformatics tool (219) was applied to detect the GOBP terms enriched by the DEGs. For each prioritized GOBP term, we computed a geneset score, using the Functional Analysis of Individual Microarray Expression (FAIME) algorithm (177). A higher FAIME score suggests an increased overall expression of a given GOBP term/geneset. All the RNA-seq datasets have been deposited in the Gene Expression Omnibus (GSE251713).

3.2.13 PANDORA-seq of sperm small RNAs

PANDORA-seq protocol has been described in detail in our recent reports (37, 59, 180). Briefly, sperm total RNAs isolated for LCD and HCD fed male LDLR$^{-/-}$ mice was ran through a 15% urea polyacrylamide gel. Small RNA of 15-50 nucleotides was visualized with SYBR Gold solution (Invitrogen, S11494) and excised (59). A sample of the eluted RNA was stored in -80˚C for Traditional-seq. The remaining RNA was eluted and then treated with T4PNK reaction mixture (5µl 10x PNK buffer, 1mM ATP, 10U T4PNK) followed by RNA isolation with TRIzol. The collected RNAs were then treated with AlkB mixture (50mM HEPES, 75µM ferrous ammonium sulfate, 1mM α-ketoglutaric acid, 2mM sodium ascorbate, 50mg/l BSA, 4µg/ml AlkB, 2,000 U/ml RNase inhibitor) followed by RNA isolation with TRIzol. The recombinant AlkB enzyme was prepared by Dr. Linlin Zhao (University of California, Riverside, CA) as previously described (59). The adapters (New England Biolabs, E7330S) were ligated sequentially (3' adapter, reverse transcription primer, then 5' adapter). First-strand cDNA synthesis was performed followed by PCR amplification with PCR Primer Cocktail and PCR Master Mix to enrich the cDNA fragments. Finally, the PCR products were purified from PAGE gel and prepared for sequencing at the Genomics Center of University of California, San Diego (Illumina system) (37, 59, 180).

Small RNA sequences were annotated using the software *SPORTS1.1* with one mismatch tolerance (*SPORTS1.1* parameter setting: -M 1). Statistical significance among different groups was determined by two-sided one-way ANOVA with uncorrected Fisher's least significant difference test. Pairwise comparison of differentially expressed sncRNAs

(average raw counts of each sncRNA >10 in the compared treatments) among different diets was performed using the R package DEseq2 with a normalized RPM fold change > 2 and $P < 0.05$. All the small RNA-seq datasets have been deposited in the Gene Expression Omnibus (GSE251713).

3.2.14 Statistics analysis

All data except the high-throughput sequencing data are presented as the mean ± S.E.M. Individual pairwise comparisons were analyzed by two-sample, two-tailed Student's t test. One-way analysis of variance (ANOVA) was used for analyzing different origins of the tsRNA/miRNA expression ratio under different treatments (uncorrected Fisher's LSD test) or when the statistical significance of more than two groups were analyzed (Bonferroni's multiple comparison test). Two-way ANOVA was used when multiple comparisons were made, followed by a Bonferroni multiple comparisons test. Data analysis was performed using the GraphPad Prism 10 software with statistical significance set at $P < 0.05$.

3.2.15 Study approval

All animal studies were performed in compliance with the IACUC protocols approved by the University of California, Riverside.

3.2.16 Data availability

All the RNA-seq datasets have been deposited in the Gene Expression Omnibus under the accession code GSE251713. Values for graphs in the figures and supplemental figures are provided in the Supporting Data Values file.

3.3 Results

3.3.1 Male LDL receptor-deficient mice fed a low-fat, high-cholesterol diet develop severe hypercholesterolemia and atherosclerosis

To investigate the effects of paternal hypercholesterolemia on offspring cardiometabolic health, 3-week-old male LDLR$^{-/-}$ mice were fed a low-fat AIN76 diet (4.3% fat) containing either 0.02% or 0.5% cholesterol for 8 weeks before mating with age matched control LDLR$^{-/-}$ female mice (159, 180) (Figure 3.1A). The HCD containing 0.5% cholesterol has been previously used to promote severe hypercholesterolemia or atherosclerosis in mice without inducing obesity and other metabolic disorders (159, 160, 178-180). Pregnant female LDLR$^{-/-}$ mice were housed separately and fed a low-cholesterol diet (LCD) containing 0.02% cholesterol after the vaginal plug was identified (embryonic day 0.5).

Consistent with our previous studies (180), LDLR$^{-/-}$ mice fed a HCD had similar body weight or growth curve and lean/fat mass as that of LCD-fed LDLR$^{-/-}$ mice (Figure 3.2, A and B). As expected, HCD feeding led to elevated serum total cholesterol levels without affecting triglyceride levels (Figure 3.1B). Lipoprotein fraction analyses showed that HCD-fed mice had significantly elevated atherogenic LDL and VLDL cholesterol levels, but similar HDL cholesterol levels as compared to LCD-fed mice (Figure 3.1C). Atherosclerotic lesions at the aortic root were then measured in those mice. As expected, HCD feeding led to larger atherosclerotic lesion sizes at the aortic root of LDLR$^{-/-}$ mice as compared with mice fed the LCD (Figure 3.1D). Thus, LDLR$^{-/-}$ mice fed with this low-

fat HCD developed severe hypercholesterolemia and large atherosclerotic lesions without increased obesity.

3.3.2 Paternal high-cholesterol diet feeding does not affect serum lipid levels and metabolic phenotypes in F1 LDL receptor-deficient offspring

F1 LDLR$^{-/-}$ litters from LCD or HCD-fed sires were weaned on postnatal day 21 and fed an LCD for 16 weeks before euthanasia at 19 weeks of age. Paternal HCD feeding did not affect the birth weight and growth curve of the F1 litters before weaning (Figure 3.3A). After weaning, both male and female offspring from HCD-fed sires also had similar growth curve and body weight as offspring from LCD-fed sires (Figure 3.3, B and C). In addition, body composition was analyzed, and paternal HCD feeding did not affect lean or fat mass of male and female offspring (Figure 3.3, D and E). There were also no changes on major organ weights between the offspring of LCD and HCD-fed sires (Figure 3.3, A and C). We also performed glucose tolerance test (GTT) in the offspring and found that paternal HCD feeding did not affect the glucose tolerance in the offspring (Figure 3.3 B and D).

We next measured the serum total cholesterol and triglyceride levels of the F1 offspring. While HCD feeding induced hypercholesterolemia in the sires, it did not affect the total cholesterol or triglyceride levels in the F1 offspring (Figure 3.4, F and G). In addition, offspring of HCD-fed sires also had similar VLDL, LDL, and HDL cholesterol levels as compared to the offspring of LCD-fed sires (Figure 3.4, H and I). Taken together, these results demonstrate that paternal HCD feeding did not affect metabolic phenotypes or serum lipid profiles in the offspring.

3.3.3 Paternal hypercholesterolemia leads to exacerbated atherosclerosis in F1 female but not male LDL receptor-deficient offspring

To investigate the impact of paternal hypercholesterolemia on atherosclerosis development in the offspring, we analyzed the atherosclerotic lesion area at the aortic root and brachiocephalic artery (BCA) of F1 $LDLR^{-/-}$ mice. Paternal HCD feeding did not significantly affect atherosclerosis development in the male offspring since F1 male $LDLR^{-/-}$ mice from HCD-fed sires had similar lesion sizes at the aortic root (63,910.06 ± 18,068.08 μm^2 vs. 83,190.78 ± 14,110.76 μm^2) and BCA (840.31 ± 397.60 μm^2 vs. 1,267.31 ± 303.04 μm^2) as compared to male offspring from LCD-fed sires (Figure 3.5, A and B). Interestingly, female offspring from HCD-fed sires developed significantly larger atherosclerotic lesions at both the aortic root (322,168.11 ± 44,583.68 μm^2 vs. 53,287.69 ± 21,105.56 μm^2) and BCA (12,388.15± 3,410.31 μm^2 vs. 3,960.33 ± 1,368.80 μm^2) as compared to female mice from LCD-fed sires (Figure 3.5, C and D).

We next evaluated the atherosclerotic plaque composition of F1 $LDLR^{-/-}$ offspring. While paternal HCD feeding did not affect the smooth muscle cell (SMC) contents in the plaques of F1 male or female offspring (Figure 3.6, A and B), paternal hypercholesterolemia led to significantly increased macrophage contents in the atherosclerotic plaques of F1 female but not male mice (Figure 3.6, C and D). We also assessed the collagen contents and necrotic cores in the atherosclerotic plaques of these mice and found that paternal HCD feeding did not affect collagen contents in male offspring but tended to increase collagen levels in female offspring (Figure 3.7, A and B).

In addition, the necrotic core sizes were not affected by paternal hypercholesterolemia in either male or female offspring (Figure 3.7, C and D).

Since inflammatory responses are the driving force of atherosclerosis development (128, 133, 161), we then analyzed the expression of key proinflammatory proteins including IL6 and MCP1 in the atherosclerotic plaques of the offspring. While MCP1 protein levels in the offspring were not affected by paternal hypercholesterolemia, paternal HCD-feeding led to significantly increased IL6 protein levels in the atherosclerotic plaques of F1 female but not male $LDLR^{-/-}$ mice (Figure 3.6, E-H). Collectively, these findings demonstrated that paternal hypercholesterolemia elicited sex-specific atherogenic effects in the offspring of $LDLR^{-/-}$ mice, which were independent of serum lipid levels.

3.3.4 Transcriptomic analysis reveals altered atherosclerosis-related gene expression in the intima of female offspring from high-cholesterol diet-fed sires

To further understand the paternal hypercholesterolemia-elicited atherogenic effects in offspring, RNAs were isolated from the intima of F1 male and female offspring for RNA sequencing (RNA-seq) analysis. RNA-seq analysis revealed that paternal HCD feeding led to 197 differentially expressed genes (DEGs) in the intima of male offspring, and most of them (164) were downregulated genes (Figure 3.8A). By contrast, paternal HCD feeding led to 147 upregulated genes but only 21 downregulated genes in the intima of female offspring (Figure 3.8B).

We then performed Gene Ontology (GO) analysis (166, 220) and the results uncovered that the upregulated genes by paternal HCD feeding in the F1 female but not male intima were enriched in several biological processes related to atherosclerosis or

inflammation including “immune system process”, “positive regulation of tumor necrosis factor production”, “neutrophil chemotaxis”, “integrin-mediated signaling pathway”, “innate immune response”, “positive regulation of phagocytosis”, and “receptor-mediated endocytosis” (Figure 3.8, C and 5D).

Functional Analysis of Individual Microarray Expression (FAIME) algorithm was then performed to evaluate the geneset scores of the GO biological process (GOBP) terms (180). FAIME results confirmed that paternal hypercholesterolemia led to significant upregulation of geneset scores of those GOBP terms associated with atherosclerosis or inflammation processes in female but not male offspring (Figure 3.9A). Consistently, the genes associated with these GOBP terms were upregulated in the intima of F1 female but not male mice from HCD-fed sires as shown in the heatmap (Figure 3.9B).

3.3.4 CCN1 and CCN2 proteins are elevated in the lesions of F1 females from high-cholesterol diet-fed sires and promote pro-atherogenic gene expression in endothelial cells in vitro

While paternal HCD feeding led to significant upregulation of some known pro-atherogenic and pro-inflammatory genes or pathways in the intima of F1 female but not male offspring, several other DEGs induced by paternal hypercholesterolemia have not been well studied. To explore novel genes or pathways that may contribute to paternal hypercholesterolemia-elicited atherogenic effects in the offspring, we investigated several candidate genes including *Ccn1* and *Ccn2*—two upregulated intimal genes in female offspring that are implicated in regulating vascular function and inflammatory responses (221-224).

We first evaluated the protein levels of CCN1 and CCN2 in the atherosclerotic plaques by immunofluorescent staining. Consistent with RNA-seq results, both CCN1 and CCN2 protein levels were significantly elevated in the atherosclerotic plaques of F1 female but not male offspring from HCD-fed sires as compared to the offspring from LCD-fed sires (Figure 3.10, A and B). Interestingly, we found that CCN1 and CCN2 proteins can be co-localized with both macrophages and endothelial cells in atherosclerotic lesions (Figure 3.11). To elucidate the potential role of CCN1 and CCN2 in regulating endothelial cell function related to atherosclerosis, we treated human endothelial cells, HMEC-1 cells (171, 180), with recombinant human CCN1 or CCN2 proteins. Interestingly, both CCN1 and CCN2 protein treatments led to increased expression of several key pro-atherogenic genes including *Vcam1*, *Icam1*, *Mcp1*, and *Il6* in HMEC-1 cells (Figure 3.12A).

To determine whether CCN1 and CCN2 can regulate endothelial cell function, we examined the impact of CCN1 and CCN2 treatment on macrophage adhesion properties to endothelial cells. Freshly isolated primary macrophages from $LDLR^{-/-}$ mice were incubated with HMEC-1 cells treated with CCN1, CCN2, or TNFα. Similar to TNFα treatment, CCN1 and CCN2 treatment increased macrophage adhesion to HMEC-1 cells (Figure 3.12B). Previous studies have demonstrated that CCN1 and CCN2 can activate NF-κB signaling in other cell types (221, 222, 225, 226). NF-κB is a master transcriptional factor that regulates immune responses and has also been shown to promote atherosclerosis development (133, 135, 161). Interestingly, we found that treatment of HMEC-1 cells with CCN1 and CCN2 led to increased phosphorylation of NF-κB p65 subunit and induction of p65 nuclear co-localization (Figure 3.13), indicative of NF-κB signaling activation. Taken

together, these results demonstrate that paternal HCD feeding leads to increased intimal expression of CCN1 and CCN2 in female offspring, which may promote endothelial cell dysfunction through NF-κB signaling pathway.

3.3.5 PANDORA-sequencing detects differentially expressed tsRNAs and rsRNAs in the sperm of hypercholesterolemic LDLR−/− male mice.

Sperm contain specific sncRNAs including tsRNAs and rsRNAs that have been reported to function as transmissible epigenetic regulators to mediate offspring's metabolic phenotypes (30, 32, 44). Many sperm tsRNAs and rsRNAs are highly modified and these RNA modifications render sncRNAs undetectable by widely used traditional RNA-seq methods. To overcome this limitation, we utilized a newly developed small RNA sequencing method, PANDORA-seq (59), which can unveil a more comprehensive tsRNA/rsRNA landscape in sperm and other tissues (59, 180).

To investigate whether exposure to HCD can elicit sncRNA changes in the sperm of $LDLR^{-/-}$ mice that may confer pro-atherogenic effects in offspring, we isolated total RNAs from sperm of LCD- and HCD-fed male $LDLR^{-/-}$ mice and conduced both traditional RNA-seq and PANDORA-seq. The sequence data were then analyzed using the *SPORTS1.1* bioinformatics tool (59, 181). Consistent with our previous results (37, 59), PANDORA-seq but not traditional RNA-seq uncovered abundant tsRNA and rsRNA populations in sperm of both LCD and HCD-fed mice (Figure 3.14A). In addition, only PANDORA-seq can detect that exposure to HCD induced differentially expressed sperm total tsRNAs and rsRNAs. We then analyzed the origins of sperm tsRNA related to their loci from tRNA precursors including 5'tsRNAs, 3'tsRNAs, 3'tsRNAs with a CCA end,

and internal tsRNAs. PANDORA-seq results showed elevated relative expression of specific genomic and mitochondrial (mt)-derived tsRNA origins (normalized to miRNAs) as compared to traditional RNA-seq results (Figure 3.14B). Interestingly, most genomic tsRNAs were derived from the 5'-end of mature tRNAs while many mitochondrial tsRNAs originated from 5'end and internal regions of tRNAs (Figure 3.14B). Overall, PANDORA-seq detected 813 differentially regulated tsRNAs and rsRNAs elicited by HCD feeding as shown in the heatmap (Figure 3.14C). Further, mapping of tsRNA and rsRNA expression patterns on selected individual tRNA or rRNA length scales including tRNA-Asp-GTC, tRNA-Ser-CGA, mt-tRNA-His-GTG, and 5.8S rRNA revealed that these tsRNAs/rsRNAs also contain distinct dynamic responses to HCD feeding (Figure 3.14, D and E, and Figure 3.15, A and B). The functions of these tsRNAs or rsRNAs as epigenetic regulators are mostly unknown, but previous studies from us and others have demonstrated that sperm sncRNA fractions enriched by tsRNAs/rsRNAs contributed to the epigenetic inheritance of paternally acquired metabolic disorder through zygotic injection (30, 31, 80, 227, 228). Thus, it is plausible that these altered tsRNAs or rsRNAs contribute to paternal hypercholesterolemia-induced intergenerational atherogenic effects.

3.3.6 Exposure to high-cholesterol diet alters sncRNA biogenesis-related genes in the epididymis

The biogenesis of sperm sncRNAs including tsRNAs mainly occurs in the epididymis rather than testis (32, 43, 75). To determine whether changes in the sperm sncRNA profile from HCD-fed LDLR$^{-/-}$ mice are due to altered tsRNA/rsRNA biogenesis in the epididymis, we examined the expression of sncRNA biogenesis-related genes in the

testis, caput and cauda epididymis (Figure 3.16A). HCD feeding did not significantly affect the expression of sncRNA biogenesis-related genes in the testis or caput epididymis (Figure 3.16, B and C). Interestingly, exposure to HCD led to increased expression of several key sncRNA biogenesis-related genes inducing tsRNA cleavage enzymes *Ang*, *Rnasel*, and *Rnaset2* and RNA modification enzymes *Mettl3* in the cauda epididymis (Figure 3.16D). There results indicate that hypercholesterolemia affects tsRNA/rsRNA biogenesis-related gene expression in the epididymis (primarily in the cauda), leading to the altered sperm sncRNA landscape.

3.3.7 Hypercholesterolemia-stimulated sperm tsRNAs/rsRNAs induce early transcription changes in murine embryoid bodies

We previously demonstrated that tsRNAs and rsRNAs can affect murine embryonic stem cell (mESC) differentiation and embryoid body (EB) transcriptome (59). To explore the potential functions of the dysregulated sperm tsRNAs/rsRNAs, we transfected a pool of selected tsRNAs and rsRNAs including tsRNA-Glu-CTC/TTC, mt-tsRNA-His-GTG, rsRNA-18S, and two rsRNAs derived from rRNA-28S that were stimulated by HCD feeding into mESCs followed EB formation. Interestingly, we found that transfection of these tsRNAs/rsRNAs led to significantly increased expression of several pro-atherogenic or endothelial dysfunction-related genes including Endothelin (*End1*), E-selectin (*Sele*), and *Il1b* (Figure 3.17). In addition, the expression levels of *Sox17*, a key transcription factor regulating cardiovascular development and endoderm differentiation (229, 230), was also elevated by transfection of those tsRNAs/rsRNAs (Figure 3.17). Thus, HCD feeding-

stimulated sperm tsRNAs and rsRNAs may have adverse effects on offspring cardiovascular development or atherogenesis.

3.4 Discussion

Increasing lines of evidence demonstrates that parental exposure-acquired diseased phenotypes can be encoded in the germline epigenome and transmitted to future generations, leading to adverse health outcomes (217, 231-234). While many studies have investigated the adverse effects of maternal exposures to suboptimal factors on offspring cardiometabolic health, little is known about the contribution of paternal factors to CVD risk in offspring. In the current study, we investigated the effects of paternal HCD feeding on offspring atherosclerosis development in LDLR$^{-/-}$ mice (Figure 3.18). We found that paternal hypercholesterolemia significantly increased atherosclerosis in F1 female but not male LDLR$^{-/-}$ mice. Interestingly, paternal hypercholesterolemia-elicited sex-specific atherogenic effects in the offspring were independent of serum lipid levels or metabolic dysfunction. RNA-seq analysis then revealed that paternal hypercholesterolemia can lead to upregulation of many known pro-atherogenic genes or pathways in the intima of F1 female mice. We then identified two potentially novel pro-atherogenic genes, *Ccn1* and *Ccn2*, that may contribute to increased atherosclerosis development in female F1 LDLR$^{-/-}$ mice by regulating pro-atherogenic gene expression in endothelial cells. Using the innovative PANDORA-seq method, we revealed that HCD feeding can alter the sperm tsRNA and rsRNA landscape, which may contribute to paternally acquired atherosclerosis in offspring. We also discovered that exposure to HCD alters sncRNA biogenesis-related

genes in the epididymis but not testis, which may lead to the altered sperm sncRNA landscape. Although the exact mechanism through which sperm tsRNAs and rsRNAs mediate paternally acquired atherosclerosis in offspring remain elusive, we found that hypercholesterolemia-stimulated sperm tsRNAs and rsRNAs can induce early transcription changes in murine embryoid bodies. Several pro-atherogenic or endothelial dysfunction-related genes were upregulated by these tsRNAs/rsRNAs in EBs, which may lead to adverse effects on cardiovascular development or increased atherosclerosis in the offspring. Our study demonstrated that paternal dietary exposure could elicit sex-specific intergenerational atherosclerosis in offspring using appropriate animal models.

Human longitudinal studies, such as the Framingham Offspring Study have suggested that the presence of parental CVD risk factors can lead to increased CVD in offspring (20, 21, 23). Moreover, clinical and animal studies have demonstrated that maternal exposures to suboptimal environmental factors such as unhealthy diets and toxicants may lead to CVD complications including hypertension (213, 235, 236), increased intima-media thickness (237, 238), altered lipid profile (239), and increased atherosclerosis (24, 25, 29, 214) in offspring. In addition to maternal influences, offspring CVD can be closely associated with paternal CVD risk factors in humans (21-23, 206). However, very limited studies have investigated paternal exposure-elicited cardiometabolic disease risk in animal models. Further, most of the paternal studies including our previous ones have focused on the intergenerational transmission of paternally acquired metabolic disorders but not CVD (30-32, 36, 37, 80, 209, 216, 217, 240). In the current study, we utilized the widely used atherosclerosis prone LDLR$^{-/-}$

mouse model to investigate the impact of paternal HCD feeding on offspring atherosclerosis development. We report that paternal hypercholesterolemia can lead to increased atherosclerosis development and intimal pro-atherogenic gene expression in female LDLR$^{-/-}$ descendants, demonstrating the atherogenic effects of paternal unhealthy diet exposure in offspring.

It is intriguing that paternal hypercholesterolemia can lead to increased atherosclerosis in female but not male offspring in LDLR$^{-/-}$ mice. Parental exposure-elicited sex-specific effects on offspring cardiometabolic health have been reported in both human and animal studies (206, 241). For example, human studies suggest that maternal undernutrition may lead to increased adiposity and body weight in middle-aged female but not male descendants (241, 242). In animal studies, maternal hypercholesterolemia also led to early atherosclerosis development in female but not male offspring in apolipoprotein E-deficient (29, 214) and circulating lipid levels were unlikely to be the main factor contributing to accelerated atherosclerosis development in the offspring. An earlier study in rats claimed that F1 female but not male offspring from HFD-fed sires had glucose tolerance impairment (209). A very recent report showed that paternal HFD feeding in mice led to increased metabolic disorders in male offspring, but female offspring were not included in the study (45). We also demonstrated that paternal exposure to a plastic-associated EDC, dicyclohexyl phthalate elicited sex-specific transgenerational effects in F2 offspring in mice (37). Interestingly, paternal EDC exposure induced glucose intolerance in F2 female but not male descendants (37). The mechanisms responsible for sex differences in the intergenerational inheritance of metabolic phenotypes remain largely

unknown. Several potential mechanisms related to sex hormones (216, 241, 243, 244), sex chromosomes (17, 245), mitochondrial function (246, 247), or developmental epigenetic reprogramming (241) have been suggested. Further, the sex-difference in offspring phenotype may also derived from the different sperm RNA information carried in X versus Y sperm (248), with mechanisms remain unknown. Sexual dimorphic responses to early life perturbations, from either ancestral side remain an important but understudied research topic. Future studies are required to understand the detailed mechanisms for sex differences in the intergenerational transmission of paternally acquired cardiometabolic phenotypes.

In addition to known pro-atherogenic genes, our RNA-seq analysis identified two potentially new pro-atherogenic genes, *Ccn1* and *Ccn2*, that may contribute to increased atherosclerosis in F1 females. CCN1 and CCN2 are matricellular proteins that are essential for cardiovascular development during embryogenesis (221, 222, 249, 250). The expression of these genes is reduced later in life and can be increased in atherosclerotic plaques of both human and rodents (221-224, 251, 252). We found that CCN1 and CCN2 can be co-localized with both endothelial cells and macrophages within atherosclerotic lesions. The function of CCNs in macrophages have been previously reported (253, 254), but their role in endothelial cell biology remains unclear. We then discovered that CCN1 and CCN2 proteins can activate NF-κB signalling and stimulate pro-atherogenic gene expression in endothelial cells in vitro. Thus, it is plausible that the increased endothelial *Ccn1/Ccn2* expression may affect other cell types such as macrophages to contribute to the exacerbated atherosclerosis in F1 female mice from HCD-fed sires.

Emerging evidence supports the notion that the paternal environment can influence offspring health, but the underlying molecular mechanisms remains largely unknow. Recent studies by us and others have demonstrated that environmental exposures including unhealthy diet, environmental toxicants, and stress, can alter the sperm RNAs to mediate intergenerational inheritance (30, 31, 37, 45, 80, 255-259). We previously discovered that mouse sperm is enriched with a subset of sncRNAs including tsRNAs and rsRNAs that contribute significantly to intergenerational inheritance of paternally acquired metabolic disorders (30-32, 43, 44, 71). The injection of sperm total RNAs or tsRNA/rsRNA-enriched RNA fractions from HFD-exposed sires can induce offspring phenotypes that fully or partially recapitulated the paternal environmental input, including obesity and altered glucose metabolism (30, 31), thus demonstrating that sperm RNAs have causal effects in mediating intergenerational inheritance in mammals. Many sperm tsRNAs/rsRNAs are highly modified and these RNA modifications may shape the RNA secondary structures and biological properties to mediate epigenetic inheritance (31, 43, 61). While RNA modifications are essential for the functions of sncRNAs such as tsRNAs (43, 260, 261), these modifications can also interfere with either reverse transcription or adaptor ligation process when constructing cDNA library for RNA-seq analysis, thereby limiting the sncRNA detection capacity of the traditional RNA-seq method. To address this obstacle, we utilized the PANDORA-seq method which enabled us to identify highly modified sncRNAs that are otherwise undetectable by traditional RNA-seq (59, 146). In the current study, PANDORA-seq revealed abundant tsRNA/rsRNA expression in the sperm of $LDLR^{-/-}$ mice as compared to traditional RNA-seq results. These results were

consistent with our recent results demonstrating that these understudied tsRNAs/rsRNAs are much more abundant than the well-studied miRNAs across many human and murine tissues or cells including sperm (37, 59, 180, 260, 261). Interestingly, HCD-feeding also led to upregulation of sperm mitochondrial tsRNAs (mt-tsRNAs) that have recently been linked to mitochondrial dysfunction in HFD-fed mice and obese humans (45, 262). These sperm sncRNAs have also been shown to affect altered early-embryo transcription which may lead to offspring metabolic disorders (45). Therefore, the sperm nuclear and mitochondrial-derived sncRNAs could act as potentially key factors in mediating paternal hypercholesterolemia-elicited atherosclerosis in offspring.

To explore how the altered sperm sncRNAs may affect offspring cardiovascular heath, we investigated the impact of a pool of sperm tsRNA/rsRNA on murine EB transcription changes. We and others have demonstrated that tsRNAs/rsRNAs including sperm mt-tsRNAs can affect EB or early-embryo transcription (45, 59). Therefore, we also included HCD-stimulate sperm mt-tsRNAs in our assays. Interestingly, we found that overexpression of these sperm tsRNAs/rsRNAs including sperm mt-tsRNA led to increased expression of pro-atherogenic genes such as *End1*, *Sel4* and *Il1b* in murine EBs. While IL-1β has been well-established to promote atherosclerosis, END1 and SELE are markers for endothelial dysfunction and may also contribute to the development of CVD (263-266). In addition, the expression levels of *Sox17* were also elevated by overexpression of those tsRNAs/rsRNAs. Sox17, an essential factor controlling endothelial and hematopoietic cell lineages (229, 230), also plays an important role in regulating endothelial cell function and can be upregulated in response to endothelial dysfunction

(229). It is plausible that tsRNAs/rsRNAs-elicited early transcription changes in EBs lead to adverse effects on of the increased expression of pro-atherogenic genes causing adverse effects on atherogenesis later in life. Future studies are needed to investigate the functions and detailed mechanisms of these tsRNAs/rsRNAs in mediating HCD feeding-induced intergenerational atherosclerosis risk.

It is interesting that HCD feeding can alter the sperm tsRNA/rsRNA landscape. The biogenesis of sperm sncRNAs including tsRNAs mainly occurs in the epididymis (32, 43, 75). Epididymal but not testicular sperm sncRNAs are also more susceptible to unhealthy diet exposures (45). While the mechanisms underlying the diet-induced sperm sncRNA changes remain unknow, it is possible that dietary changes altered the levels or activities of related enzymes for RNA modifications and cleavage enzymes, leading to altered tsRNA/rsRNA biogenesis. We found that HCD feeding mainly affects the expression of RNA biogenesis-related genes in cauda epididymis but not in testis and caput epididymis. Specifically, exposure to HCD led to significantly increased expression of cleavage enzymes *Ang*, *Rnasel* and *Rnaset2*, and modification enzymes *Mettl3* in cauda epididymis. *Ang*, *Rnasel* and *Rnaset2* are ribonucleases that cleave tRNAs into tsRNAs, have been shown to alter the sperm tsRNA/rsRNA composition (62, 80). *Ang* has also been well-documented to be induced under various stress conditions including inflammation (80, 267). *Mettl3* is a m^6A methyltransferase that can also regulate RNA translation and many biological processes (268). It is plausible that the high cholesterol environment affects the expression levels or activities of these enzymes to modulate sperm sncRNA biogenesis in the epididymis, leading to an altered "sperm RNA code" that impacts offspring health (32,

44, 55). Future studies are required to study the detailed mechanism through which consumption of unhealthy diets affects sperm tsRNA/rsRNA biogenesis to mediate intergenerational transmission of paternally acquired CVD and other chronic diseases.

In summary, we investigated the impact of paternal hypercholesterolemia on offspring atherosclerosis development in $LDLR^{-/-}$ mice and revealed that paternal hypercholesterolemia induced sex-specific atherogenic effects in $LDLR^{-/-}$ offspring. Paternal HCD feeding led to significantly increased atherosclerosis in F1 female but not male $LDLR^{-/-}$ mice. The increased atherosclerosis in female offspring was also corelated with elevated pro-atherogenic gene expression in the intima. PANDORA-seq then uncovered that HCD feeding can lead to altered sperm tsRNA and rsRNA profiles, which could be key contributing factors that convey intergenerational transmission of paternally acquired atherosclerosis in offspring. The altered sperm sncRNA profiles were probably due to HCD-elicited changes in epididymal RNA modification and cleavage enzymes. Lastly, hypercholesterolemia-stimulated sperm tsRNAs and rsRNAs can induce early transcription changes of cardiovascular development and atherosclerosis-related genes in murine EBs. Our findings will hopefully stimulate further investigations of the impact of parental exposures on offspring cardiovascular health and the underlying mechanisms of parentally acquired CVD and other chronic diseases.

3.5 Figures and Tables

Table 3.1. Primer Sequences used for QPCR

Genes	Primer sequences	Genes	Primer sequences
hGAPDH	5'- GGCCTCCAAGGAGTAAGACC-3'	hIL-1β	5'- CGCCAATGACTCAGAGGAAGA-3'
	5'- AGGGGAGATTCAGTGTGGTG-3'		5'- AGGGCGTCATTCAGGATGAA-3'
hMCP-1	5'- GATGCAATCAATGCCCCAGTC-3'	hICAM-1	5'- ATGCCCAGACATCTGTGTCC-3'
	5'- TCCTTGGCCACAATGGTCTT-3'		5'- GGGGTCTCTATGCCCAACAA-3'
hIL-6	5'- GGTACATCCTCGACGGCATCT-3'	hVCAM-1	5'- TTTGACAGGCTGGAGATAGACT-3'
	5'- GTGCCTCTTTGCTGCTTTCAC-3'		5'- TCAATGTGTAATTTAGCTCGGCA-3'
mGAPDH	5'-AACTTTGGCATTGTGGAAGG-3'	mALKBH3	5'-GCCAGGTAGCCATCCCTT-3'
	5'-GGATGCAGGGATGATGTTCT-3'		5'-AGGGGAAGCTGGCTGAGT-3'
mDNMT2	5'-AGCCTGTGGCTTTCAGTATCA-3'	mRNase L	5'-TAGGCGAACACATCAATGAGGA-3'
	5'-TTGGCTGACTTTCTTCAACTACTGC-3'		5'-CTGCCTCTGGAACGCTGAG-3'
mNSUN2	5'-TTGGACGACGACGAGGA-3'	mRNase T2	5'-ACTATGGCCCGATAGAGCAGA-3'
	5'-CCATTCTCCTCTAGCGAACATG-3'		5'-ATTGGCTGCGATTAGAAGACC-3'
mMETTL3	5'-CAGTGCTACAGGATGACGGCTT-3'	mDICER1	5'-GGTCCTTTCTTTGGACTGCCA-3'
	5'-CCGTCCTAATGATGCGCTGCAG-3'		5'-GCGATGAACGTCTTCCCTGA-3'
mADAR1	5'-TGAGCATAGCAAGTGGAGATACC-3'	mANG	5'-CATCCCAACAGGAAGGAAGGA-3'
	5'-GCCGCCCTTTGAGAAACTCT-3'		5'-ACCTGGAGTCATCCTGAGCC-3'
mALKBH1	5'-AAGCGAAGACCCCGAAGTTTA-3'	mBMP4	5'-TTCCTGGTAACCGAATGCTGA-3'
	5'-CAGTGGCGACTTGCTCTGA-3'		5'-CCTGAATCTCGGCGACTTTTT-3'
mSox17	5'-GATGCGGGATACGCCAGTG-3'	mID1	5'-CCTAGCTGTTCGCTGAAGGC-3'
	5'-CCACCACCTCGCCTTTCAC-3'		5'-CTCCGACAGACCAAGTACCAC-3'
mIL-1β	5'-TTCAGGCAGGCAGTATCACTC-3'	mTMEM1000	5'-GACAATGGAGAAAAACCCCAAGA-3'
	5'-GAAGGTCCACGGGAAAGACAC-3'		5'-GGTAGCAGGAGAGTTCGGC-3'
mE-Selectin	5'-ATGCCTCGCGCTTTCTCTC-3'	mTGFB1	5'-CCACCTGCAAGACCATCGAC-3'
	5'-GTAGTCCCGCTGACAGTATGC-3'		5'-CTGGCGAGCCTTAGTTTGGAC-3'
mEndothelin	5'-GCACCGGAGCTGAGAATGG-3'		
	5'-GTGGCAGAAGTAGACACACTC-3'		

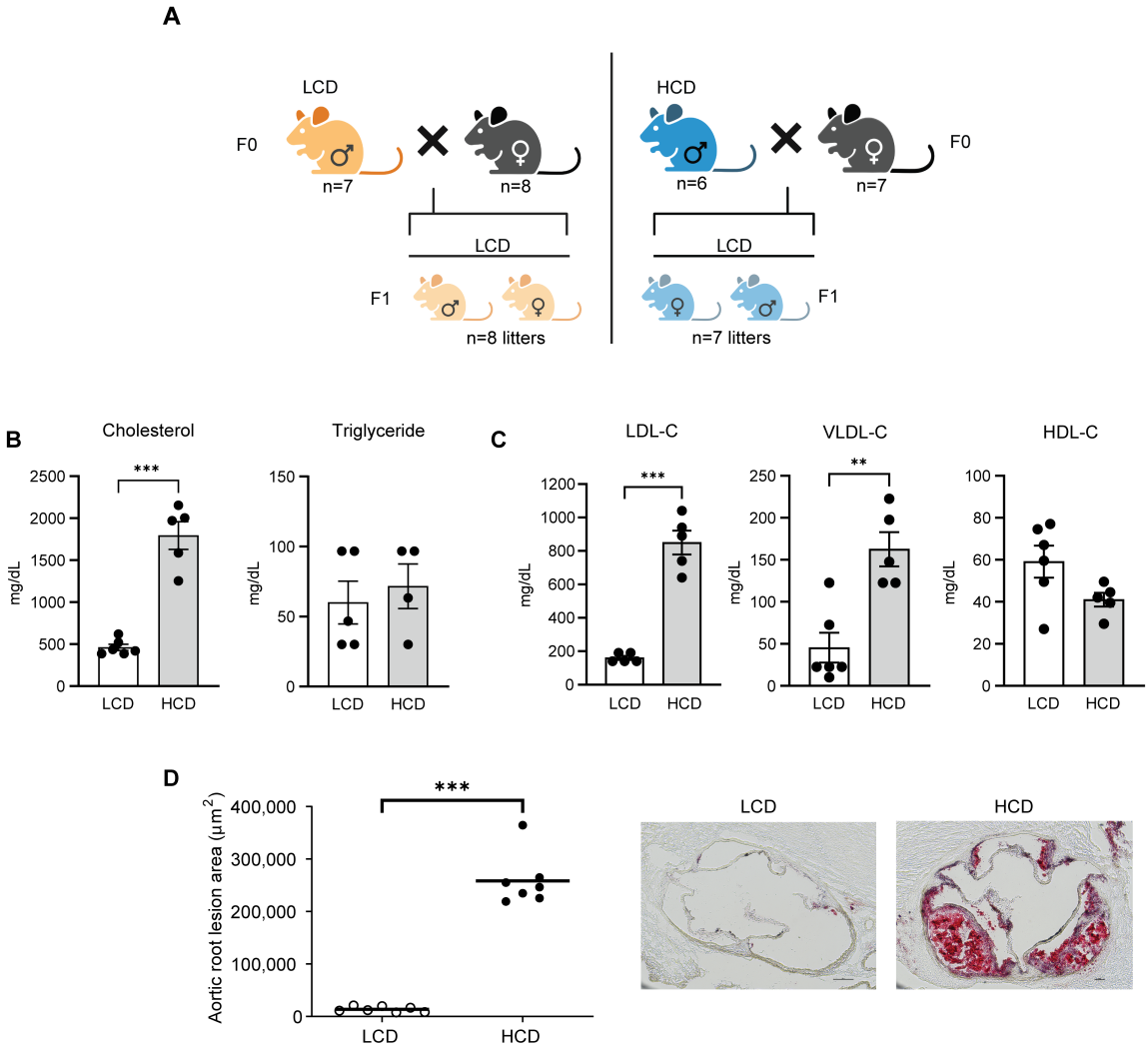
A
LCD
HCD
F0
n=7
n=8
n=6
n=7
F0
LCD
LCD
F1
F1
n=8 litters
n=7 litters
B
Cholesterol
Triglyceride
mg/dL
***
LCD
HCD
C
LDL-C
VLDL-C
HDL-C
**
D
Aortic root lesion area (μm²)
400,000
300,000
200,000
100,000
0
LCD
HCD

Figure 3.1. Male LDL receptor deficient mice fed a low-fat, high-cholesterol diet develop severe hypercholesterolemia-mediated atherosclerosis.

Three-week-old male $LDLR^{-/-}$ mice were fed a low-cholesterol diet (LCD, 0.02% cholesterol) or high-cholesterol diet (HCD, 0.5% cholesterol) for 8 weeks before mating with female $LDLR^{-/-}$ mice. The F1 offspring were weaned at 3-week-old and were fed an LCD for 16 weeks. (A) Schematic representation of experimental design and generation of F1 offspring. (B) Serum total cholesterol and triglyceride levels were measured (n=4-6, ***P<0.001, two-sample, two tailed Student's t-test). (C) Lipoprotein fractions (VLDL-C, LDL-C, and HDL-C) were isolated from serum, and the cholesterol levels of each fraction were measured (n=5-6, **P<0.01, ***P<0.001; two-sample, two tailed Student's t-test). (D) Quantitative analysis of the lesion area in the aortic root of LCD and HCD-fed $LDLR^{-/-}$ mice (n=7, ***P<0.05, two-sample, two tailed Student's t-test). Representative images are shown to the right. VLDL-C, very low-density lipoprotein cholesterol; LDL-C, low density lipoprotein cholesterol; HDL-C, high density lipoprotein cholesterol. All data are plotted as means ± S.E.M.

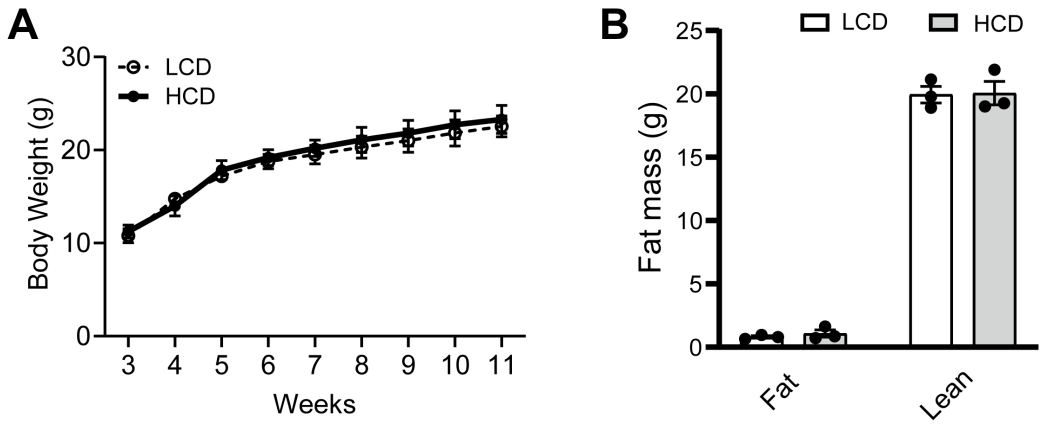

Figure 3.2. High-cholesterol diet feeding does not affect body weight and adiposity in LDLR$^{-/-}$ mice.

Three-week-old male LDLR$^{-/-}$ mice were fed an LCD or HCD for 9 weeks. (A) Growth curves were measured (n=5-6, two-way *ANOVA* followed by Bonferroni's multiple comparison test). (B) Body composition of LDLR$^{-/-}$ mice fed an LCD or HCD were measured (n=3, two-sample, two tailed Student's t-test). All data are plotted as means ± S.E.M.

F1 Males

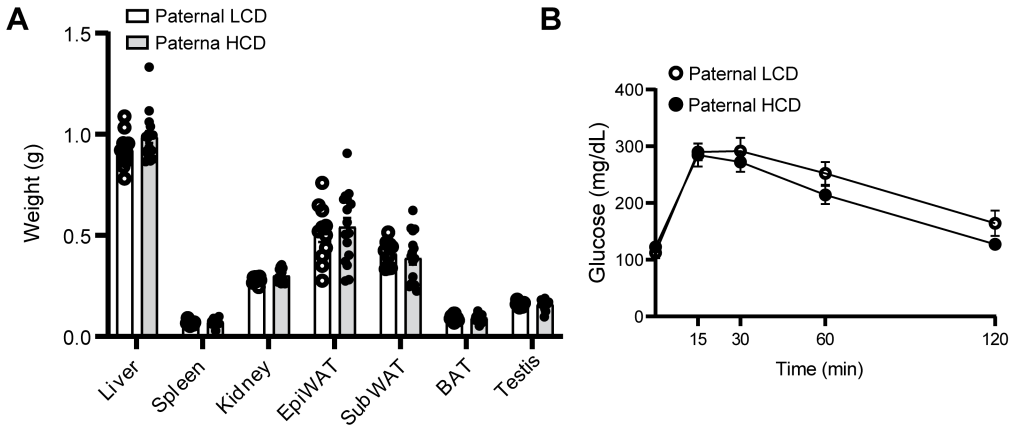

F1 Females

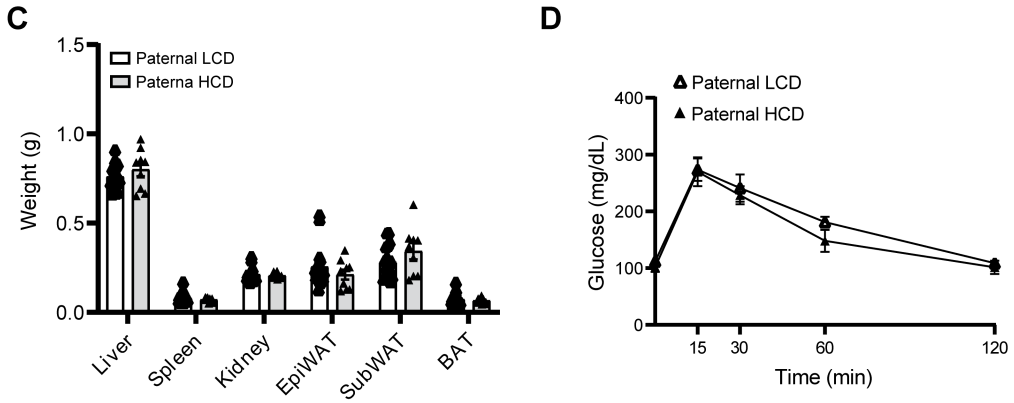

Figure 3.3. Paternal hypercholesterolemia does not affect organ weight or glucose tolerance tests in F1 LDLR$^{-/-}$ offspring.

Three-week-old male LDLR$^{-/-}$ mice were fed an LCD or HCD diet for 8 weeks before mating with female LDLR$^{-/-}$ mice. Three-week-old F1 offspring were fed an LCD for 16 weeks and euthanized at 19 weeks of age. Major organ weights (A and C) of male and female offspring were measured (n=9-18, *P<0.05, two-sample, two tailed Student's t-test). (B and D) Intraperitoneal glucose tolerance test (IPGTT) of male and female offspring was performed (n=8-10, two-way *ANOVA* followed by Bonferroni's multiple comparison test). All data are plotted as means ± S.E.M.

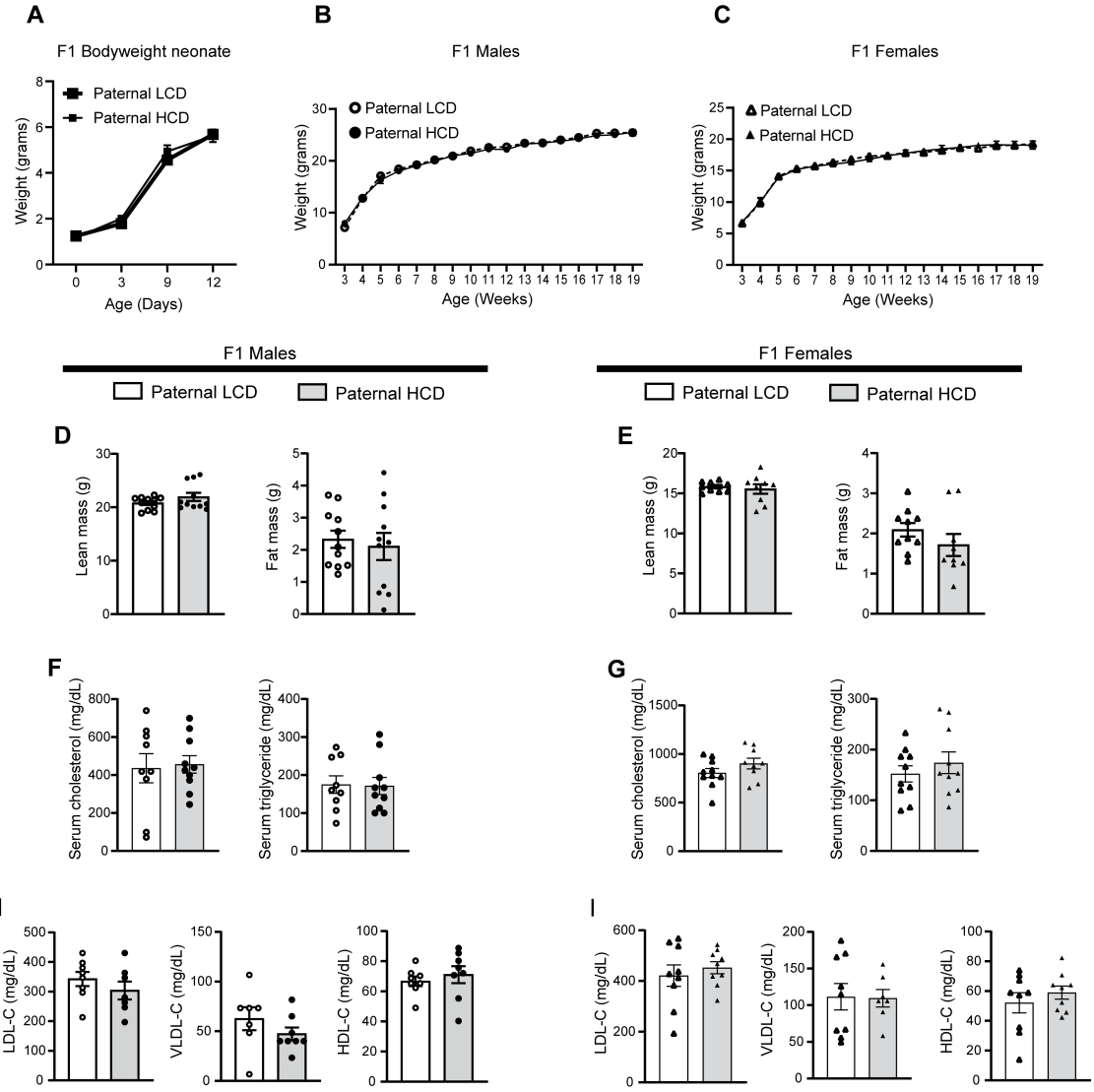
A
F1 Bodyweight neonate
Paternal LCD
Paternal HCD
Weight (grams)
Age (Days)
B
F1 Males
Paternal LCD
Paternal HCD
Weight (grams)
Age (Weeks)
C
F1 Females
Paternal LCD
Paternal HCD
Weight (grams)
Age (Weeks)
F1 Males
Paternal LCD
Paternal HCD
F1 Females
Paternal LCD
Paternal HCD
D
Lean mass (g)
Fat mass (g)
E
Lean mass (g)
Fat mass (g)
F
Serum cholesterol (mg/dL)
Serum triglyceride (mg/dL)
G
Serum cholesterol (mg/dL)
Serum triglyceride (mg/dL)
H
LDL-C (mg/dL)
VLDL-C (mg/dL)
HDL-C (mg/dL)
I
LDL-C (mg/dL)
VLDL-C (mg/dL)
HDL-C (mg/dL)

Figure 3.4. Paternal high-cholesterol diet feeding does not affect body weight and serum lipid levels in F1 offspring.

Three-week-old male LDLR$^{-/-}$ mice were fed an LCD or HCD diet for 8 weeks before mating with control female LDLR$^{-/-}$ mice. Three-week-old F1 offspring were fed an LCD for 16 weeks and euthanized at 19-weeks of age. (A) Birth weight (Day 0) and body weight of F1 pups before weaning (n=5; two-way ANOVA followed by Bonferroni's multiple comparison test). (B and C) Growth curves of male (B) and female (C) F1 offspring were measured (n = 9–14; two-way ANOVA followed by Bonferroni's multiple comparison test). (D and E) Lean and fat mass were measure in male (D) and female (E) F1 offspring (n=9-11, two-sample, two tailed Student's t-test). (F and G) Serum cholesterol and triglyceride levels were measured in male and female offspring (n=9-10, two-sample, two tailed Student's t-test). (H and I) Serum lipoprotein fractions (VLDL-C, LDL-C, and HDL-C) were isolated from male (H) and female (I) F1 offspring and cholesterol levels from each fraction were measured (n=7-9, two-sample, two tailed Student's t-test). VLDL-C, very low-density lipoprotein cholesterol; LDL-C, low density lipoprotein cholesterol; HDL-C, high density lipoprotein cholesterol. All data are plotted as means ± S.E.M.

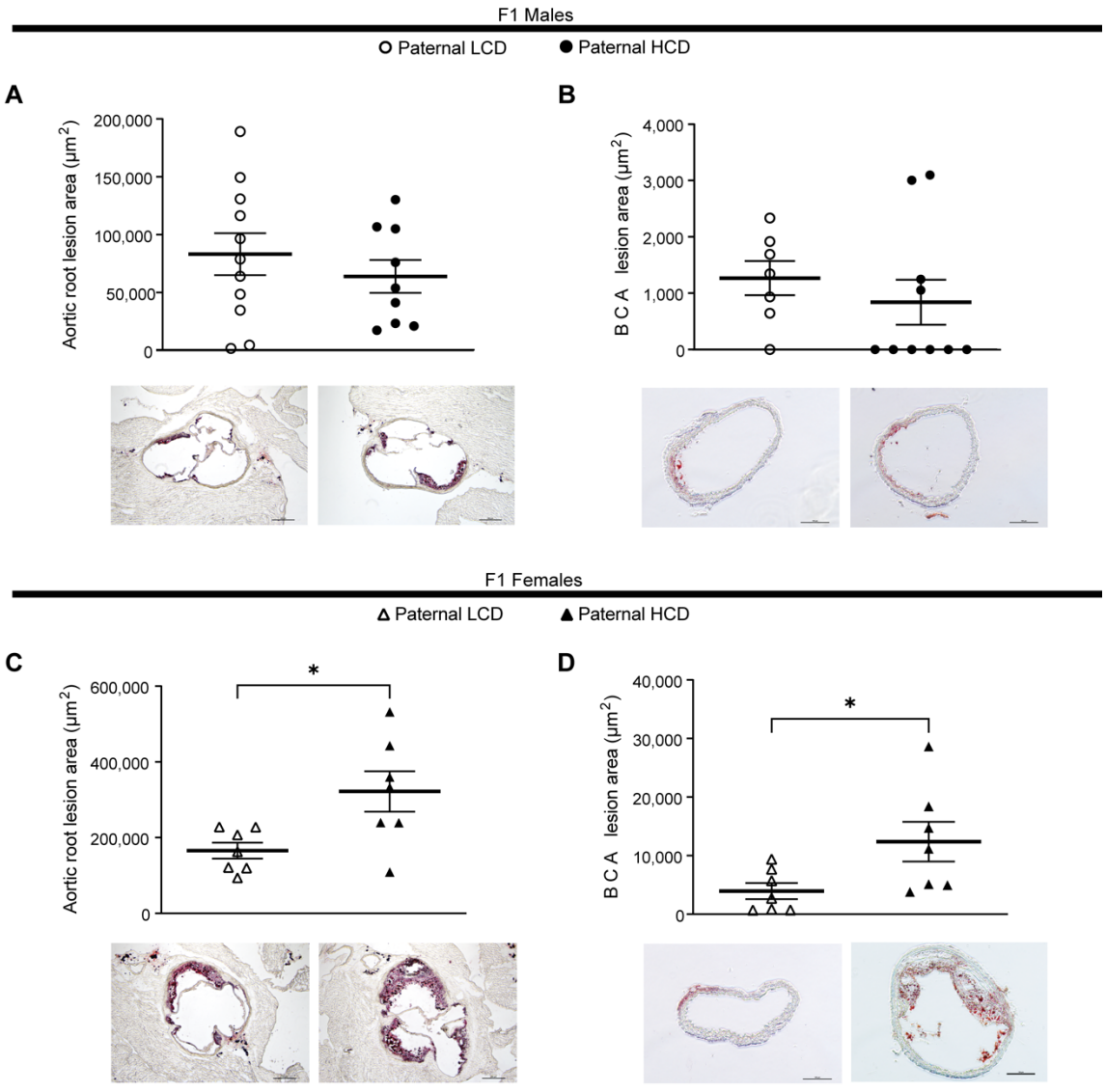
F1 Males
Paternal LCD
Paternal HCD
A
Aortic root lesion area (μm2)
200,000
150,000
100,000
50,000
0
B
B C A lesion area (μm2)
4,000
3,000
2,000
1,000
0
F1 Females
Paternal LCD
Paternal HCD
C
Aortic root lesion area (μm2)
600,000
400,000
200,000
0
*
D
B C A lesion area (μm2)
40,000
30,000
20,000
10,000
0
*

Figure 3.5. Paternal hypercholesterolemia increases atherosclerosis development in F1 female LDL receptor-deficient offspring.

Three-week-old male $LDLR^{-/-}$ mice were fed an LCD or HCD diet for 8 weeks before mating with control female $LDLR^{-/-}$ mice. Three-week-old F1 descendants were fed an LCD for 16 weeks. (A-D) Quantitative analysis of the lesion area at the aortic root (A and C) or brachiocephalic artery (B and D) of male (A and B) and female (C and D) offspring (n=7-11, *P<0.05, two-sample, two tailed Student's t-test). Representative oil red O-stained sections displayed below the quantification data (scale bar = 200μm). All data are plotted as means ± S.E.M.

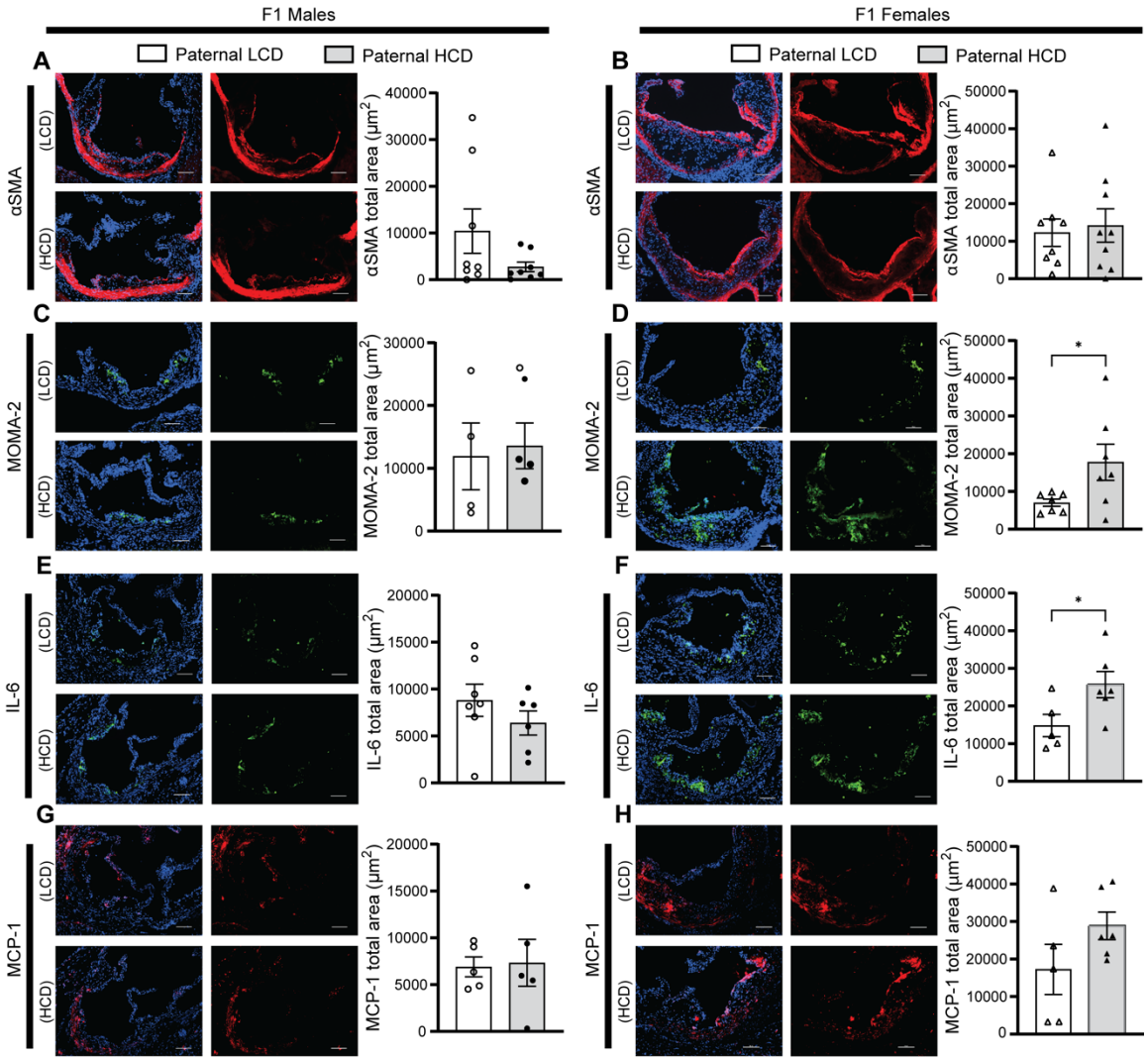
F1 Males
F1 Females
Paternal LCD
Paternal HCD
A
B
C
D
E
F
G
H
αSMA
MOMA-2
IL-6
MCP-1
(LCD)
(HCD)
αSMA total area (μm²)
MOMA-2 total area (μm²)
IL-6 total area (μm²)
MCP-1 total area (μm²)
*

Figure 3.6. Paternal high-cholesterol diet feeding elicits macrophage accumulation and inflammation in atherosclerotic plaques of F1 offspring.

Three-week-old male LDLR$^{-/-}$ mice were fed an LCD or HCD diet for 8 weeks before mating with control female LDLR$^{-/-}$ mice. Three-week-old F1 descendants were fed an LCD for 16 weeks (A-H) Representative images of immunofluorescence staining of αSMA (A and B), MOMA-2 (C and D), IL-6 (E and F), and MCP-1 (G and H) at the aortic root of male and female offspring (scale bar=100μm). The nuclei were stained with DAPI (blue). Quantification analysis of staining areas is displayed as indicated (n=4-9, *P<0.05, two-sample, two tailed Student's t-test). All data are plotted as means ± S.E.M.

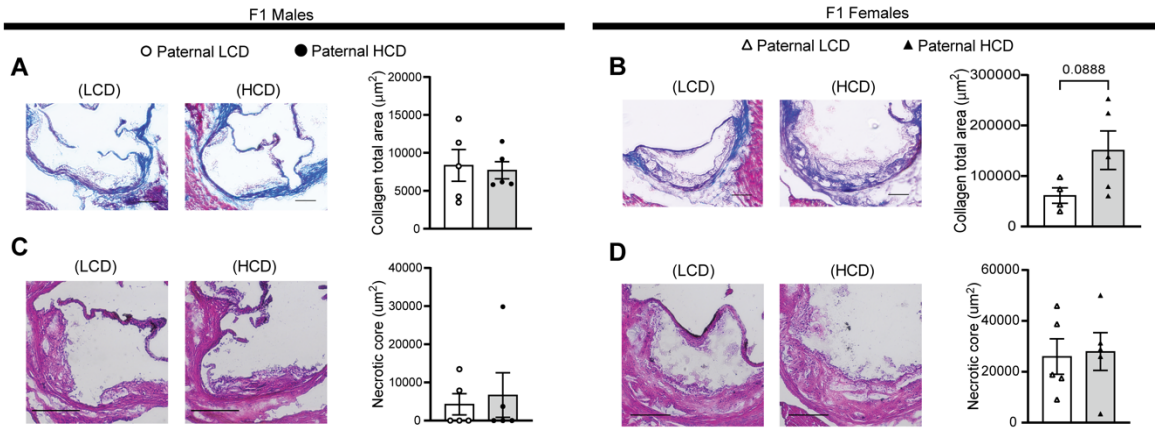

Figure 3.7. Paternal high cholesterol diet does not affect collagen production or necrotic core formation in the aortic root of F1 offspring.

Three-week-old male C57BL/6 LDLR$^{-/-}$ littermates were fed an LCD or HCD diet for 8 weeks before mating with female LDLR$^{-/-}$ mice. Three-week-old F1 offspring were fed a LCD for 16 weeks and euthanized at 19-weeks of age. (A and B) Masson's Trichrome stain was used to measure the collagen content at the aortic root of male (A) and female (B) offspring. Representative images are shown to the left of each data set (scale bar=100µm). (C and D) Hematoxylin and eosin staining was used for analyzing the necrotic core at the aortic root of male (C) and female (D) offspring. Representative images are shown to the left of each data set (scale bar=200µm). Statistical significance was determined by independent t-test. All data are plotted as means ± S.E.M. (n=4-5).

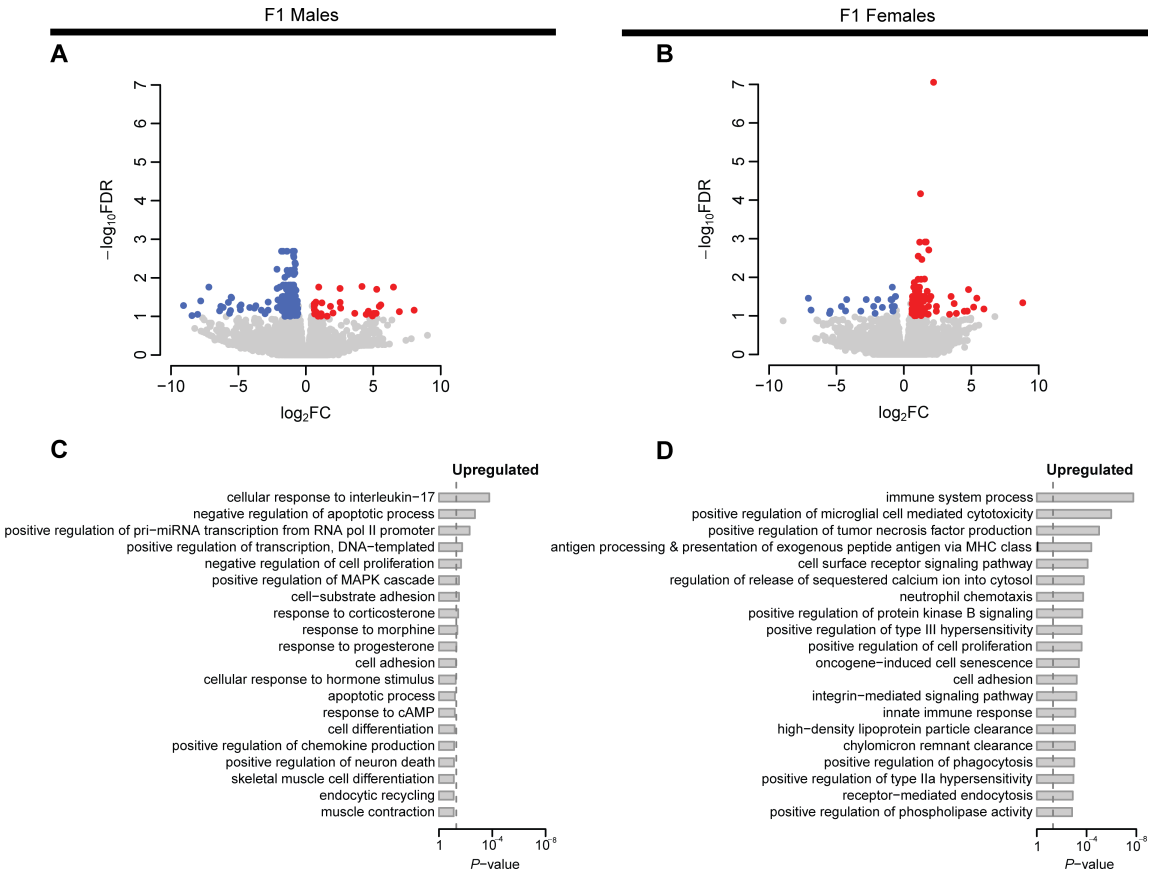
F1 Males
F1 Females
A
B
C
D
−log10FDR
log2FC
Upregulated
cellular response to interleukin−17
negative regulation of apoptotic process
positive regulation of pri−miRNA transcription from RNA pol II promoter
positive regulation of transcription, DNA−templated
negative regulation of cell proliferation
positive regulation of MAPK cascade
cell−substrate adhesion
response to corticosterone
response to morphine
response to progesterone
cell adhesion
cellular response to hormone stimulus
apoptotic process
response to cAMP
cell differentiation
positive regulation of chemokine production
positive regulation of neuron death
skeletal muscle cell differentiation
endocytic recycling
muscle contraction
P−value
immune system process
positive regulation of microglial cell mediated cytotoxicity
positive regulation of tumor necrosis factor production
antigen processing & presentation of exogenous peptide antigen via MHC class
cell surface receptor signaling pathway
regulation of release of sequestered calcium ion into cytosol
neutrophil chemotaxis
positive regulation of protein kinase B signaling
positive regulation of type III hypersensitivity
positive regulation of cell proliferation
oncogene−induced cell senescence
cell adhesion
integrin−mediated signaling pathway
innate immune response
high−density lipoprotein particle clearance
chylomicron remnant clearance
positive regulation of phagocytosis
positive regulation of type IIa hypersensitivity
receptor−mediated endocytosis
positive regulation of phospholipase activity

Figure 3.8. Paternal hypercholesterolemia elicits transcriptomic changes in the intima of F1 LDL receptor-deficient mice.

Three-week-old male $LDLR^{-/-}$ mice were fed an LCD or HCD diet for 8 weeks before mating with control female $LDLR^{-/-}$ mice. Three-week-old F1 descendants were fed a LCD for 16 weeks. Total RNAs were isolated from the intima of F1 offspring and used for RNA-seq analysis. (A and B) Volcano plot of differentially expressed genes (DEGs) in the intima of male offspring (A) and female offspring (B) from HCD-fed $LDLR^{-/-}$ sires. Colored dots represent the enriched (red dots) or depleted (blue dots) DEGs with a false discovery rate (FDR) of < 0.1 and a fold change (FC) > 1.5 as a cut-off threshold. (C and D) Gene Ontology Biological Process (GOBP) terms significantly associated with upregulated DEGs in intima of male offspring (C) and female offspring (D) from HCD-fed sires. The P-values were computed by the modified Fisher's exact test using the DAVID bioinformatics tool. The vertical dash line indicates the significance level of $\alpha = 0.05$. The y-axis displays the GOBP terms while the x-axis displays the P-values. (n = 4-7 each group).

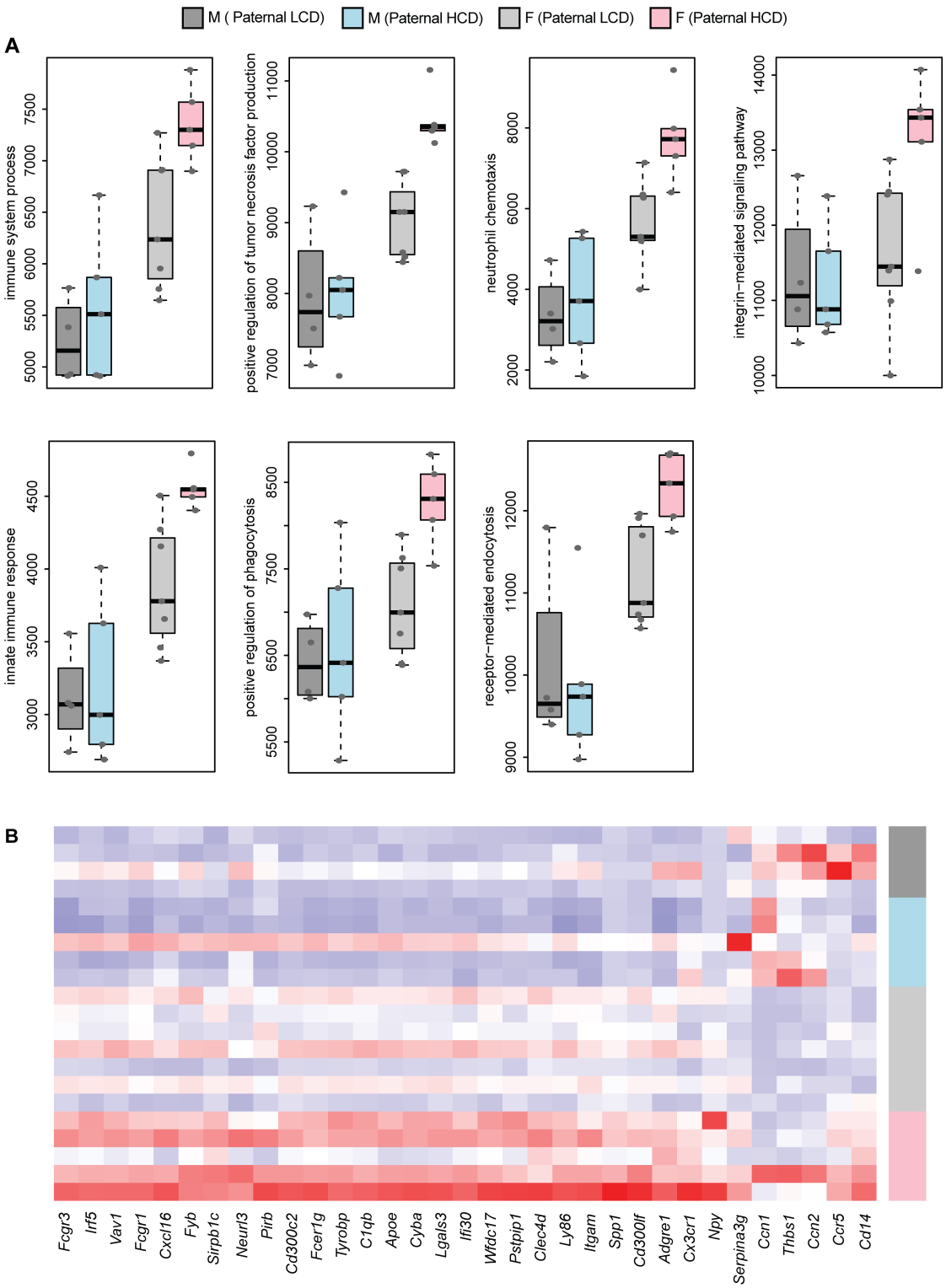
M (Paternal LCD)
M (Paternal HCD)
F (Paternal LCD)
F (Paternal HCD)
A
immune system process
positive regulation of tumor necrosis factor production
neutrophil chemotaxis
integrin−mediated signaling pathway
innate immune response
positive regulation of phagocytosis
receptor−mediated endocytosis
B
Fcgr3
Irf5
Vav1
Fcgr1
Cxcl16
Fyb
Sirpb1c
Neurl3
Pirb
Cd300c2
Fcer1g
Tyrobp
C1qb
Apoe
Cyba
Lgals3
Ifi30
Wfdc17
Pstpip1
Clec4d
Ly86
Itgam
Spp1
Cd300lf
Adgre1
Cx3cr1
Npy
Serpina3g
Ccn1
Thbs1
Ccn2
Ccr5
Cd14

Figure 3.9. Paternal hypercholesterolemia alters atherosclerosis-related gene expression in the intima of female F1 offspring.

Three-week-old male LDLR$^{-/-}$ mice were fed an LCD or HCD diet for 8 weeks before mating with control female LDLR$^{-/-}$ mice. Three-week-old F1 descendants were fed a LCD for 16 weeks. Total RNAs were isolated from the intima of F1 offspring and used for RNA-seq analysis. (A) Geneset scores of the prioritized GOBP terms of male and female offspring from LCD or HCD-fed sires. The geneset score was calculated using the FAIME algorithm. (B) Heatmap representation of DEGs involved in the indicated GOBP terms. Each column shows one individual gene, and each row shows a biological replicate of mouse. Red represents relatively increased gene expression, whereas blue denotes downregulation (n = 4-7 each group).

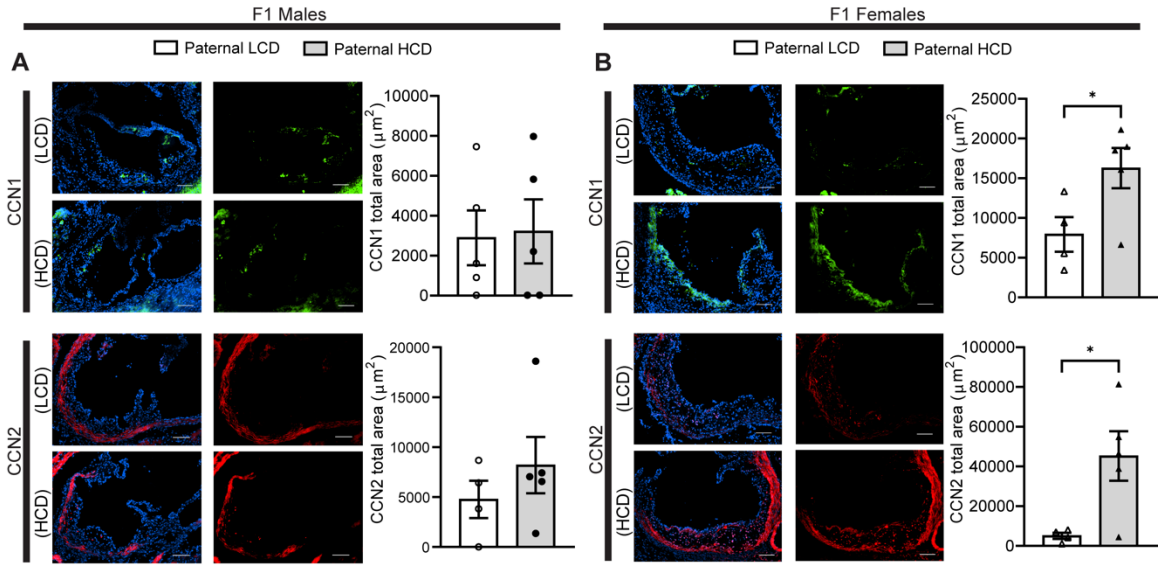

Figure 3.10. CCN1 and CCN2 proteins are elevated in the atherosclerotic lesions of F1 female LDL receptor-deficient descendants from high-cholesterol diet-fed sires.

Three-week-old male LDLR$^{-/-}$ mice were fed an LCD or HCD diet for 8 weeks before mating with control female LDLR$^{-/-}$ mice. Three-week-old F1 descendants were fed an LCD for 16 weeks. (A-B) Representative immunofluorescence images of CCN1 (green) and CCN2 (red) at the aortic root of F1 male (A) and female (B) offspring. The nuclei were stained with DAPI (blue) (scale bar=100µm). Quantification analysis of stating areas is displayed as indicated (n=4-5, *P<0.05, two-sample, two tailed Student's t-test). All data are plotted as means ± S.E.M.

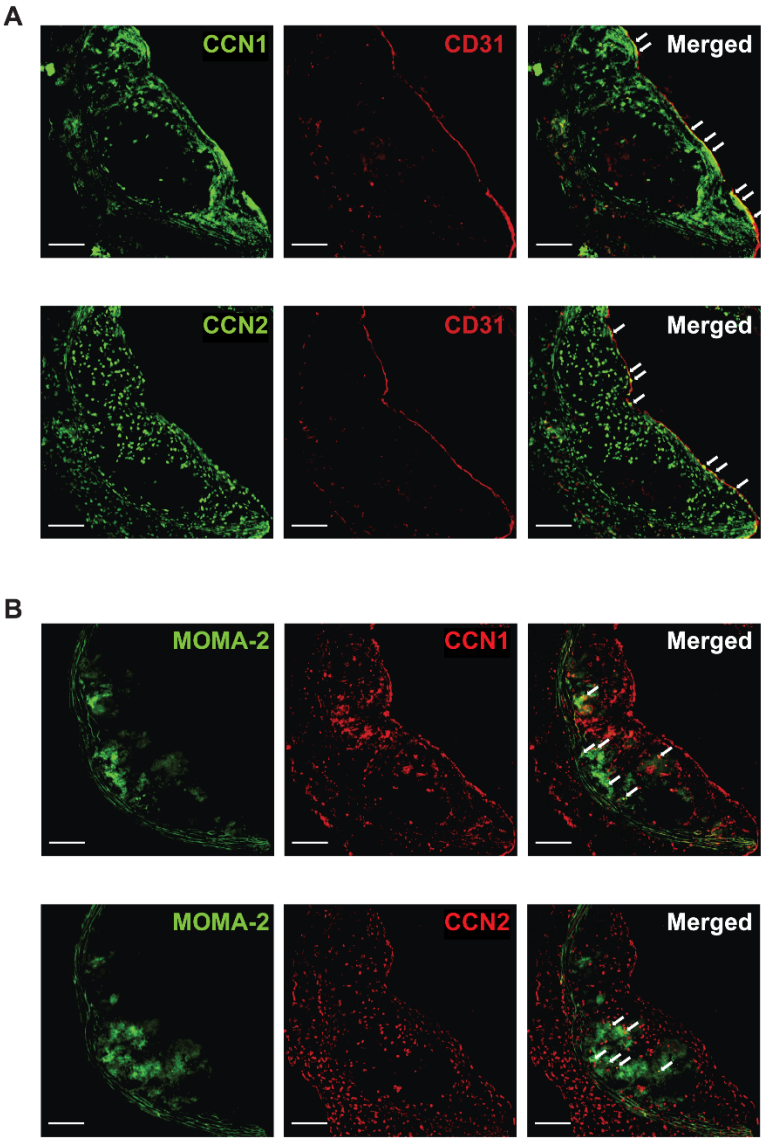

Figure 3.11. CCN proteins are co-localized with macrophage and endothelial cells in atherosclerotic lesions.

(A) Representative images of CD31 and CCN1 or CCN2 immunofluorescent staining in the aortic root of $LDLR^{-/-}$ mice (scale bar=100μm). (B) Representative images of 3 experimental replicates for MOMA-2 and CCN1 or CCN2 immunofluorescent staining in the aortic root of $LDLR^{-/-}$ mice (scale bar=100μm).

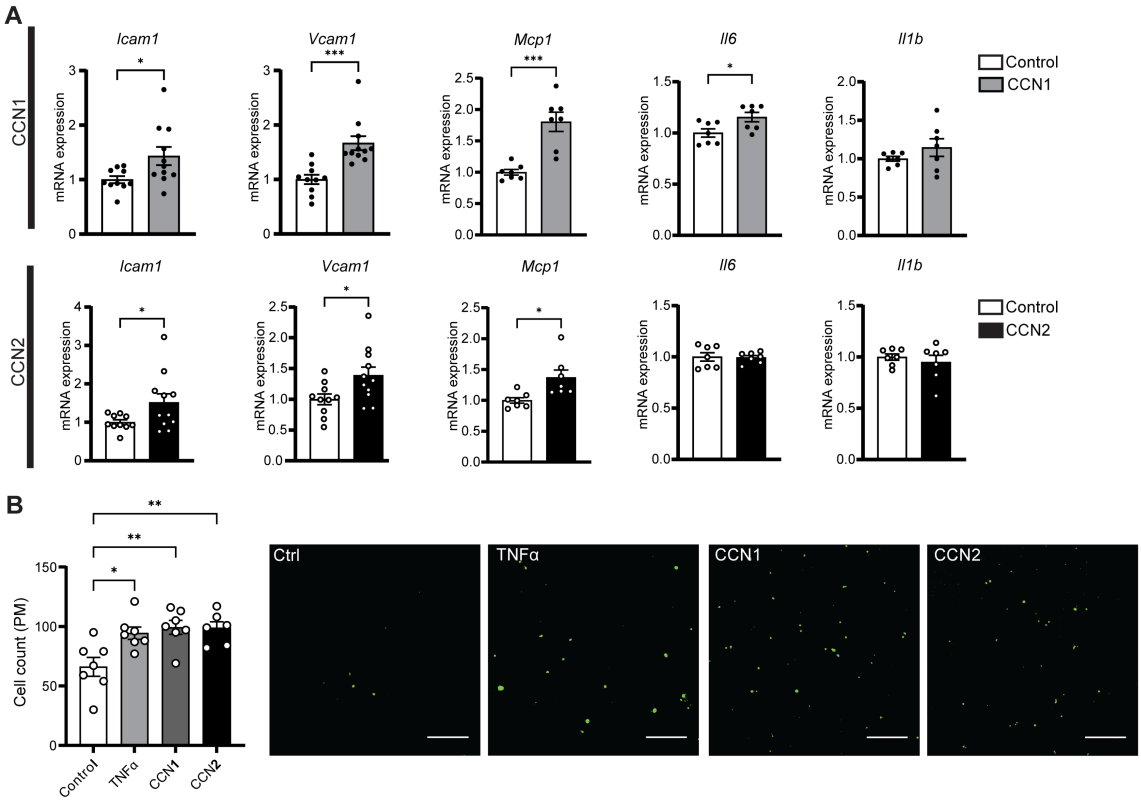
A
CCN1
Icam1
Vcam1
Mcp1
Il6
Il1b
mRNA expression
Control
CCN1
CCN2
Control
CCN2
B
Cell count (PM)
Control
TNFα
CCN1
CCN2
Ctrl
TNFα
CCN1
CCN2

Figure 3.12. CCN1 and CCN2 proteins promote pro-atherogenic gene expression in endothelial cells in vitro.

(A) Human endothelial cells, HMEC-1 cells, were treated with 1μg/ml CCN1 or CCN2 for 4 hours followed by total RNA isolation. The expression levels of indicated genes were analyzed by quantitative real-time PCR (n=7-11, *P<0.05, ***P<0.001, two-sample, two tailed Student's t-test). (B) HMEC-1 endothelial cells were pre-treated with 50 ng/ml CCN1 or CCN2 or 10ng/mL TNFα for 24 hours before incubating with calcein acetoxymethyl-stained peritoneal macrophages isolated from $LDLR^{-/-}$ mice for 4 hours. Adhered cells were counted under a fluorescence microscope. Quantitative analysis of the adhered cells is displayed to the left of representative images (scale bar=250μm, n=6-7, *P<0.05, **P<0.01, one-way ANOVA followed by Bonferroni's multiple comparison test). All data are plotted as means ± S.E.M.

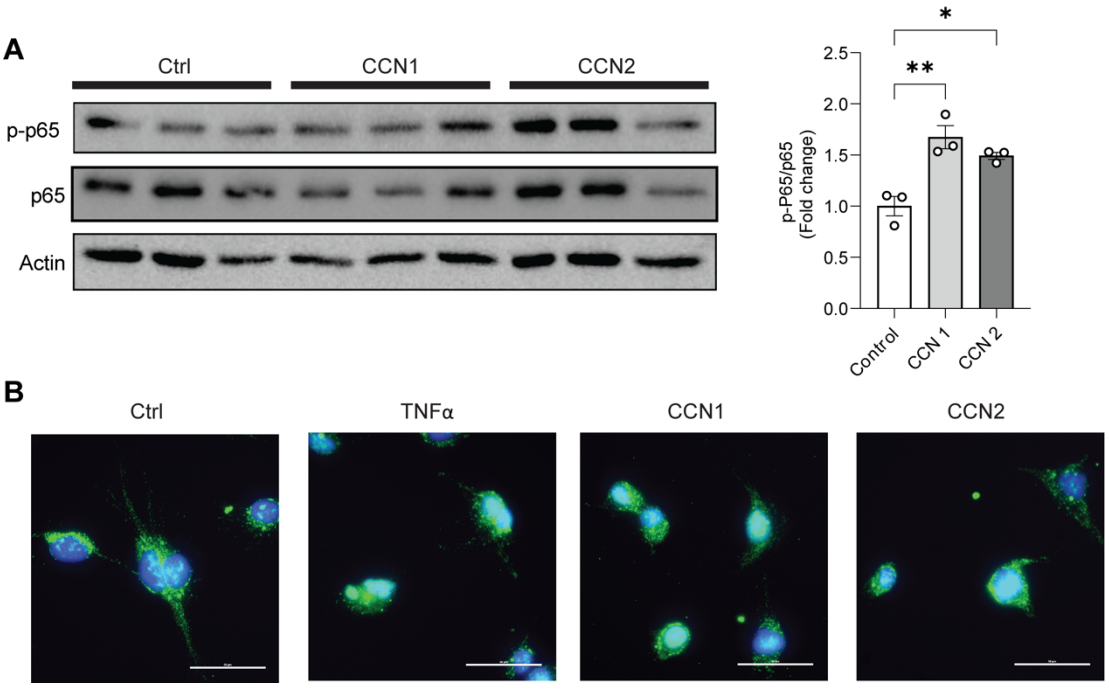

Figure 3.13. CCN proteins stimulate NF-κB activation in human endothelial cells.

(A) Human endothelial cells, HMEC-1 cells, were treated with 1 µg/ml CCN1 or CCN2 for 1 hour followed by protein extraction. Immunoblotting of phosphorylated NF-κB subunit p65, total 65, and Actin (left) and quantification data (right) (n=3, *P<0.05, *P<0.05, one-way *ANOVA* followed by Bonferroni's multiple comparison test). (B) Representative immunofluorescence staining images of 3 experimental replicates for NF-κB p65 (green) in HMEC-1 cells treated with vehicle control or 1 µg/ml CCN1 or CCN2 for 3 hours. The nuclei were stained with DAPI (blue). (scale bar= 50µm). All data are plotted as means ± S.E.M.

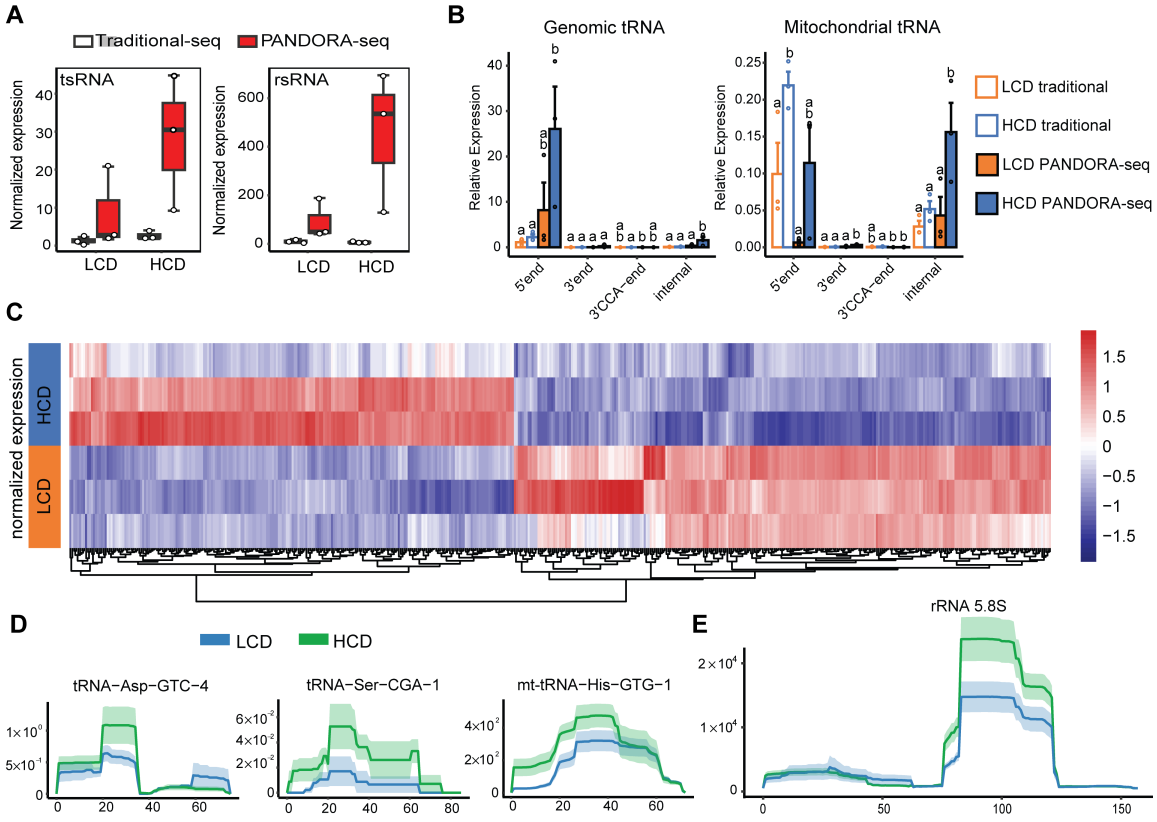
A
Traditional-seq
PANDORA-seq
tsRNA
rsRNA
Normalized expression
LCD
HCD
B
Genomic tRNA
Mitochondrial tRNA
Relative Expression
5'end
3'end
3'CCA-end
internal
LCD traditional
HCD traditional
LCD PANDORA-seq
HCD PANDORA-seq
C
normalized expression
HCD
LCD
D
LCD
HCD
tRNA-Asp-GTC-4
tRNA-Ser-CGA-1
mt-tRNA-His-GTG-1
E
rRNA 5.8S

Figure 3.14. PANDORA-seq reveals significantly changed sperm tsRNAs and rsRNAs induced by high-cholesterol diet feeding in male LDL receptor-deficient mice.

Three-week-old male LDLR$^{-/-}$ mice were fed an LCD or HCD for 9 weeks. Total RNAs were isolated from the sperm and used for PANDORA-seq and traditional small RNA sequencing. (A) Sperm tsRNA and rsRNA relative expression (normalized to miRNAs) under traditional-seq and PANDORA-seq protocols. (B) Sperm tsRNA responses to traditional-seq and PANDORA-seq in regard to different genomic or mitochondria tRNA origins (5' tsRNA, 3' tsRNA, 3' tsRNA-CCA end, and internal tsRNAs). The y -axes represent the relative expression levels compared with total reads of miRNA. Different letters above the bars indicate statistically significant differences ($P<0.05$). Same letters indicate $P>0.05$. Statistical significance was determined by two-sided one-way ANOVA with uncorrected Fisher's least significant difference test. All data are plotted as means ± SEM. (C) Heatmap representation of differentially expressed sperm tsRNAs detected by PANDORA-Seq. Biological replicates are represented in each row. Red represents relatively increased expression, whereas blue represents decreased expression with adjusted P value<0.05 and fold change (FC) >2 as the cutoff threshold. (D and E) Dynamic responses to LCD or HCD of representative sperm tsRNAs (D) and rsRNAs (E) detected by PANDORA-seq. Mapping plots are presented as mean ± SEM (n=3 in each group).

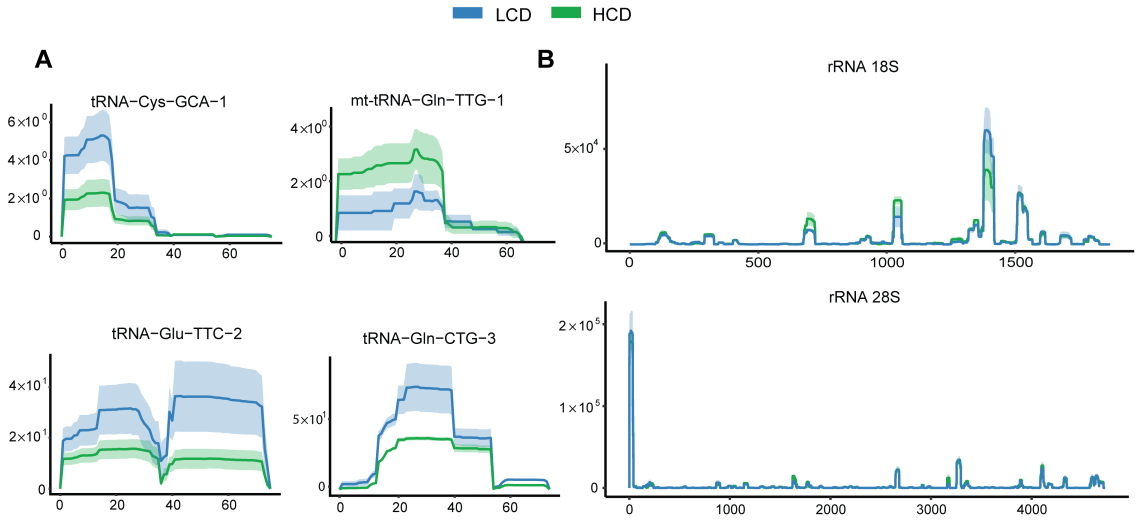

Figure 3.15. PANDORA-seq reveals dynamic changes to high-cholesterol diet feeding of representative sperm tsRNAs and rsRNAs.

Three-week-old male LDLR$^{-/-}$ mice were fed an LCD or HCD for 9 weeks. Total RNAs were isolated from the sperm and used for PANDORA-seq. (A-B) Dynamic responses to the LCD or HCD of representative individual sperm tsRNAs (A) and sperm rsRNAs (B) detected by PANDORA-seq. Mapping plots are presented as mean ± SEM (n = 3 in each group).

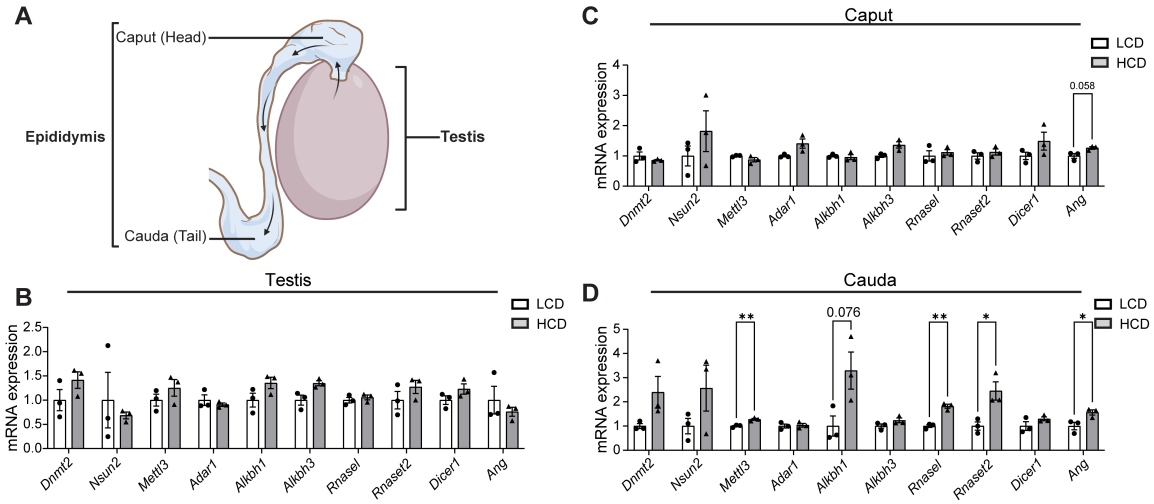

Figure 3.16. Hypercholesterolemia alters the expression of sncRNA biogenesis-related genes in cauda epididymis.

(A) Schematic of the testis and epididymis. Sperm generated in the testis undergo maturational changes during transiting through the caput and cauda epididymis. (B-D) Three-week-old male LDLR$^{-/-}$ mice were fed an LCD or HCD for 9 weeks. Total RNAs were isolated from the testis (B), and caput (C) and cauda (D) epididymis. The expression levels of indicated genes related to sncRNA biogenesis were analyzed by quantitative real-time PCR (n=3, *P<0.05, **P<0.01, two-sample, two tailed Student's t-test). All data are plotted as means ± S.E.M.

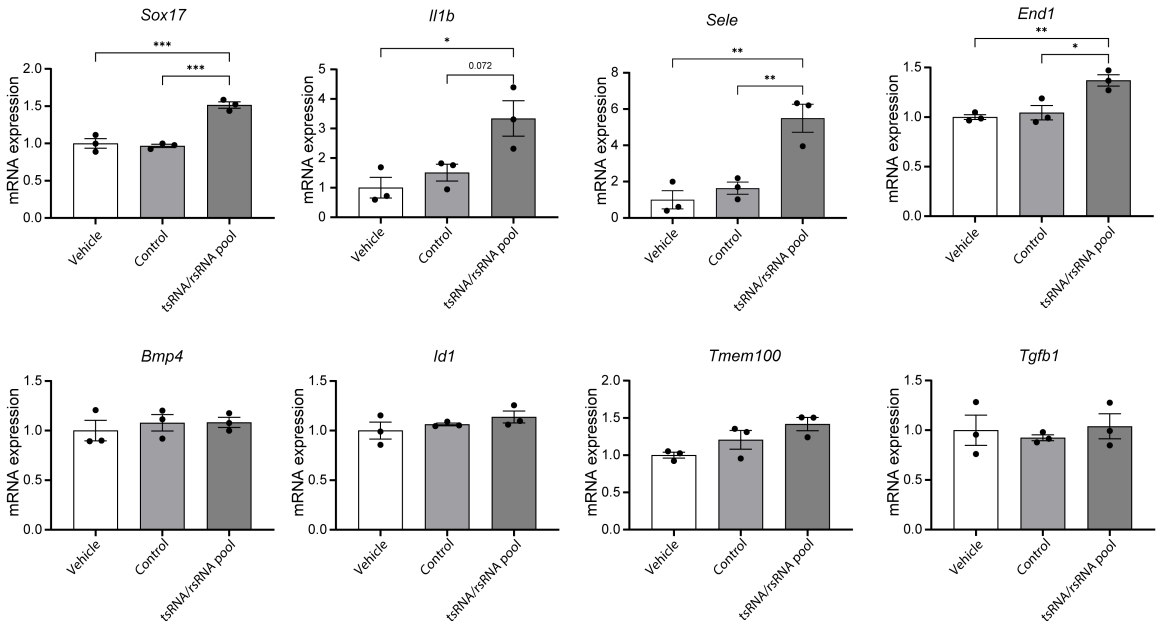

Figure 3.17. Hypercholesterolemia-stimulated sperm tsRNAs/rsRNAs induce early transcription changes in murine embryoid bodies.

Murine embryonic stem cells were transfected with a pool of tsRNA/rsRNAs, control oligo or vehicle followed by 24 hours of embryoid body (EB) formation assay. Total RNA was isolated from EBs for gene expression analysis. The expression levels of indicated genes were analyzed by quantitative real-time PCR (n=3, *P<0.05, **P<0.01). Statistical significance was determined by one-way ANOVA followed by Bonferroni's multiple comparison test. All data are plotted as means ± S.E.M.

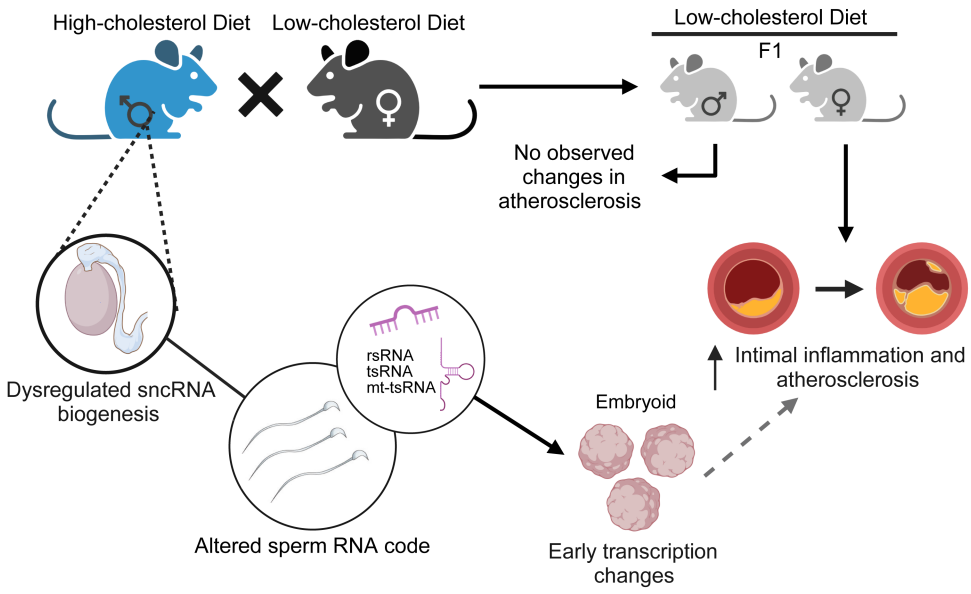

Figure 3.18 Schematic of the impact of paternal exposure to the high-cholesterol diet on sperm sncRNAs and offspring atherosclerosis development. Paternal high-cholesterol feeding led to significantly increased atherosclerosis and intimal inflammation in F1 female, but not male, LDLR$^{-/-}$ offspring. PANDORA-seq identified an altered sncRNA landscape in the sperm of high-cholesterol diet-fed LDLR$^{-/-}$ sires. Overexpression of a pool of sperm tsRNAs/rsRNAs that were upregulated in the sperm of hypercholesterolemic sires induced transcription changes in embryoid bodies that may contribute the increased atherosclerosis in the adult offspring. The image was created with BioRender.com.

4. Chapter 4: Fibroblast IKKβ deficiency impairs plaque stability in LDLR$^{-/-}$ mice

4.1 Abstract

Atherosclerosis is a chronic inflammatory disease involving the contribution of multiple cell types in the vasculature and immune cells. IKKβ is a well-known proatherogenic molecule that contributes to chronic inflammation in the vasculature. Besides inflammation, IKKβ can also participate in cell survival and differentiation. Adventitial fibroblasts are metabolically active cells that help to maintain a balance in immune response and structural integrity within the vasculature. However, their contribution to atherosclerotic plaque development remains elusive. To investigate the function of fibroblast IKKβ in atherosclerosis development, we generated an inducible fibroblast IKKβ-deficient LDLR$^{-/-}$ mouse model. We report the important role of fibroblast IKKβ on atherosclerotic plaque stability. Fibroblast IKKβ-deficient LDLR$^{-/-}$ mice developed features of a vulnerable plaque including a thin fibrous cap, large necrotic core, and reduced extracellular matrix. Single cell analysis revealed downregulation in fibroblast to smooth muscle cell differentiation leading to decreased smooth muscle cell population in fibroblast IKKβ-deficient aortas. These findings reveal the important role of fibroblast IKKβ in maintaining plaque stability through fibroblast to smooth muscle cell differentiation.

4.2 Introduction

Atherosclerosis is a complex inflammatory disease characterized by the gradual and chronic accumulation of lipids and immune cells into the subintimal space of arteries (7).

Inflammation is recognized as a main driver for atherosclerosis development, leading to increases in plaque size, which reduces blood supply to major organs. If left untreated, atherosclerotic plaques may rupture causing significant blood flow obstruction and leading to stroke, heart attack, or other deadly cardiovascular events. (269, 270). Characteristics of a vulnerable (or unstable) plaque include a large necrotic core, thin fibrous cap, small extracellular matrix (ECM) component, and increased immune cell accumulation (270). Vascular smooth muscle cells (VSMCs) contribute to plaque stability since they are the main cell type found at the fibrous cap and can synthesize ECM (271, 272). Additionally, ruptured plaques in human samples are often devoid of VSMCs (12), further supporting their importance in plaque stabilization. However, the origins of plaque VSMCs are controversial, with medial, circulating, and adventitial origins being suggested (13, 14, 272).

The NF-κB/ IKKβ signaling pathway is one of the most well-established inflammatory pathways to be activated in atherosclerosis (84, 90, 96). Transgenic mouse models have been utilized to target the NF-κB/ IKKβ signaling pathway to elucidate its atherogenic roles in endothelial cells, macrophages, and VSMCs (5, 8). For example, NF-κB inhibition or IKKβ deletion in endothelial and myeloid cells decreases macrophage intimal accumulation and protects mice from atherosclerosis (4, 106). IKKβ can interact with several important signaling molecules besides NF-κB such as β-catenin, BAD, and IRS-1 that are essential for regulating cell survival, differentiation, and insulin signaling (133). Thus, IKKβ can be implicated in more than just inflammation, and may also contribute to cell survival and differentiation (111, 126, 165).

While the intima and media in atherosclerosis development has been well studied (133), the outer adventitial layer has been overlooked and its role in atherosclerosis remains incompletely understood. Though initially thought to provide only structural support, the adventitia is the most complex layer of the vascular wall which contains fibroblasts, progenitor cells, immune cells, nerves, and its own blood supply (vaso vasorum) (273, 274). Adventitial fibroblasts respond to various external stressors and act as an "injury sensor." Some of these responses include proliferation, alteration of the ECM, differentiation into other cell types and their migration to the other layers, and the release of inflammatory factors affecting neighboring VSMCs and ECs (274). Furthermore, a previous study showed that monocyte chemoattractant protein-1 (MCP-1) is expressed in the adventitia prior to atherosclerosis development (275). Other evidence of early adventitial activation includes neovascularization and immune cell infiltration in the vaso vasorum of the adventitia (276-278). A more recent study found that adventitial progenitor cells may differentiate to fibroblast-like smooth muscle cells (also called myofibroblasts) that contribute to plaque stability (14). These studies support the notion that adventitial activation may be a crucial component involved in atherosclerosis, termed the "outside-in" hypothesis (273).

To explore the role of adventitial fibroblast IKKβ on atherosclerosis development, we utilized C57BL/6 mice and the inducible Cre-LoxP system to generate a fibroblast specific (Col1a2-CreERT) knockout of IKKβ mouse model crossed with LDLR deficient background ($IKK\beta^{\Delta Fib}LDLR^{-/-}$). We revealed that fibroblast IKKβ deficiency resulted in features of vulnerable plaque formation including a thin fibrous cap, decreased collagen

deposition, and large necrotic core as compared with control littermates. Single cell-sequencing analysis demonstrated a marked decrease in the VSMC population in IKKβ$^{\Delta Fib}$LDLR$^{-/-}$ mice correlating with a decrease in fibroblast to smooth muscle cell differentiation. This study provides further insight into the implications of adventitial cells, such as fibroblasts, on atherosclerosis development and the potential for IKKβ in mediating fibroblast to VSMC differentiation.

4.3 Methods

4.3.1 Animals

Fibroblast-specific IKKβ-knockout (IKKβ$^{\Delta Fib}$) mice were previously generated by breeding mice carrying loxP-flanked IKKβ alleles (IKKβF/F) with the indicible Col1a2-CreERT transgenic mice (163). To increase the susceptibility to atherosclerotic plaque development, IKKβ$^{\Delta Fib}$ mice were then bred with LDLR$^{-/-}$ mice to generate IKKβ$^{F/F}$LDLR$^{-/-}$ and IKKβ$^{\Delta Fib}$LDLR$^{-/-}$ mice. All mice used in this study had the IKKβ$^{F/F}$LDLR$^{-/-}$ double-mutant background, and IKKβ$^{\Delta Fib}$LDLR$^{-/-}$ mice carried the heterozygous knock-in for the inducible Col1a2-CreERT. To induce cre expression, 4-week-old male IKKβ$^{F/F}$LDLR$^{-/-}$ and IKKβ$^{\Delta Fib}$LDLR$^{-/-}$ littermates were injected with 75 mg tamoxifen/kg body weight for 5 consecutive days followed by 1 week clearance. At 6-weeks-old, mice were fed a Western-type HFD (21% fat and 0.2% cholesterol) for 12 weeks until they were euthanized at age 18 weeks. All experimental mice used in this study were male. There are limitations in studying a single sex because sex differences have been widely reported in various mouse atherosclerosis studies. Body weight was measured

weekly, and body composition was analyzed by EchoMRI (EchoMRI Corp) for measuring the fat and lean masses of mice at the end of the study. On the day of euthanasia, mice were fasted for 6 hrs following the dark cycle (feeding cycle), and major tissues were collected. All animals were housed in an animal facility under a protocol approved by the University of California, Riverside institutional animal care and use committee.

4.3.2 Atherosclerotic Lesion Analysis

To quantify the plaque area at the aortic root, Optimal Cutting Temperature (OCT)-compound-embedded hearts were sectioned at a 12-μm thickness keeping all the three valves of the aortic root in the same plane. Sections were then stained with oil red O. Images were taken and plaque size was quantified using a Nikon microscope as previously described (135, 138, 168, 169). (Nikon, Melville, NY, USA).

4.3.3 Histopathology analysis

Aortic root OCT sections were fixed in 4% PFA for 15 minutes and washed with 1x PBS. Aortic root necrotic cores and cap thickness were analyzed via H&E staining as previously described (279). The cap thickness was measured for each H&E image by measuring the average distance of cap at each necrotic core using the InteredgeDistance Image J macro. Picrosirius red stain kit (Polysciences; 24901) was used to stain collagen fibers according to the manufacturer's instructions and as previously described (279), and the total area was measured.

4.3.4 Immunofluorescence staining

Aortic roots OCT sections were used for immunofluorescence staining. Samples were first fixed in 4% PFA for 15 minutes and washed with 1x PBS. Fixed slides were

blocked for 1 hr in 5% BSA. After blocking, slides were washed 3x and then incubated in CD68 (Bio-Rad; MCA1957) and aSMA (Abcam; ab5694) primary antibodies in 4°C overnight. The next day, the slides were washed 3x and incubated in secondary antibodies (Life Technologies) for 1 hr at room temperature. Tissues were mounted with DAPI mounting media (Vectashield) and imaged on a Nikon microscope (Nikon, Melville, NY, USA).

4.3.5 RNA isolation and qPCR

Total RNA was isolated from the adventitia, media/intima, and mouse tissues using TRIZOL Reagent (Sigma-Aldrich, T9424), and quantitative reverse transcription polymerase chain reaction was performed using gene-specific primers and the SYBR Green PCR Kit (Bio-Rad Laboratories) on a Bio-Rad CFX Real-Time-PCR Machine as previously described (37, 138, 164). The sequences of the primer sets used in this study are listed in Table 4.1.

4.3.6 Single cell-RNA sequencing

Single cell preparation

Aorta from mice were dissected and maintained in HBSS for the harvest to maintain cell viability. After the harvest, tissues were rinsed in HBSS to remove red blood cells. The digestion enzyme cocktail was prepared fresh in HBSS containing Hyaluronidase (60U/mL), Liberase TM (5mg/mL), and DNase I (12U/mL). Three aortas for each condition were pooled and minced with dissection scissors in 20ml of digestion cocktail. The minced tissue was then digested in 1.5mL digestion cocktail at 37°C for 30 min. The single-cell suspension was centrifuged at 600 rcf for 10 min and washed with FACS buffer

in 1xPBS containing 2% FBS (Sigma; F4135), 5mM EDTA, 20mM HEPES (Gibco; 15630080), 1mM sodium pyruvate (Corning; MT25000Cl) 2x before filtering through a 70mm filter. Samples with >70% viability were then fixed with the Chromium Next GEM Single Cell Fixed RNA Sample Preparation Kit (10x Genomics; 1000414) for 16 hours and stored according to the manufacturer's instructions in -80°C until further processing using the 10x Genomics Single Cell Gene expression Flex kits (10x Genomics; 1000495, 1000422, 1000251) and Chromium X instrument.

Single cell RNA-sequencing and Data Analysis

The processed samples were sequenced at the Genomics Center of University of California, San Diego (Illumina system). The raw single-cell RNA sequencing data was preprocessed using CellRanger v8.0.0 (10x Genomics), including aligning reads to the mouse reference genome (mm10-2020-A), and generating cellxgene expression count matrices. Using the generated gene expression count matrices, an in-house single-cell RNA-seq pipeline was built based on the Seurat R package (R v4.2.3, Seurat v4.3.0) (280), including ambient RNA removal, quality control, cell filtering, clustering, cell type annotation, differential gene expression, and visualization. Ambient RNA was removed using SoupX v1.6.2 (281). Doublets were identified by cxds function using scds v1.14.0 (282). Only the identified singlets expressing 200 to 8000 genes that were detected in at least three cells and with mitochondrial gene content below 20% were kept for further analysis.

Cells of good quality from the two experimental groups were integrated using Harmony (283). Principal component analysis (PCA) over the identified 2000 highly

variable genes was applied for dimension reduction (dimensions = 25) and clustering. Cell clustering was performed on integrated data with a shared nearest-neighbor (SNN) graph-based method using the FindNeighbors function included in Seurat, followed by the Louvain algorithm for modularity optimization (resolution = 0.8) using FindClusters function. After the cell clusters were determined, their top 5 marker genes were identified with the FindMarkers function. For cell type annotation, the top marker genes based on the adjusted p value were manually curated to match canonical cell types and their marker genes based on literature research and public resources from scRNA-seq databases. Cell type annotation was also consolidated by enrichR v3.1 using top 100 markers and by SingleR v2.0.0.

Differentially expressed genes (DEG) between the positive group and negative group were identified in each cell type. Gene Ontology (GO) enrichment analyses were conducted for up-regulated DEGs and down-regulated DEGs in each cell type using clusterProfiler v4.6.2 (284). A GO term was deemed significantly enriched if the adjusted p-value (with Benjamini-Hochberg correction) was below 0.05.

4.4 Results

4.4.1 Generation of inducible fibroblast-specific IKKβ–deficient mice without altering metabolic phenotypes

To investigate the role of fibroblast IKKβ on atherosclerosis development in vivo, we generated LDLR knockout ($LDLR^{-/-}$) mice with inducible fibroblast-specific IKKβ deficiency (termed $IKK\beta^{\Delta Fib}LDLR^{-/-}$) by crossing $IKK\beta^{\Delta Fib}$ mice with $LDLR^{-/-}$ mice. All

mice used in this study had IKKβ$^{F/F}$LDLR$^{-/-}$ double mutant background, and IKKβ$^{\Delta Fib}$ LDLR$^{-/-}$ mice contained heterozygous Col1a2-CreERT knock-in. Four-week-old male IKKβ$^{\Delta Fib}$LDLR$^{-/-}$ mice were I.P. injected with 75 mg tamoxifen/kg body weight per day for 5 days to induce Cre expression (163). IKKβ$^{\Delta Fib}$LDLR$^{-/-}$ mice remained viable and healthy with no obvious phenotypic deviations after tamoxifen treatment (data not shown).

After 1 week of tamoxifen clearance, adventitia and intimal fractions from aortas along with major organs were isolated from male IKKβ$^{F/F}$LDLR$^{-/-}$ and IKKβ$^{\Delta Fib}$LDLR$^{-/-}$ littermates to confirm knock out of IKKβ in adventitial fibroblasts. The results confirmed significant decrease in *Ikkb* mRNA exoression in the adventitia of IKKβ$^{\Delta Fib}$LDLR$^{-/-}$ mice as compared with IKKβ$^{F/F}$LDLR$^{-/-}$ control littermates (Figure 4.1A). There were no significant changes in *Ikkb* expression in the intima or other major organs including liver, kidney, white adipose tissue, or intestine (Figure 4.1A).

4.4.2 Deficiency of IKKβ alters plaque stability in LDLR−/− mice

To investigate whether deficiency of fibroblast IKKβ affects atherosclerosis development, six-week-old mice were fed a high fat diet (HFD; 42% kcal from fat) for 12 weeks to induce atherosclerosis plaque development. Since we previously identified IKKβ as a key regulator in adipose differentiation and survival (109, 111, 126), we first analyzed the metabolic phenotype of these mice. There was no difference in body weights, organ weights, body composition, or glucose tolerance between IKKβ$^{F/F}$LDLR$^{-/-}$ and IKKβ$^{\Delta Fib}$LDLR$^{-/-}$ mice fed a HFD (Figure 4.1, B-D), suggesting fibroblast IKKβ knock out does not affect the metabolic phenotypes of these mice. Atherosclerotic plaque areas were then quantified at the aortic roots of IKKβ$^{\Delta Fib}$LDLR$^{-/-}$ and IKKβ$^{F/F}$LDLR$^{-/-}$

littermates. Interestingly, IKKβ$^{\Delta Fib}$LDLR$^{-/-}$ mice developed similar atherosclerotic plaque size to those of IKKβ$^{\Delta F/F}$LDLR$^{-/-}$ mice (Figure 4.2A). We next sought to determine if fibroblast IKKβ deficiency affects features of plaque stability which are characterized by fibrous cap thickness, collagen contents, necrotic core size, macrophage accumulation, and smooth muscle cell contents. Quantification of collagen deposition in the plaques of the aortic root showed reduced collagen contents in IKKβ$^{\Delta Fib}$LDLR$^{-/-}$ mice compared with control littermates (Figure 4.2B). Immunostaining for macrophage and smooth muscle cell (SMC) markers at the aortic roots revealed no changes in macrophage or SMC contents between IKKβ$^{\Delta Fib}$LDLR$^{-/-}$ and IKKβ$^{\Delta F/F}$LDLR$^{-/-}$ mice (Figure 4.2, C and D). We then measured the plaque necrotic core size and cap thickness at the aortic roots. We observed an increase in necrotic core size and thinner fibrous caps in IKKβ$^{\Delta Fib}$LDLR$^{-/-}$ mice compared with their control littermates (Figure 4.2E). Consistently, gene expression analysis showed increase expression of pro-apoptotic genes *Bak1* and *Bax* and decreased *Bcl-2* gene expression in the aortas of IKKβ$^{\Delta Fib}$LDLR$^{-/-}$ mice (Figure 4.3B).

Adventitial fibroblasts have been shown to respond to changes in the microenvironment and become activated during atherosclerosis (274). Thus, we also analyzed the aorta for genes related to fibroblast activation including *Tgfb,* which promotes fibroblast to myofibroblast transition, and *Acta2* (also known as aSMA), which is a marker for myofibroblasts. Aortas from IKKβ$^{\Delta Fib}$LDLR$^{-/-}$ mice exhibited a decrease in *Tgfb* gene expression and a trending decrease in *Acta2* suggesting a decrease fibroblast response and transition to myofibroblasts (Figure 4.3A). Together, this data demonstrates a dysfunction

in fibroblast activation due to IKKβ deficiency linked to features of a vulnerable atherosclerotic plaque in $LDLR^{-/-}$ mice.

4.4.3 scRNA-Seq identifies shifts in vascular cell phenotypes induced by fibroblast IKKβ deficiency

To further elucidate the role of IKKβ on fibroblasts function in atherosclerosis development, three aortas were pooled from $IKK\beta^{F/F}LDLR^{-/-}$ and $IKK\beta^{\Delta Fib}LDLR^{-/-}$ mice and subjected to single-cell RNA-sequencing (scRNA-seq). Datasets from $IKK\beta^{F/F}LDLR^{-/-}$ and $IKK\beta^{\Delta Fib}LDLR^{-/-}$ samples were combined for filtering and quality check, and then process through the Seurat pipeline, which yielded 30 clusters (Figure 4.4A). The clusters were annotated using known gene markers for aortic cells (Figure 4.4, B and C) resulting in 10 main cell types consisting of Endothelial cells (clusters 10, 14, 25), VSMCs (clusters 0, 2, 4, 5, 12, 23, 28), Transitioning cells (cluster 6, 29), Fibroblasts (clusters 1, 3, 8, 15, 17, 22), Proliferating or stem-like cells (cluster 24), Macrophages (clusters 7, 9, 13, 19, 21, 26), Oligodendrocytes (clusters 11, 20), T cells, (clusters 18, 27), B cells (cluster 30), and Erythrocytes (cluster 16). The transitioning cell clusters express both fibroblast and VSMC markers (Figure 4.4D). Further supporting this annotation, Gene Ontology (GO) gene enrichment pathway analysis of the transitional cell cluster compared with FibroblastCol1 revealed features resembling VSMCs including muscle cell development, differentiation, and migration (Figure 4.4 E). On the contrary, GO gene enrichment pathway analysis of the transitional cell cluster compared with the VSMC cluster revealed features resembling fibroblasts including extracellular organization

(Figure 4.4 E). This data confirms this cell cluster represents a transitional state between fibroblasts and SMCs.

4.4.4 Fibroblasts from IKKβ -deficient aortas display a decreased VSMC population associated with a reduction in smooth muscle cell differentiation

Next, we analyzed the changes in cell populations between control and fibroblast IKKβ-deficient aortas. There were no changes in the two fibroblast clusters, but we identified a decrease in the SMC cluster and an increase in immune cell clusters including macrophages, T cells, and B cells (Figure 4.5, A-C). VSMCs comprised 53.4% of the total cell population in control aortas, whereas fibroblast IKKβ-deficient aortas only contained 34.4% of VSMCs (Figure 4.5 C).

We further investigated the changes in the FibroblastCol1 cluster between control and the fibroblast IKKβ-deficient aortas since there was no change in their population size. GO gene enrichment pathway analysis revealed a decrease in pathways related to VMSC differentiation including “muscle cell differentiation,” “muscle cell migration,” “muscle cell development,” smooth muscle cell migration,” vascular associated smooth muscle cell proliferation,” and “muscle cell proliferation” (Figure 4.6 A). We then generated violin plots to confirm the decrease in genes associated with SMC development including *Acta2, Itga8, Myh11, Csrp2, Myl9, Nr1d2, Tpm1, Rock1, Postn,* and *Dmpk* (Figure 4.6 B). This data suggests a decrease in fibroblast-to-SMC differentiation and potential migration to the cap of the plaque, which would explain the vulnerable plaque phenotype in IKKβ$^{\Delta Fib}$LDLR$^{-/-}$ mice compared with control littermates. Interestingly, FibroblastCol1 cells also demonstrate an increase in antigen processing and presentation by GO gene

enrichment analysis including “antigen processing and presentation”, “antigen processing and presentation of peptide antigen”, “antigen processing and presentation of exogenous antigen”, “antigen processing and presentation of endogenous peptide antigen”, and more can be seen in Figure 4.6 A. Fibroblasts can act as antigen presenting cells (APCs), which may lead to an increase in immune cell recruitment via the vaso vasorum and adventitial lymphatic system, or activation of adventitial resident immune cells (292). Together this data suggests IKKβ is necessary for fibroblast differentiation into VSMCs, proliferation, and migration.

4.5 Discussion

Atherosclerotic plaque instability leading to rupture is the major cause of thrombotic events. In the current study, we investigated the role of fibroblast IKKβ on atherosclerosis development in HFD-fed male $LDLR^{-/-}$ mice. While fibroblast IKKβ knockout did not affect plaque size, the plaques of $IKK\beta^{\Delta Fib}LDLR^{-/-}$ mice contained features of a vulnerable plaque including a large necrotic core, thin fibrous cap, and decreased collagen composition compared to their control littermates. Single cell-sequencing further revealed a decrease VSMC and increase immune cell population in the aortas of $IKK\beta^{\Delta Fib}LDLR^{-/-}$ mice compared with controls. Interestingly, gene enrichment analysis revealed a decrease in fibroblast to VSMC differentiation and migration in the aortas. These results suggest that IKKβ may be necessary for fibroblast to VSMC differentiation, and adventitial fibroblasts may be a more important contributor to

atherosclerosis than previously thought. Overall, we show that fibroblast IKKβ may be necessary for plaque stability and beneficial to prevent thrombotic events.

The origins of plaque cells are complex and are often derived from various sources. For example, VSMCs or -like cells are believed to be derived from a variety of sources including activated adventitial fibroblasts (fibromyocytes or myofibroblasts), adventitial progenitor cells (14), circulating progenitor cells (13), or even endothelial and macrophage cells (285). Adventitial fibroblasts remain in a quiescent state and become activated under pathological conditions where they proliferate, alter the ECM, and differentiate into aSMA-expressing myofibroblasts or VSMCs (286). It is unclear whether a portion fibrous cap cells are derived from activated adventitial fibroblasts since aSMA is a marker for VSMCs and activated fibroblasts. Nonetheless, myofibroblasts are known to migrate to the intima during neointimal formation of injured arteries (287, 288). A recent study also identified cells of adventitial progenitor origin at the media, plaque core (possible foam cells), and the cap of the plaque (14). Interestingly, we found that fibroblasts contribute significantly to plaque stability in an IKKβ-dependent manner. Single-cell RNA analysis revealed that aortas from IKKβ$^{\Delta Fib}$LDLR$^{-/-}$ mice contained a fibroblast cluster with significantly decreased genes involved in muscle cell differentiation, development, and migration. We hypothesize that fibroblasts contribute to plaque stability by differentiation to smooth muscle-like cells that migrate to the cap and provide structural stability. To confirm this hypothesis, future studies will involve the use of a reporter mouse line to track Col1a2-CreERT expressing fibroblasts after 12 weeks of HFD. Like Dubner et al. (14), we expect

to find cells of fibroblast origin at the fibrous cap of the plaque and a decrease of these cells with IKKβ knockout.

Besides fibroblasts, the adventitia is home to populations of resident immune cells including macrophages, T cells, and B cells (289). In addition, it is believed that immune cells can infiltrate through the vasa vasorum of the adventitia under inflammatory conditions leading to the development of arterial tertiary lymphoid organs (ATLOs) in the adventitia. Indeed, several studies have demonstrated an increase in immune cell infiltration and adventitial ATLO formation in rodent and human plaques (191, 290, 291). Interestingly, the stage of ATLOs in human plaques positively correlated with plaque instability (291). Fibroblasts can also function as antigen presenting cells (APCs) (292), which is a crucial step in the hosts adaptive immune response and for presenting antigens to activate T cells. In addition to a decrease in VSMC differentiations, we identified an increase in genes involved in antigen presenting, which may have led to the increase in immune cell clusters in our single cell data. The contribution of adventitial fibroblasts as APCs on atherosclerosis development has not been well studied and requires further investigation.

It is intriguing we identified a protective role of fibroblast IKKβ since previous reports have consistently shown that IKKβ in other vascular cells, such as endothelial cells and macrophages, increases plaque burden due to its pro-inflammatory effects (133). However, the role of IKKβ has not been well studied and we provide evidence that IKKβ is necessary for normal fibroblast function and response to changes in their microenvironment. We previously reported that IKKβ deficient cardiac fibroblasts can

blunt angiotensin-II-induced expression of aSMA (279). Fibroblast IKKβ deficiency also decreases collagen production in mouse hearts and in vitro (279), suggesting IKKβ may also be necessary for collagen synthesis. In the current study, we show that IKKβ-deficient fibroblasts result in plaque formation with decreased collagen deposition and thinner fibrous cap, suggesting that adventitial fibroblasts contribute to plaque stability. Collectively, these results reveal IKKβ as a potential regulator of fibroblast to VSMC differentiation in the context of atherosclerosis. Deficiency of IKKβ in fibroblasts may lead to features of an unstable plaque via decreased VSCM differentiation during atherosclerosis. However, in vitro studies are needed to confirm the role of IKKβ in fibroblasts.

In summary, we investigated the role of fibroblast IKKβ signaling on atherosclerosis development and revealed a key role of fibroblast IKKβ on maintaining plaque stability. IKKβ$^{\Delta Fib}$LDLR$^{-/-}$ mice developed vulnerable plaques with a thin fibrous cap, large necrotic core, and small ECM component. Plaque instability in these mice was correlated with a decrease in VSMC population and increase immune cell population in the aortas. The reduction in aortic VSMCs was probably due to a decrease in fibroblast to VSMC differentiation with IKKβ ablation. Likewise, the increase in immune cells could have been due to the increase in fibroblast APC function, though the role of IKKβ in fibroblast antigen presentation remains unknown. We anticipate our findings will stimulate further studies on the complexity of the adventitia and its role in atherosclerosis development.

4.6 Figures and Tables

Table 4.1. Primer Sequences used for QPCR

Genes	Primer sequences	Genes	Primer sequences
mGAPDH	5'-AACTTTGGCATTGTGGAAGG-3'	mIKKβ	5'-AAGGAGGAGATCTCCGAAGATACTT -3'
	5'-GGATGCAGGGATGATGTTCT-3'		5'-TAAGAGCCGATGCGATGTCA -3'
mB-actin	5'- GGCTGTATTCCCCTCCATCG-3'	mBlc2	5'-TTCGCAGCGATGTCCAGTCAGCT-3'
	5'- CCAGTTGGTAACAATGCCATGT-3'		5'-TGAAGAGTTCTTCCACCACCGT-3'
mTGFb	5'- TGACGTCACTGGAGTTGTACGG-3'	mBax	5'-TGAAGACAGGGGCCTTTTTG-3'
	5'- GGTTCATGTCATGGATGGTGC-3'		5'- AATTCGCCGGAGACACTCG-3'
maSMA	5'- TCCTGACGCTGAAGTATCCGATA-3'	mBid	5'- TCCACAACATTGCCAGACTA-3'
	5'- GGCCACACGAAGCTCGTTAT-3'		5'- CACTCAAGCTGAACGCAGAG-3'
		mBak1	5'- CAGCTTGCTCTCATCGGAGAT-3'
			5'- GGTGAAGAGTTCGTAGGCATTC-3'

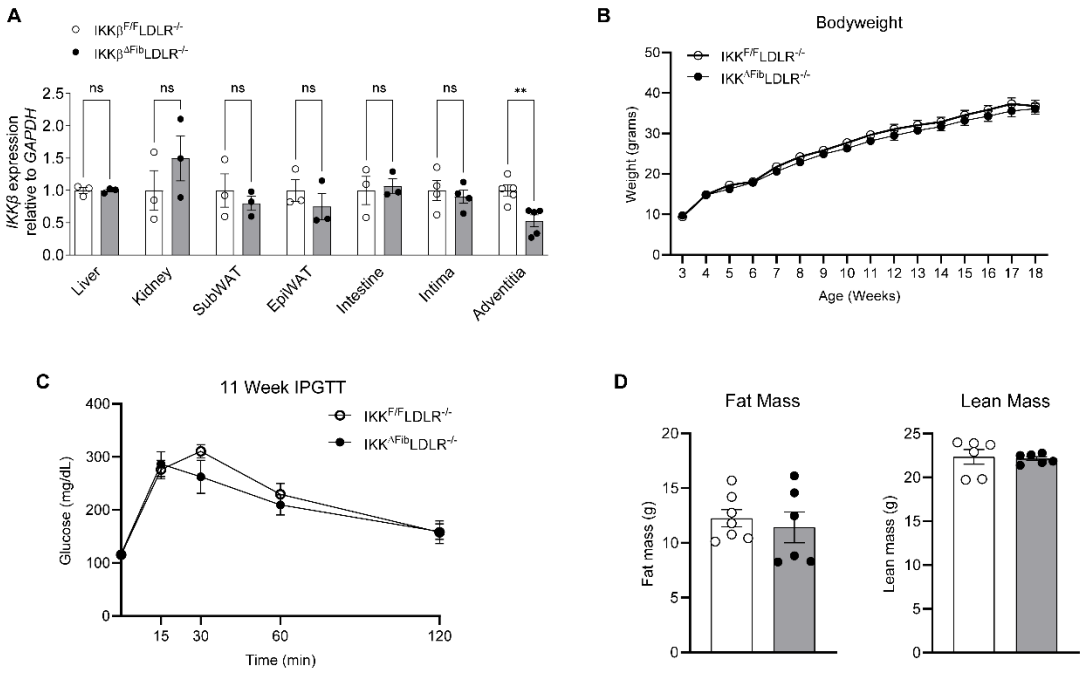
A
IKKβ^F/F LDLR-/-
IKKβ^ΔFib LDLR-/-
IKKβ expression relative to GAPDH
ns
ns
ns
ns
ns
ns
**
Liver
Kidney
SubWAT
EpiWAT
Intestine
Intima
Adventitia
B
Bodyweight
IKK^F/F LDLR-/-
IKK^ΔFib LDLR-/-
Weight (grams)
Age (Weeks)
C
11 Week IPGTT
IKK^F/F LDLR-/-
IKK^ΔFib LDLR-/-
Glucose (mg/dL)
Time (min)
D
Fat Mass
Lean Mass
Fat mass (g)
Lean mass (g)

Figure 4.1. Generation of LDLR$^{-/-}$ mice with inducible fibroblast-specific IKKβ–deficiency without affecting metabolic phenotypes of LDLR$^{-/-}$ mice.

Four-week-old male IKKβ$^{\Delta Fib}$LDLR$^{-/-}$ and IKKβ$^{F/F}$LDLR$^{-/-}$ mice were i.p. injected with 75mg/kg tamoxifen per day for 5 days to induce Cre expression. At six-weeks-old those mice were fed a HFD for twelve weeks. (**A**) Major organs and aorta fractions were collected from IKKβ$^{\Delta Fib}$LDLR$^{-/-}$ and IKKβ$^{F/F}$LDLR$^{-/-}$ mice 1 week after completion of tamoxifen injections followed by total RNA isolation. IKKβ mRNA expression levels in major organs of IKKβ$^{\Delta Fib}$LDLR$^{-/-}$ and IKKβ$^{F/F}$LDLR$^{-/-}$ were analyzed by quantitative real-time PCR (n=3-5, two-sample, two-tailed Student's t-test). (**B**) Growth curves of male IKKβ$^{\Delta Fib}$LDLR$^{-/-}$ and IKKβ$^{F/F}$LDLR$^{-/-}$ mice on HFD for twelve weeks were measured (n=7; two-way *ANOVA* followed by Bonferroni's multiple comparison test). (**C**) Intraperitoneal glucose tolerance test was performed 11 weeks after diet (n=5; two-way *ANOVA* followed by Bonferroni's multiple comparison test). (**D**) Fat mass and lean mass were measured in both IKKβ$^{\Delta Fib}$LDLR$^{-/-}$ and IKKβ$^{F/F}$LDLR$^{-/-}$ mice (n=6-7; two-sample, two tailed Student's t-test). HFD, high fat diet. All data are plotted as means ± S.E.M.

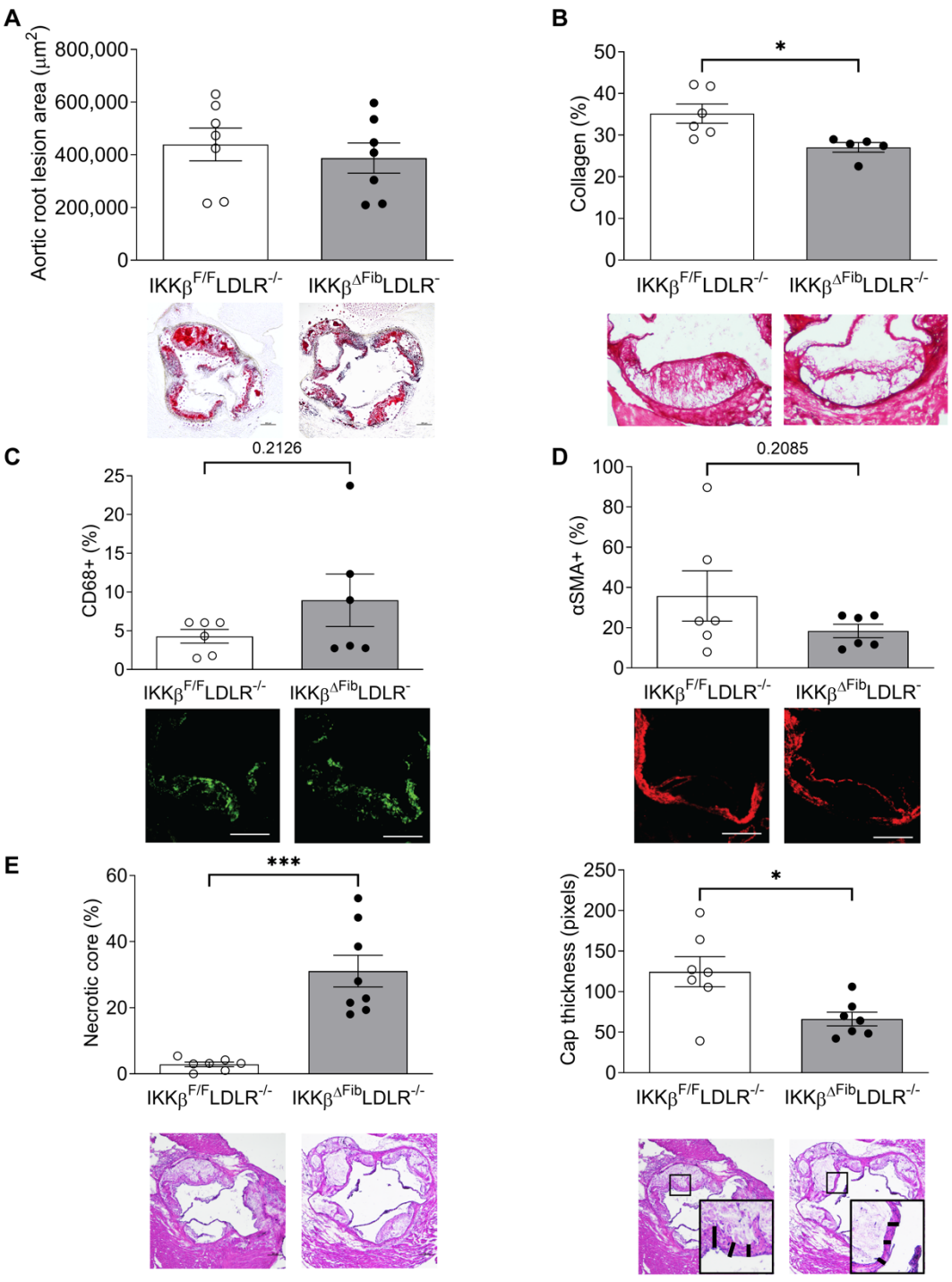
A
Aortic root lesion area (μm²)
800,000
600,000
400,000
200,000
0
IKKβF/FLDLR-/-
IKKβΔFibLDLR-
B
Collagen (%)
50
40
30
20
10
0
*
IKKβF/FLDLR-/-
IKKβΔFibLDLR-/-
C
CD68+ (%)
25
20
15
10
5
0
0.2126
IKKβF/FLDLR-/-
IKKβΔFibLDLR-
D
αSMA+ (%)
100
80
60
40
20
0
0.2085
IKKβF/FLDLR-/-
IKKβΔFibLDLR-
E
Necrotic core (%)
60
40
20
0
***
IKKβF/FLDLR-/-
IKKβΔFibLDLR-/-
Cap thickness (pixels)
250
200
150
100
50
0
*
IKKβF/FLDLR-/-
IKKβΔFibLDLR-/-

Figure 4.2. Fibroblast IKKβ deficiency causes plaque vulnerability in HFD-fed LDLR$^{-/-}$ mice.

Four-week-old male IKKβ$^{\Delta Fib}$LDLR$^{-/-}$ and IKKβ$^{F/F}$LDLR$^{-/-}$ mice were i.p. injected with 75mg/kg tamoxifen per day for 5 days to induce Cre expression. At six-weeks-old those mice were fed a HFD for twelve weeks. (**A**) Quantitative analysis of the lesion area at the aortic root of IKKβ$^{\Delta Fib}$LDLR$^{-/-}$ and IKKβ$^{F/F}$LDLR$^{-/-}$ mice (n=7). Representative oil red O-stained sections displayed below the quantification data (scale bar= 200μm). (**B**) Quantitative analysis of collagen deposition at the aortic root of IKKβ$^{\Delta Fib}$LDLR$^{-/-}$ and IKKβ$^{F/F}$LDLR$^{-/-}$ mice (n=5-6, *P<0.05, two-sample, two tailed Student's t-test). Representative Sirius red-stained sections displayed below the quantification data (scale bar= 200μm). (**C-D**) Quantitative analysis of the macrophage (CD68) (**C**) and smooth muscle cell (αSMA) (**D**) at the aortic root of IKKβ$^{\Delta Fib}$LDLR$^{-/-}$ and IKKβ$^{F/F}$LDLR$^{-/-}$ mice (n=6, two-sample, two tailed Student's t-test). Representative immunofluorescent staining displayed below the quantification data. Nuclei were stained with DAPI (scale bar= 200μm). (**E**) Quantitative analysis of the necrotic core area (left) and cap thickness (right) at the aortic root of IKKβ$^{\Delta Fib}$LDLR$^{-/-}$ and IKKβ$^{F/F}$LDLR$^{-/-}$ mice (n=7, *P<0.05, ***P<0.001, two-sample, two tailed Student's t-test). Representative H&E-stained sections displayed below the quantification data (scale bar= 200μm). All data are plotted as means ± S.E.M.

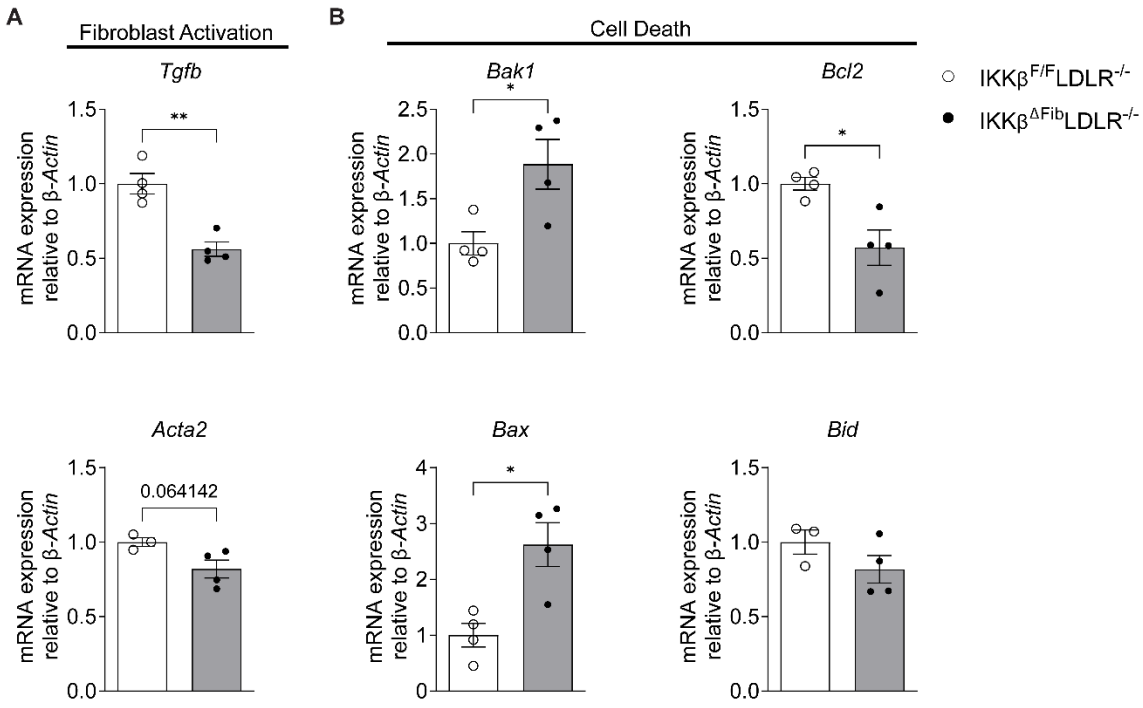

Figure 4.3. IKKβ deletion in fibroblasts decrease markers of fibroblast activation and increase apoptosis in aortas. Four-week-old male IKKβ$^{\Delta Fib}$LDLR$^{-/-}$ and IKKβ$^{F/F}$LDLR$^{-/-}$ mice were i.p. injected with 75mg/kg tamoxifen per day for 5 days to induce Cre expression. At six-weeks-old those mice were fed a HFD for twelve weeks. Total RNA form aortas were isolated. (**A-B**) The expression of fibroblast activation (**A**) or (**B**) apoptotic genes were analyzed by quantitative real-time PCR. (n=3-4, *P<0.05, **P<0.01, two-sample, two tailed Student's t-test). All data are plotted as means ± S.E.M.

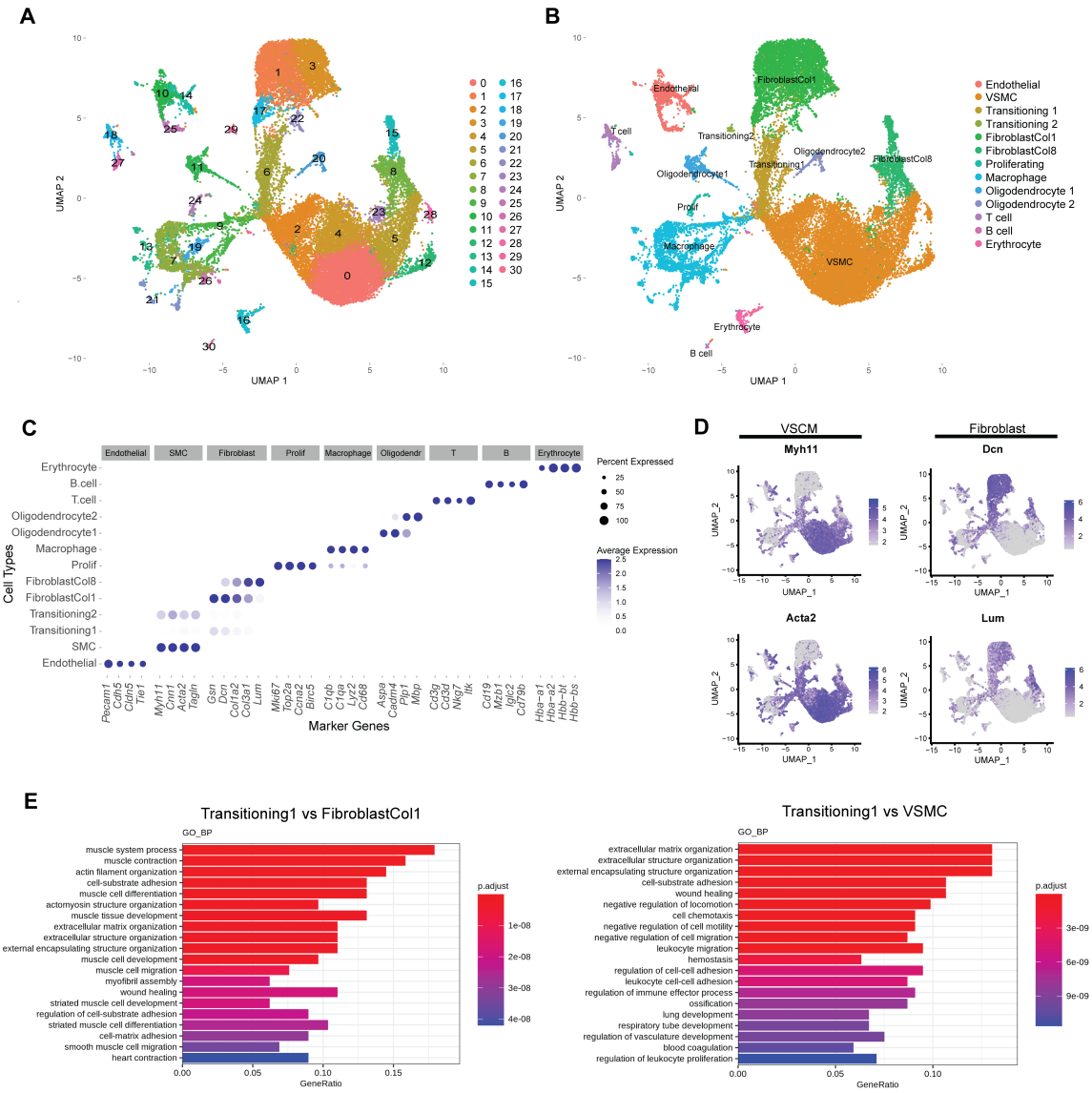
A
B
C
D
E
UMAP 1
UMAP 2
Endothelial
VSMC
Transitioning 1
Transitioning 2
FibroblastCol1
FibroblastCol8
Proliferating
Macrophage
Oligodendrocyte 1
Oligodendrocyte 2
T cell
B cell
Erythrocyte
Cell Types
Marker Genes
Percent Expressed
Average Expression
VSCM
Fibroblast
Myh11
Dcn
Acta2
Lum
Transitioning1 vs FibroblastCol1
Transitioning1 vs VSMC
GO_BP
GeneRatio
p.adjust
muscle system process
muscle contraction
actin filament organization
cell-substrate adhesion
muscle cell differentiation
actomyosin structure organization
muscle tissue development
extracellular matrix organization
extracellular structure organization
external encapsulating structure organization
muscle cell development
muscle cell migration
myofibril assembly
wound healing
striated muscle cell development
regulation of cell-substrate adhesion
striated muscle cell differentiation
cell-matrix adhesion
smooth muscle cell migration
heart contraction
extracellular matrix organization
extracellular structure organization
external encapsulating structure organization
cell-substrate adhesion
wound healing
negative regulation of locomotion
cell chemotaxis
negative regulation of cell motility
negative regulation of cell migration
leukocyte migration
hemostasis
regulation of cell-cell adhesion
leukocyte cell-cell adhesion
regulation of immune effector process
ossification
lung development
respiratory tube development
regulation of vasculature development
blood coagulation
regulation of leukocyte proliferation

Figure 4.4. Identification of cell clusters in IKKβ$^{\Delta Fib}$LDLR$^{-/-}$ and IKKβ$^{F/F}$LDLR$^{-/-}$ mouse aortas by scRNA-seq

Four-week-old male IKKβ$^{\Delta Fib}$LDLR$^{-/-}$ and IKKβ$^{F/F}$LDLR$^{-/-}$ mice were i.p. injected with 75mg/kg tamoxifen per day for 5 days to induce Cre expression. At six-weeks-old those mice were fed a HFD for twelve weeks. The aortic arch, brachiocephalic artery, and carotid arteries were isolated and processed for scRNA-seq. 3 mice per condition were pooled for analysis. (**A**) UMAP of all cells that passed quality assessment, and the identity of each cluster was assigned using marker genes. (**B**) UMAP of annotated cell clusters based on marker genes. (**C**) Feature plots showing VSMC markers (*Myh11, Acta2*) and Fibroblast markers (*Dcn, Lum*) (**D**) Gene Ontology (GO) biological process pathway analysis showing the differences between the Transitioning1 cluster and the FibroblasCol1 clusters or VSMC clusters.

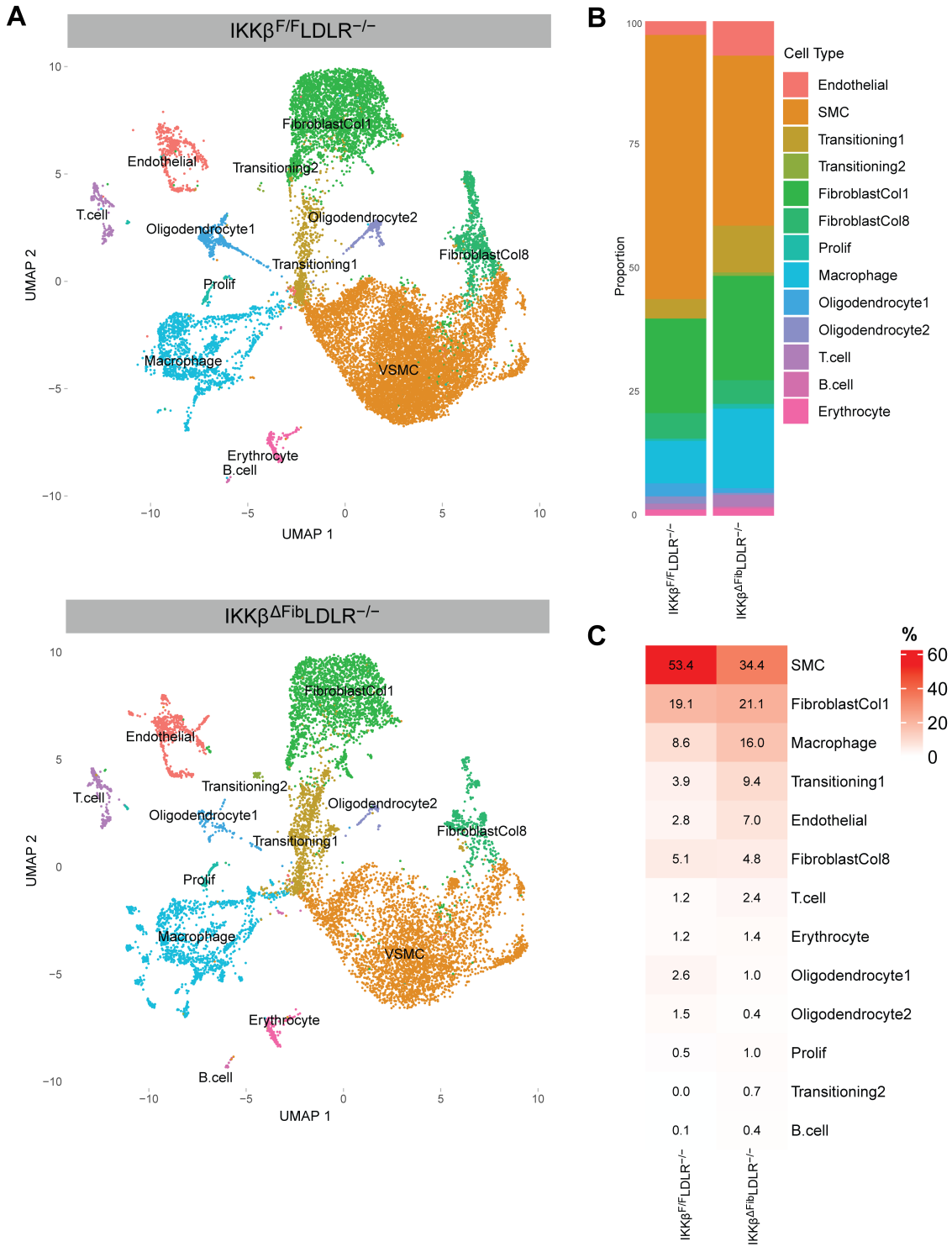
A
IKKβF/FLDLR−/−
FibroblastCol1
Endothelial
Transitioning2
T.cell
Oligodendrocyte1
Oligodendrocyte2
Transitioning1
FibroblastCol8
Prolif
Macrophage
VSMC
Erythrocyte
B.cell
UMAP 2
UMAP 1
IKKβΔFibLDLR−/−
B
Proportion
Cell Type
Endothelial
SMC
Transitioning1
Transitioning2
FibroblastCol1
FibroblastCol8
Prolif
Macrophage
Oligodendrocyte1
Oligodendrocyte2
T.cell
B.cell
Erythrocyte
C
%
SMC 53.4 34.4
FibroblastCol1 19.1 21.1
Macrophage 8.6 16.0
Transitioning1 3.9 9.4
Endothelial 2.8 7.0
FibroblastCol8 5.1 4.8
T.cell 1.2 2.4
Erythrocyte 1.2 1.4
Oligodendrocyte1 2.6 1.0
Oligodendrocyte2 1.5 0.4
Prolif 0.5 1.0
Transitioning2 0.0 0.7
B.cell 0.1 0.4

Figure 4.5. scRNA-seq analysis reveals shift in VSCM population in IKKβ deficient aortas.

Four-week-old male IKKβ$^{\Delta Fib}$LDLR$^{-/-}$ and IKKβ$^{F/F}$LDLR$^{-/-}$ mice were i.p. injected with 75mg/kg tamoxifen per day for 5 days to induce Cre expression. At six-weeks-old those mice were fed a HFD for twelve weeks. The aortic arch, brachiocephalic artery, and carotid arteries were isolated and processed for scRNA-seq. 3 mice per condition were pooled for analysis. (**A**) UMAP of cell clusters between the two conditions. (**B**) Stacked bar plot of the relative proportions of each cell cluster per condition. (**C**) Percentage value of the proportion of each cell cluster per condition.

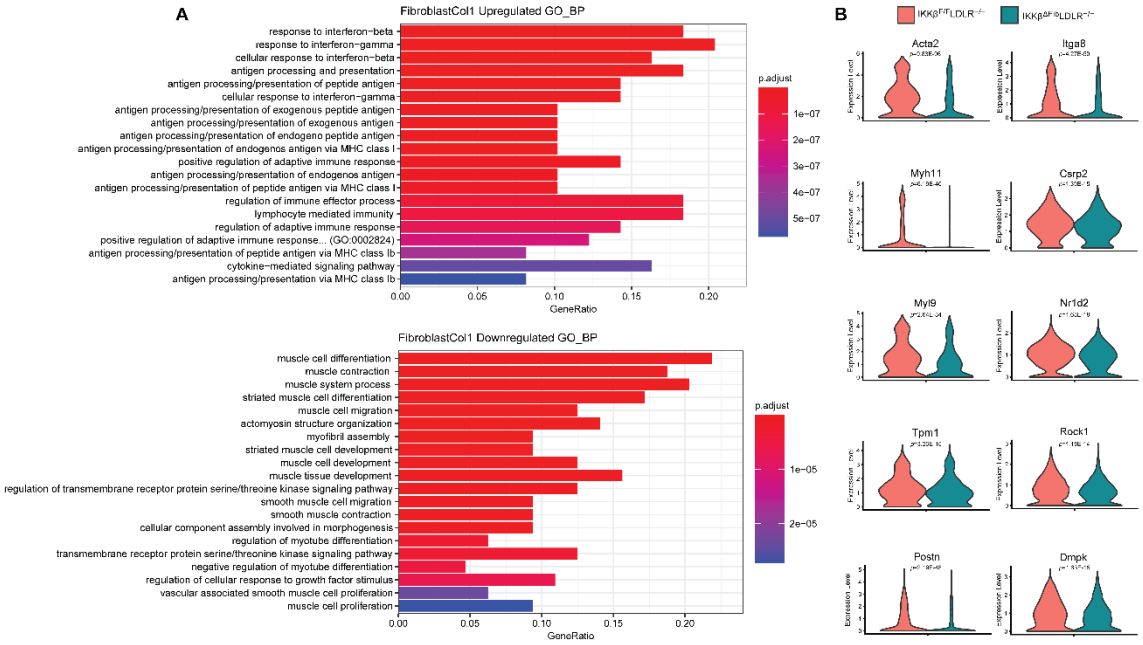

Figure 4.6 scRNA-seq analysis reveals Fibroblast IKKβ deficiency decreases SMC differentiation in aortas.

Four-week-old male IKKβ$^{\Delta Fib}$LDLR$^{-/-}$ and IKKβ$^{F/F}$LDLR$^{-/-}$ mice were i.p. injected with 75mg/kg tamoxifen per day for 5 days to induce Cre expression. At six-weeks-old those mice were fed a HFD for twelve weeks. The aortic arch, brachiocephalic artery, and carotid arteries were isolated and processed for scRNA-seq. 3 mice per condition were pooled for analysis. (**A**) Gene Ontology (GO) Biological Process enrichment analysis of the FibroblastCol1 cluster between IKKβ$^{\Delta Fib}$LDLR$^{-/-}$ and IKKβ$^{F/F}$LDLR$^{-/-}$ aortas. (**B**) Violin plots of the expression of selected genes from the downregulated GO BP analysis for the FibroblastCol1 cluster from IKKβ$^{\Delta Fib}$LDLR$^{-/-}$ and IKKβ$^{F/F}$LDLR$^{-/-}$ aortas.

5. Chapter 5: Conclusion and Future Directions

Atherosclerosis has remained the leading cause of mortality worldwide despite significant advancements in the understanding of its etiology. This compilation of studies revealed the role of unexpected contributors of atherosclerosis development including tsRNAs/rsRNAs, paternal diet, and adventitial fibroblasts. The following sections in this chapter will discuss the main findings and future directions needed to confirm our results and hypothesis, or to expand on the current findings.

5.1 tsRNAs in atherosclerosis development

Research surrounding tsRNAs and rsRNAs has been gaining much attention recently, and progress has been made in elucidating their functions in cancers and neurological diseases (56, 293, 294). However, highly modified sncRNAs, such as tsRNAs and rsRNAs, often escape detection due to the limitations of traditional-sequencing methods. The newly developed PANDORA-seq method overcomes the limitations of traditional-seq and detects tsRNAs/rsRNAs at a higher capacity (59). We revealed a large population of dysregulated tsRNAs/rsRNAs in the intima of high cholesterol-fed atherogenic mice, which may have inflammatory functions. One of the HCD-stimulated upregulated tsRNAs, tsRNA-Arg-CCG, induced genes related to endothelial dysfunction in vitro.

5.1.1 Exploring the mechanism of tsRNA-Arg-CCG

It is important to point out that although modifications on tsRNAs hinder their detection, these modifications are essential for their structure and function (31, 61, 72,

146). For example, the tsRNA modification pseudouridylation is essential for controlling translation that dictates stem cell fates. Dysregulation of pseudouridylation on tsRNAs was implicated in diseases such as myelodysplastic syndrome (295). Endogenous modifications on HCD-induced tsRNA-Arg-CCG were not investigated and the synthetic tsRNA-Arg-CCG oligo used in our study did not contain modifications. Therefore, our in vitro studies do not entirely reflect endogenous conditions, and it is possible that endogenous tsRNA-Arg-CCG may elicit an exacerbated response. To test this, tsRNA-Arg-CCG can be isolated from mouse tissue via a biotinylated pull-down method using a complimentary synthesized biotinylated tsRNA oligo, and further purifying the sample through size selection. The purified endogenous tsRNA-Arg-CCG can then be used in future experiments to assess its role in vascular inflammation and endothelial dysfunction. Whether tsRNAs/rsRNAs identified by PANDORA-seq can also be used as biomarkers for advanced or unstable plaques would be of great translational interest and should be investigated in future studies.

Besides regulating gene expression, tsRNA fragments can also act as “sponges” to sequester proteins and prevent them from interacting with their targets. For instance, tRNA-Glu, tRNA-Asp, tRNA-Gly, and tRNA-Tyr fragments can sequester the oncogenic Y-box binding protein to suppress tumor formation. It would be interesting to investigate whether tsRNA-Arg-CCG regulates atherogenic inflammatory genes via IkB sponging to increase Nf-kB nuclear localization, which can be determined via the pull-down method mentioned previously to identify tsRNA-protein interactions via LC-MS/MS (296, 297).

Results from these experiments would provide insight into the pro-atherogenic roles and mechanism of action of tsRNA-Arg-CCG, which would advance the field.

5.2 The effects of paternal hypercholesterolemia on atherosclerosis and sperm sncRNA profile

Studies have suggested that the presence of parental risk factors can transmit cardiovascular disease to their offspring (21, 24, 25, 29). However, majority of these studies have only investigated inheritance through the maternal side. Whether the paternal presence of atherogenic risk factors can also affect offspring cardiovascular health remains elusive. In addition, small non-coding RNAs (sncRNAs) in sperm act as epigenetic agents in mediating offspring's metabolic phenotypes (32) and are sensitive to changes in expression and modification patterns by dietary exposures (30, 61, 71, 79, 298, 299). It has been previously demonstrated that that the expression patterns of tsRNAs and rsRNAs in sperm, along with their associated RNA modifications establishes the "sperm RNA code" required for intergenerational transmission of paternally acquired metabolic disorders (30, 32, 79). Several studies have confirmed that injection of dysregulated sperm small RNAs into zygotes can transmit paternal phenotypes to offspring (30, 79, 80, 257, 300, 301).

In our study, we identified paternal exposure to a HCD led to increased atherosclerosis in their female offspring. We also revealed that a high cholesterol diet (HCD) can alter the expression patterns of sperm tsRNAs/rsRNAs, which were associated with expression changes in sncRNA-biogenesis related genes in the epididymis. Collectively, these results support the idea that paternal hypercholesterolemia alters components of the sperm RNA code, possibly linked to increased atherosclerosis of the

offspring. A pool of upregulated tsRNAs and rsRNAs that were identified with PANDORA-seq were able to induce early transcription changes in embryoid bodies, but whether this translates to atherosclerosis development in the offspring remains to be explored. Nonetheless, these studies suggest paternal hypercholesterolemia may be imprinted in the germline that affects atherosclerosis development in the offspring. These studies also provide a foundation to facilitate more research on tsRNA/rsRNA epigenetic regulation of atherosclerosis.

5.2.1 Exploring tsRNAs/rsRNAs as epigenetic carriers of atherosclerosis

Several groups have confirmed that the injection of sperm RNA can elicit health-related dysfunction in offspring (30, 79, 80, 257, 300, 301). We hypothesize that features of atherosclerosis are imprinted in the "sperm RNA code" from HCD-fed mice. To test this hypothesis, sperm sncRNA fragments from HCD or LCD-fed LDLR−/− mice can be injected into normal zygotes to generate viable offspring. The cardiometabolic phenotype of the offspring from injected zygotes would determine if HCD-derived sperm sncRNAs can recapitulate similar phenotypes observed in our studies, thus providing evidence that sperm may carry an atherogenic "RNA code."

Besides investigating the phenotypic effects of sperm sncRNAs on offspring cardiometabolic health, their effects on early embryonic development would provide additional insight into their mechanism of action. Several studies have investigated the impact of sperm sncRNAs on early embryonic development. These studies have found essential pathways dysregulated in embryos form injected zygotes such as metabolic regulation (30) and mitochondria energy production (45) that proceeds to affect adult

offspring health. To establish a mechanism of sperm sncRNA-mediated atherogenesis in the offspring, we would need to analyze the altered pathways during embryonic development and correlate these findings with the offspring phenotype. Together these studies will identify the effects of HCD-induced dysregulated sperm on offspring cardiometabolic health and contribute to the advancement of sperm RNA as an epigenetic regulator.

5.3 The role of fibroblast IKKβ on atherosclerotic plaque stability

The study of the adventitial layer in atherogenesis has been largely ignored due to the lack of understanding of its contribution to vascular disease. The adventitia is a complex layer consisting of multiple cell populations with the fibroblast being the most abundant cell type. Fibroblasts become activated in response to external factors and changes in the microenvironment (276). However, their role in atherosclerosis development has not been well studied. IKKβ is a known pro-atherogenic molecule that drives the inflammatory response in the inner vascular wall. However, IKKβ has many other substrates whose downstream roles include cell survival, proliferation, and differentiation (133) and its function in fibroblasts remains elusive.

We investigated the function of adventitial fibroblast IKKβ on atherosclerosis development. While we did not observe any changes in plaque size from fibroblast IKKβ-deficient mice compared with controls, we did observe a decrease in plaque stability. Interestingly, single cell-sequencing revealed a decrease in the smooth muscle cell population in fibroblast IKKβ-deficient aortas, consistent with human studies showing VSMCs are reduced in ruptured plaques (12). Gene enrichment pathway analysis revealed

that the reduced VSMC population could be a result of impaired fibroblast-to-VSMC differentiation. These results reveal the important role of fibroblast IKKβ signaling in plaque stabilization via VSMC differentiation, but more studies are needed to confirm and strengthen these results.

5.3.1 Exploring the role and mechanism of IKKβ on fibroblast activity

Several studies have reported that fibroblasts migrate to the intima to contribute to neointima formation (287, 288). However, fewer studies have reported on the role of fibroblasts on atherosclerosis development despite early reports of adventitial pathology in patients with atherosclerosis (191, 275, 290, 291). We hypothesize that plaque VSMCs can be derived from adventitial fibroblasts, and IKKβ deficiency decreases fibroblast to VSMC differentiation and migration. Future studies will utilize a reporter mouse model (mTmG) to track the fate of Col1a2-CreERT-expressing fibroblasts after 12 weeks of HFD. The reporter model would reveal whether Col1a2-CreERT expressing cells migrate from the adventitia to the cap or other areas of the plaque (i.e., necrotic core). scRNA-seq may also be performed on aortas of reporter mice to confirm the cellular identities of Col1a2-CreERT expressing cells after 12 weeks HFD and whether they do indeed contribute to VSMC clusters.

We previously demonstrated that angiotensin-II treatment on primary cardiac fibroblasts increases aSMA expression, which is attenuated by IKKβ knockout (279). To confirm the current single cell-sequencing results, in vitro experiments will be conducted to determine if fibroblast IKKβ deficiency can reduce fibroblast-to-VSMC differentiation after free fatty acid (FFA) treatment. Further in vitro mechanistic experiments may be

performed to determine whether IKKβ regulates fibroblast to VSMC transition via b-catenin degradation or other pathways. Together these experiments will confirm our current hypothesis that plaque VSMCs can be derived from adventitial fibroblasts in an IKKβ-dependent manner.

References

1. Raggi, P., J. Genest, J. T. Giles, K. J. Rayner, G. Dwivedi, R. S. Beanlands, and M. Gupta. 2018. Role of inflammation in the pathogenesis of atherosclerosis and therapeutic interventions. *Atherosclerosis* **276**: 98-108.

2. Ross, R., J. Glomset, and L. Harker. 1977. Response to injury and atherogenesis. *Am J Pathol* **86**: 675-684.

3. Ross, R. 1999. Atherosclerosis--an inflammatory disease. *N Engl J Med* **340**: 115-126.

4. Gareus, R., E. Kotsaki, S. Xanthoulea, I. van der Made, M. J. J. Gijbels, R. Kardakaris, A. Polykratis, G. Kollias, M. P. J. de Winther, and M. Pasparakis. 2008. Endothelial Cell-Specific NF-κB Inhibition Protects Mice from Atherosclerosis. *Cell Metabolism* **8**: 372-383.

5. Hansson, G. K. 2017. Inflammation and Atherosclerosis: The End of a Controversy. *Circulation* **136**: 1875-1877.

6. Libby, P. 2002. Inflammation in atherosclerosis. *Nature* **420**: 868-874.

7. Libby, P. 2012. Inflammation in atherosclerosis. *Arterioscler Thromb Vasc Biol* **32**: 2045-2051.

8. Lusis, A. J. 2000. Atherosclerosis. *Nature* **407**: 233-241.

9. Libby, P., and K. E. Bornfeldt. 2020. How Far We Have Come, How Far We Have Yet to Go in Atherosclerosis Research. *Circ Res* **126**: 1107-1111.

10. Chen, Y. C., A. L. Huang, T. S. Kyaw, A. Bobik, and K. Peter. 2016. Atherosclerotic Plaque Rupture: Identifying the Straw That Breaks the Camel's Back. *Arterioscler Thromb Vasc Biol* **36**: e63-72.

11. Campbell, J. H., and G. R. Campbell. 2012. Smooth muscle phenotypic modulation--a personal experience. *Arterioscler Thromb Vasc Biol* **32**: 1784-1789.

12. van der Wal, A. C., A. E. Becker, C. M. van der Loos, and P. K. Das. 1994. Site of intimal rupture or erosion of thrombosed coronary atherosclerotic plaques is characterized by an inflammatory process irrespective of the dominant plaque morphology. *Circulation* **89**: 36-44.

13. Bentzon, J. F., and E. Falk. 2010. Circulating smooth muscle progenitor cells in atherosclerosis and plaque rupture: current perspective and methods of analysis. *Vascul Pharmacol* **52**: 11-20.

14. Dubner, A. M., S. Lu, A. J. Jolly, K. A. Strand, M. F. Mutryn, T. Hinthorn, T. Noble, R. A. Nemenoff, K. S. Moulton, M. W. Majesky, and M. C. Weiser-Evans. 2023. Smooth muscle-derived adventitial progenitor cells direct atherosclerotic plaque composition complexity in a Klf4-dependent manner. *JCI Insight* **8**.

15. Leong, D. P., P. G. Joseph, M. McKee, S. S. Anand, K. K. Teo, J. D. Schwalm, and S. Yusuf. 2017. Reducing the Global Burden of Cardiovascular Disease, Part 2: Prevention and Treatment of Cardiovascular Disease. *Circ Res* **121**: 695-710.

16. Joseph, P., D. Leong, M. McKee, S. S. Anand, J. D. Schwalm, K. Teo, A. Mente, and S. Yusuf. 2017. Reducing the Global Burden of Cardiovascular Disease, Part 1: The Epidemiology and Risk Factors. *Circ Res* **121**: 677-694.

17. Pembrey, M. E., L. O. Bygren, G. Kaati, S. Edvinsson, K. Northstone, M. Sjöström, J. Golding, and A. S. T. The. 2006. Sex-specific, male-line transgenerational responses in humans. *European Journal of Human Genetics* **14**: 159-166.

18. Kaati, G., L. O. Bygren, and S. Edvinsson. 2002. Cardiovascular and diabetes mortality determined by nutrition during parents' and grandparents' slow growth period. *Eur J Hum Genet* **10**: 682-688.

19. Ravelli, G. P., Z. A. Stein, and M. W. Susser. 1976. Obesity in young men after famine exposure in utero and early infancy. *N Engl J Med* **295**: 349-353.

20. Jawaid, A., K. L. Jehle, and I. M. Mansuy. 2021. Impact of Parental Exposure on Offspring Health in Humans. *Trends Genet* **37**: 373-388.

21. Lloyd-Jones, D. M., B. H. Nam, R. B. D'Agostino, D. Levy, J. M. Murabito, T. J. Wang, P. W. Wilson, and C. J. O'Donnell. 2004. Parental cardiovascular disease as a risk factor for cardiovascular disease in middle-aged adults: a prospective study of parents and offspring. *JAMA* **291**: 2204-2211.

22. Sesso, H. D., I. M. Lee, J. M. Gaziano, K. M. Rexrode, R. J. Glynn, and J. E. Buring. 2001. Maternal and paternal history of myocardial infarction and risk of cardiovascular disease in men and women. *Circulation* **104**: 393-398.

23. Parikh, N. I., S. J. Hwang, M. G. Larson, L. A. Cupples, C. S. Fox, E. S. Manders, J. M. Murabito, J. M. Massaro, U. Hoffmann, and C. J. O'Donnell. 2007. Parental occurrence of premature cardiovascular disease predicts increased coronary artery and abdominal aortic calcification in the Framingham Offspring and Third Generation cohorts. *Circulation* **116**: 1473-1481.

24. Napoli, C., F. P. D'Armiento, F. P. Mancini, A. Postiglione, J. L. Witztum, G. Palumbo, and W. Palinski. 1997. Fatty streak formation occurs in human fetal aortas and is greatly enhanced by maternal hypercholesterolemia. Intimal

accumulation of low density lipoprotein and its oxidation precede monocyte recruitment into early atherosclerotic lesions. *J Clin Invest* **100**: 2680-2690.

25. Napoli, C., C. K. Glass, J. L. Witztum, R. Deutsch, F. P. D'Armiento, and W. Palinski. 1999. Influence of maternal hypercholesterolaemia during pregnancy on progression of early atherosclerotic lesions in childhood: Fate of Early Lesions in Children (FELIC) study. *Lancet* **354**: 1234-1241.

26. Napoli, C., F. de Nigris, J. S. Welch, F. B. Calara, R. O. Stuart, C. K. Glass, and W. Palinski. 2002. Maternal hypercholesterolemia during pregnancy promotes early atherogenesis in LDL receptor-deficient mice and alters aortic gene expression determined by microarray. *Circulation* **105**: 1360-1367.

27. Napoli, C., J. L. Witztum, F. Calara, F. de Nigris, and W. Palinski. 2000. Maternal hypercholesterolemia enhances atherogenesis in normocholesterolemic rabbits, which is inhibited by antioxidant or lipid-lowering intervention during pregnancy: an experimental model of atherogenic mechanisms in human fetuses. *Circ Res* **87**: 946-952.

28. Palinski, W., F. P. D'Armiento, J. L. Witztum, F. de Nigris, F. Casanada, M. Condorelli, M. Silvestre, and C. Napoli. 2001. Maternal hypercholesterolemia and treatment during pregnancy influence the long-term progression of atherosclerosis in offspring of rabbits. *Circ Res* **89**: 991-996.

29. Chen, S. Y., Y. Z. Chen, Y. J. Lee, C. L. Jiang, S. C. Lu, and F. J. Lin. 2021. Maternal hypercholesterolemia exacerbates atherosclerosis lesions in female offspring through potentiating macrophage polarization toward an inflammatory M1 phenotype. *J Nutr Biochem* **90**: 108575.

30. Chen, Q., M. Yan, Z. Cao, X. Li, Y. Zhang, J. Shi, G. H. Feng, H. Peng, X. Zhang, J. Qian, E. Duan, Q. Zhai, and Q. Zhou. 2016. Sperm tsRNAs contribute to intergenerational inheritance of an acquired metabolic disorder. *Science* **351**: 397-400.

31. Zhang, Y., X. Zhang, J. Shi, F. Tuorto, X. Li, Y. Liu, R. Liebers, L. Zhang, Y. Qu, J. Qian, M. Pahima, Y. Liu, M. Yan, Z. Cao, X. Lei, Y. Cao, H. Peng, S. Liu, Y. Wang, H. Zheng, R. Woolsey, D. Quilici, Q. Zhai, L. Li, T. Zhou, W. Yan, F. Lyko, Y. Zhang, Q. Zhou, E. Duan, and Q. Chen. 2018. Dnmt2 mediates intergenerational transmission of paternally acquired metabolic disorders through sperm small non-coding RNAs. *Nat Cell Biol* **20**: 535-540.

32. Zhang, Y., J. Shi, M. Rassoulzadegan, F. Tuorto, and Q. Chen. 2019. Sperm RNA code programmes the metabolic health of offspring. *Nat Rev Endocrinol* **15**: 489-498.

33. Morgan, H. L., P. Paganopoulou, S. Akhtar, N. Urquhart, R. Philomin, Y. Dickinson, and A. J. Watkins. 2020. Paternal diet impairs F1 and F2 offspring vascular function through sperm and seminal plasma specific mechanisms in mice. *J Physiol* **598**: 699-715.

34. Watkins, A. J., and K. D. Sinclair. 2014. Paternal low protein diet affects adult offspring cardiovascular and metabolic function in mice. *Am J Physiol Heart Circ Physiol* **306**: H1444-1452.

35. Watkins, A. J., S. Sirovica, B. Stokes, M. Isaacs, O. Addison, and R. A. Martin. 2017. Paternal low protein diet programs preimplantation embryo gene expression, fetal growth and skeletal development in mice. *Biochim Biophys Acta Mol Basis Dis* **1863**: 1371-1381.

36. Watkins, A. J., I. Dias, H. Tsuro, D. Allen, R. D. Emes, J. Moreton, R. Wilson, R. J. M. Ingram, and K. D. Sinclair. 2018. Paternal diet programs offspring health through sperm- and seminal plasma-specific pathways in mice. *Proc Natl Acad Sci U S A* **115**: 10064-10069.

37. Liu, J., J. Shi, R. Hernandez, X. Li, P. Konchadi, Y. Miyake, Q. Chen, T. Zhou, and C. Zhou. 2023. Paternal phthalate exposure-elicited offspring metabolic disorders are associated with altered sperm small RNAs in mice. *Environ Int* **172**: 107769.

38. Gong, Y., Y. Xue, X. Li, Z. Zhang, W. Zhou, P. Marcolongo, A. Benedetti, S. Mao, L. Han, G. Ding, and Z. Sun. 2021. Inter- and Transgenerational Effects of Paternal Exposure to Inorganic Arsenic. *Adv Sci (Weinh)* **8**: 2002715.

39. Lee, M. K., and B. Blumberg. 2019. Transgenerational effects of obesogens. *Basic Clin Pharmacol Toxicol*.

40. Heindel, J. J., and B. Blumberg. 2019. Environmental Obesogens: Mechanisms and Controversies. *Annu Rev Pharmacol Toxicol* **59**: 89-106.

41. Cao, N., C. Lan, C. Chen, Z. Xu, H. Luo, S. Zheng, X. Gong, H. Ren, Z. Li, S. Qu, C. Yu, J. Yang, P. A. Jose, Y. Chen, G. Wu, C. Hu, J. Yu, and C. Zeng. 2022. Prenatal Lipopolysaccharides Exposure Induces Transgenerational Inheritance of Hypertension. *Circulation* **146**: 1082-1095.

42. Fitz-James, M. H., and G. Cavalli. 2022. Molecular mechanisms of transgenerational epigenetic inheritance. *Nat Rev Genet* **23**: 325-341.

43. Chen, Q., W. Yan, and E. Duan. 2016. Epigenetic inheritance of acquired traits through sperm RNAs and sperm RNA modifications. *Nat Rev Genet* **17**: 733-743.

44. Chen, Q. 2022. Sperm RNA-mediated epigenetic inheritance in mammals: challenges and opportunities. *Reprod Fert Develop* **35**: 118-124.

45. Tomar, A., M. Gomez-Velazquez, R. Gerlini, G. Comas-Armangué, L. Makharadze, T. Kolbe, A. Boersma, M. Dahlhoff, J. P. Burgstaller, M. Lassi, J. Darr, J. Toppari, H. Virtanen, A. Kühnapfel, M. Scholz, K. Landgraf, W. Kiess, M. Vogel, V. Gailus-Durner, H. Fuchs, S. Marschall, M. Hrabě de Angelis, N. Kotaja, A. Körner, and R. Teperino. 2024. Epigenetic inheritance of diet-induced and sperm-borne mitochondrial RNAs. *Nature*: doi:10.1038/s41586-41024-07472-41583.

46. Orgel, L. E., and F. H. Crick. 1980. Selfish DNA: the ultimate parasite. *Nature* **284**: 604-607.

47. Fang, Y., and M. J. Fullwood. 2016. Roles, Functions, and Mechanisms of Long Non-coding RNAs in Cancer. *Genomics Proteomics Bioinformatics* **14**: 42-54.

48. Statello, L., C. J. Guo, L. L. Chen, and M. Huarte. 2021. Gene regulation by long non-coding RNAs and its biological functions. *Nat Rev Mol Cell Biol* **22**: 96-118.

49. Holoch, D., and D. Moazed. 2015. RNA-mediated epigenetic regulation of gene expression. *Nat Rev Genet* **16**: 71-84.

50. Kärkkäinen, E., S. Heikkinen, M. Tengström, V. M. Kosma, A. Mannermaa, and J. M. Hartikainen. 2022. Expression profiles of small non-coding RNAs in breast cancer tumors characterize clinicopathological features and show prognostic and predictive potential. *Sci Rep* **12**: 22614.

51. Badowski, C., B. He, and L. X. Garmire. 2022. Blood-derived lncRNAs as biomarkers for cancer diagnosis: the Good, the Bad and the Beauty. *NPJ Precis Oncol* **6**: 40.

52. Viereck, J., and T. Thum. 2017. Circulating Noncoding RNAs as Biomarkers of Cardiovascular Disease and Injury. *Circ Res* **120**: 381-399.

53. Das, S., R. Shah, S. Dimmeler, J. E. Freedman, C. Holley, J. M. Lee, K. Moore, K. Musunuru, D. Z. Wang, J. Xiao, K. J. Yin, A. H. A. C. o. G. a. P. Medicine, T. r. a. V. B. Council on Arteriosclerosis, C. o. C. a. S. Nursing, and a. C. o. C. Cardiology. 2020. Noncoding RNAs in Cardiovascular Disease: Current Knowledge, Tools and Technologies for Investigation, and Future Directions: A Scientific Statement From the American Heart Association. *Circ Genom Precis Med* **13**: e000062.

54. Xie, Y., L. Yao, X. Yu, Y. Ruan, Z. Li, and J. Guo. 2020. Action mechanisms and research methods of tRNA-derived small RNAs. *Signal Transduct Target Ther* **5**: 109.

55. Chen, Q., X. Zhang, J. Shi, M. Yan, and T. Zhou. 2021. Origins and evolving functionalities of tRNA-derived small RNAs. *Trends in biochemical sciences* **46**: 790-804.

56. Wen, J. T., Z. H. Huang, Q. H. Li, X. Chen, H. L. Qin, and Y. Zhao. 2021. Research progress on the tsRNA classification, function, and application in gynecological malignant tumors. *Cell Death Discov* **7**: 388.

57. He, X., Y. Yang, Q. Wang, J. Wang, S. Li, C. Li, T. Zong, X. Li, Y. Zhang, Y. Zou, and T. Yu. 2021. Expression profiles and potential roles of transfer RNA-derived small RNAs in atherosclerosis. *J Cell Mol Med* **25**: 7052-7065.

58. Hrabeta-Robinson, E., E. Marcus, A. E. Cozen, E. M. Phizicky, and T. M. Lowe. 2017. High-Throughput Small RNA Sequencing Enhanced by AlkB-Facilitated RNA de-Methylation (ARM-Seq). *Methods Mol Biol* **1562**: 231-243.

59. Shi, J., Y. Zhang, D. Tan, X. Zhang, M. Yan, R. Franklin, M. Shahbazi, K. Mackinlay, S. Liu, B. Kuhle, E. R. James, L. Zhang, Y. Qu, Q. Zhai, W. Zhao, L. Zhao, C. Zhou, W. Gu, J. Murn, J. Guo, D. T. Carrell, Y. Wang, X. Chen, B. R. Cairns, X. L. Yang, P. Schimmel, M. Zernicka-Goetz, S. Cheloufi, T. Zhou, and Q. Chen. 2021. PANDORA-seq expands the repertoire of regulatory small RNAs by overcoming RNA modifications. *Nat Cell Biol* **23**: 424-436.

60. Wang, L. K., C. D. Lima, and S. Shuman. 2002. Structure and mechanism of T4 polynucleotide kinase: an RNA repair enzyme. *EMBO J* **21**: 3873-3880.

61. Zhang, X., A. E. Cozen, Y. Liu, Q. Chen, and T. M. Lowe. 2016. Small RNA Modifications: Integral to Function and Disease. *Trends Mol Med* **22**: 1025-1034.

62. Ma, Z., J. Li, L. Fu, R. Fu, N. Tang, Y. Quan, Z. Xin, Z. Ding, and Y. Liu. 2023. Epididymal RNase T2 contributes to astheno-teratozoospermia and intergenerational metabolic disorder through epididymosome-sperm interaction. *BMC Med* **21**: 453.

63. Gibney, E. R., and C. M. Nolan. 2010. Epigenetics and gene expression. *Heredity (Edinb)* **105**: 4-13.

64. Siomi, M. C., K. Sato, D. Pezic, and A. A. Aravin. 2011. PIWI-interacting small RNAs: the vanguard of genome defence. *Nat Rev Mol Cell Biol* **12**: 246-258.

65. Rajasethupathy, P., I. Antonov, R. Sheridan, S. Frey, C. Sander, T. Tuschl, and E. R. Kandel. 2012. A role for neuronal piRNAs in the epigenetic control of memory-related synaptic plasticity. *Cell* **149**: 693-707.

66. Iwasaki, Y. W., M. C. Siomi, and H. Siomi. 2015. PIWI-Interacting RNA: Its Biogenesis and Functions. *Annu Rev Biochem* **84**: 405-433.

67. Zhang, X., X. He, C. Liu, J. Liu, Q. Hu, T. Pan, X. Duan, B. Liu, Y. Zhang, J. Chen, X. Ma, H. Luo, and H. Zhang. 2016. IL-4 Inhibits the Biogenesis of an Epigenetically Suppressive PIWI-Interacting RNA To Upregulate CD1a Molecules on Monocytes/Dendritic Cells. *J Immunol* **196**: 1591-1603.

68. Couvillion, M. T., R. Sachidanandam, and K. Collins. 2010. A growth-essential Tetrahymena Piwi protein carries tRNA fragment cargo. *Genes Dev* **24**: 2742-2747.

69. Kuscu, C., P. Kumar, M. Kiran, Z. Su, A. Malik, and A. Dutta. 2018. tRNA fragments (tRFs) guide Ago to regulate gene expression post-transcriptionally in a Dicer-independent manner. *RNA* **24**: 1093-1105.

70. Boskovic, A., X. Y. Bing, E. Kaymak, and O. J. Rando. 2020. Control of noncoding RNA production and histone levels by a 5' tRNA fragment. *Genes Dev* **34**: 118-131.

71. Peng, H., J. Shi, Y. Zhang, H. Zhang, S. Liao, W. Li, L. Lei, C. Han, L. Ning, Y. Cao, Q. Zhou, Q. Chen, and E. Duan. 2012. A novel class of tRNA-derived small RNAs extremely enriched in mature mouse sperm. *Cell research* **22**: 1609-1612.

72. Chen, Q., M. Yan, Z. Cao, X. Li, Y. Zhang, J. Shi, G. H. Feng, H. Peng, X. Zhang, Y. Zhang, J. Qian, E. Duan, Q. Zhai, and Q. Zhou. 2016. Sperm tsRNAs contribute to intergenerational inheritance of an acquired metabolic disorder. *Science* **351**: 397-400.

73. Skinner, M. K., M. Ben Maamar, I. Sadler-Riggleman, D. Beck, E. Nilsson, M. McBirney, R. Klukovich, Y. Xie, C. Tang, and W. Yan. 2018. Alterations in sperm DNA methylation, non-coding RNA and histone retention associate with DDT-induced epigenetic transgenerational inheritance of disease. *Epigenetics Chromatin* **11**: 8.

74. Schuster, A., M. K. Skinner, and W. Yan. 2016. Ancestral vinclozolin exposure alters the epigenetic transgenerational inheritance of sperm small noncoding RNAs. *Environ Epigenet* **2**.

75. Sharma, U., C. C. Conine, J. M. Shea, A. Boskovic, A. G. Derr, X. Y. Bing, C. Belleannee, A. Kucukural, R. W. Serra, F. Sun, L. Song, B. R. Carone, E. P. Ricci, X. Z. Li, L. Fauquier, M. J. Moore, R. Sullivan, C. C. Mello, M. Garber, and O. J. Rando. 2016. Biogenesis and function of tRNA fragments during sperm maturation and fertilization in mammals. *Science* **351**: 391-396.

76. Yamasaki, S., P. Ivanov, G. F. Hu, and P. Anderson. 2009. Angiogenin cleaves tRNA and promotes stress-induced translational repression. *J Cell Biol* **185**: 35-42.

77. Li, S., and G. F. Hu. 2012. Emerging role of angiogenin in stress response and cell survival under adverse conditions. *J Cell Physiol* **227**: 2822-2826.

78. Su, Z., B. Wilson, P. Kumar, and A. Dutta. 2020. Noncanonical Roles of tRNAs: tRNA Fragments and Beyond. *Annu Rev Genet* **54**: 47-69.

79. Zhang, Y., X. Zhang, J. Shi, F. Tuorto, X. Li, Y. Liu, R. Liebers, L. Zhang, Y. Qu, J. Qian, M. Pahima, M. Yan, Z. Cao, X. Lei, Y. Cao, H. Peng, S. Liu, Y. Wang, H. Zheng, R. Woolsey, D. Quilici, Q. Zhai, L. Li, T. Zhou, W. Yan, F. Lyko, Q. Zhou, E. Duan, and Q. Chen. 2018. Dnmt2 mediates intergenerational transmission of paternally acquired metabolic disorders through sperm small non-coding RNAs. *Nat Cell Biol* **20**: 535-540.

80. Zhang, Y., L. Ren, X. Sun, Z. Zhang, J. Liu, Y. Xin, J. Yu, Y. Jia, J. Sheng, G. F. Hu, R. Zhao, and B. He. 2021. Angiogenin mediates paternal inflammation-induced metabolic disorders in offspring through sperm tsRNAs. *Nat Commun* **12**: 6673.

81. Chan, J. C., C. P. Morgan, N. Adrian Leu, A. Shetty, Y. M. Cisse, B. M. Nugent, K. E. Morrison, E. Jašarević, W. Huang, N. Kanyuch, A. B. Rodgers, N. V. Bhanu, D. S. Berger, B. A. Garcia, S. Ament, M. Kane, C. Neill Epperson, and T. L. Bale. 2020. Reproductive tract extracellular vesicles are sufficient to transmit intergenerational stress and program neurodevelopment. *Nat Commun* **11**: 1499.

82. Sharma, U., C. C. Conine, J. M. Shea, A. Boskovic, A. G. Derr, X. Y. Bing, C. Belleannee, A. Kucukural, R. W. Serra, F. Sun, L. Song, B. R. Carone, E. P. Ricci, X. Z. Li, L. Fauquier, M. J. Moore, R. Sullivan, C. C. Mello, M. Garber, and O. J. Rando. 2016. Biogenesis and function of tRNA fragments during sperm maturation and fertilization in mammals. *Science* **351**: 391-396.

83. Hayden, M. S., and S. Ghosh. 2008. Shared principles in NF-kappaB signaling. *Cell* **132**: 344-362.

84. Baker, R. G., M. S. Hayden, and S. Ghosh. 2011. NF-κB, Inflammation, and Metabolic Disease. *Cell Metabolism* **13**: 11-22.

85. Ma, B., and M. O. Hottiger. 2016. Crosstalk between Wnt/β-Catenin and NF-κB Signaling Pathway during Inflammation. *Frontiers in Immunology* **7**: 378.

86. Lawrence, T. 2009. The nuclear factor NF-kappaB pathway in inflammation. *Cold Spring Harbor perspectives in biology* **1**: a001651-a001651.

87. Zhang, Q., M. J. Lenardo, and D. Baltimore. 2017. 30 Years of NF-kappaB: A Blossoming of Relevance to Human Pathobiology. *Cell* **168**: 37-57.

88. Hinz, M., and C. Scheidereit. 2014. The IκB kinase complex in NF-κB regulation and beyond. *EMBO Rep* **15**: 46-61.

89. Liu, F., Y. Xia, A. S. Parker, and I. M. Verma. 2012. IKK biology. *Immunological reviews* **246**: 239-253.

90. Brand, K., S. Page, G. Rogler, A. Bartsch, R. Brandl, R. Knuechel, M. Page, C. Kaltschmidt, P. A. Baeuerle, and D. Neumeier. 1996. Activated transcription factor nuclear factor-kappa B is present in the atherosclerotic lesion. *The Journal of Clinical Investigation* **97**: 1715-1722.

91. Hajra, L., A. I. Evans, M. Chen, S. J. Hyduk, T. Collins, and M. I. Cybulsky. 2000. The NF-kappa B signal transduction pathway in aortic endothelial cells is primed for activation in regions predisposed to atherosclerotic lesion formation. *Proceedings of the National Academy of Sciences of the United States of America* **97**: 9052-9057.

92. Brand, K., T. Eisele, U. Kreusel, M. Page, S. Page, M. Haas, A. Gerling, C. Kaltschmidt, F. J. Neumann, N. Mackman, P. A. Baeurele, A. K. Walli, and D. Neumeier. 1997. Dysregulation of monocytic nuclear factor-kappa B by oxidized low-density lipoprotein. *Arterioscler Thromb Vasc Biol* **17**: 1901-1909.

93. Bennett, B. L., R. G. Lacson, C. C. Chen, R. Cruz, J. S. Wheeler, R. F. Kletzien, A. G. Tomasselli, R. L. Heinrikson, and A. M. Manning. 1996. Identification of signal-induced IkappaB-alpha kinases in human endothelial cells. *J Biol Chem* **271**: 19680-19688.

94. Bourcier, T., G. Sukhova, and P. Libby. 1997. The nuclear factor kappa-B signaling pathway participates in dysregulation of vascular smooth muscle cells in vitro and in human atherosclerosis. *J Biol Chem* **272**: 15817-15824.

95. Monaco, C., E. Andreakos, S. Kiriakidis, C. Mauri, C. Bicknell, B. Foxwell, N. Cheshire, E. Paleolog, and M. Feldmann. 2004. Canonical pathway of nuclear factor kappa B activation selectively regulates proinflammatory and prothrombotic responses in human atherosclerosis. *Proc Natl Acad Sci U S A* **101**: 5634-5639.

96. de Winther Menno, P. J., E. Kanters, G. Kraal, and H. Hofker Marten. 2005. Nuclear Factor κB Signaling in Atherogenesis. *Arteriosclerosis, Thrombosis, and Vascular Biology* **25**: 904-914.

97. Meiler, S. E., R. R. Hung, R. E. Gerszten, J. Gianetti, L. Li, T. Matsui, J. M. A. Gimbrone, and A. Rosenzweig. 2002. Endothelial IKK β Signaling is Required for

Monocyte Adhesion under Laminar Flow Conditions. *Journal of Molecular and Cellular Cardiology* **34**: 349-359.

98. Mussbacher, M., M. Salzmann, B. Haigl, J. Basílio, B. Hochreiter, V. Gleitsmann, B. Moser, B. Hoesel, B. E. Suur, F. Puhm, C. Ungerböck, M. Kuttke, M. J. Forteza, C. J. Binder, D. F. J. Ketelhuth, A. Assinger, and J. A. Schmid. 2020. Ikk2-mediated inflammatory activation of arterial endothelial cells promotes the development and progression of atherosclerosis. *Atherosclerosis* **307**: 21-31.

99. Lesniewski, L. A., J. R. Durrant, M. L. Connell, B. J. Folian, A. J. Donato, and D. R. Seals. 2011. Salicylate treatment improves age-associated vascular endothelial dysfunction: potential role of nuclear factor kappaB and forkhead Box O phosphorylation. *J Gerontol A Biol Sci Med Sci* **66**: 409-418.

100. Yang, S., H. Q. Yuan, Y. M. Hao, Z. Ren, S. L. Qu, L. S. Liu, D. H. Wei, Z. H. Tang, J. F. Zhang, and Z. S. Jiang. 2020. Macrophage polarization in atherosclerosis. *Clin Chim Acta* **501**: 142-146.

101. Fong, C. H., M. Bebien, A. Didierlaurent, R. Nebauer, T. Hussell, D. Broide, M. Karin, and T. Lawrence. 2008. An antiinflammatory role for IKKbeta through the inhibition of "classical" macrophage activation. *J Exp Med* **205**: 1269-1276.

102. Porta, C., M. Rimoldi, G. Raes, L. Brys, P. Ghezzi, D. Di Liberto, F. Dieli, S. Ghisletti, G. Natoli, P. De Baetselier, A. Mantovani, and A. Sica. 2009. Tolerance and M2 (alternative) macrophage polarization are related processes orchestrated by p50 nuclear factor kappaB. *Proc Natl Acad Sci U S A* **106**: 14978-14983.

103. Kanters, E., M. Pasparakis, M. J. J. Gijbels, M. N. Vergouwe, I. Partouns-Hendriks, R. J. A. Fijneman, B. E. Clausen, I. Förster, M. M. Kockx, K. Rajewsky, G. Kraal, M. H. Hofker, and M. P. J. de Winther. 2003. Inhibition of NF-κB activation in macrophages increases atherosclerosis in LDL receptor–deficient mice. *The Journal of Clinical Investigation* **112**: 1176-1185.

104. Goossens, P., M. N. Vergouwe, M. J. J. Gijbels, D. M. J. Curfs, J. H. G. van Woezik, M. A. Hoeksema, S. Xanthoulea, P. J. M. Leenen, R. A. Rupec, M. H. Hofker, and M. P. J. de Winther. 2011. Myeloid IκBα deficiency promotes atherogenesis by enhancing leukocyte recruitment to the plaques. *PloS one* **6**: e22327-e22327.

105. Ferreira, V., K. W. van Dijk, A. K. Groen, R. M. Vos, J. van der Kaa, M. J. J. Gijbels, L. M. Havekes, and H. Pannekoek. 2007. Macrophage-specific inhibition of NF-κB activation reduces foam-cell formation. *Atherosclerosis* **192**: 283-290.

106. Park, S.-H., Y. Sui, F. Gizard, J. Xu, J. Rios-Pilier, N. Helsley Robert, S.-S. Han, and C. Zhou. 2012. Myeloid-Specific IκB Kinase β Deficiency Decreases

Atherosclerosis in Low-Density Lipoprotein Receptor–Deficient Mice. *Arteriosclerosis, Thrombosis, and Vascular Biology* **32**: 2869-2876.

107. Basatemur, G. L., H. F. Jørgensen, M. C. H. Clarke, M. R. Bennett, and Z. Mallat. 2019. Vascular smooth muscle cells in atherosclerosis. *Nat Rev Cardiol* **16**: 727-744.

108. Sasu, S., and D. Beasley. 2000. Essential roles of IκB kinases α and β in serum- and IL-1-induced human VSMC proliferation. *American Journal of Physiology-Heart and Circulatory Physiology* **278**: H1823-H1831.

109. Sui, Y., S.-H. Park, J. Xu, S. Monette, R. N. Helsley, S.-S. Han, and C. Zhou. 2014. IKKβ links vascular inflammation to obesity and atherosclerosis. *Journal of Experimental Medicine* **211**: 869-886.

110. Helsley, R. N., Y. Sui, S.-H. Park, Z. Liu, R. G. Lee, B. Zhu, P. A. Kern, and C. Zhou. 2016. Targeting IκB kinase β in Adipocyte Lineage Cells for Treatment of Obesity and Metabolic Dysfunctions. *STEM CELLS* **34**: 1883-1895.

111. Sui, Y., Z. Liu, S.-H. Park, S. E. Thatcher, B. Zhu, J. P. Fernandez, H. Molina, P. A. Kern, and C. Zhou. 2018. IKKβ is a β-catenin kinase that regulates mesenchymal stem cell differentiation. *JCI Insight* **3**.

112. Ross, S. E., N. Hemati, K. A. Longo, C. N. Bennett, P. C. Lucas, R. L. Erickson, and O. A. MacDougald. 2000. Inhibition of adipogenesis by Wnt signaling. *Science* **289**: 950-953.

113. Rosen, E. D., and O. A. MacDougald. 2006. Adipocyte differentiation from the inside out. *Nature reviews. Molecular cell biology* **7**: 885-896.

114. Nandipati, K. C., S. Subramanian, and D. K. Agrawal. 2017. Protein kinases: mechanisms and downstream targets in inflammation-mediated obesity and insulin resistance. *Mol Cell Biochem* **426**: 27-45.

115. Gual, P., Y. Le Marchand-Brustel, and J. F. Tanti. 2005. Positive and negative regulation of insulin signaling through IRS-1 phosphorylation. *Biochimie* **87**: 99-109.

116. Gao, Z., D. Hwang, F. Bataille, M. Lefevre, D. York, M. J. Quon, and J. Ye. 2002. Serine phosphorylation of insulin receptor substrate 1 by inhibitor kappa B kinase complex. *J Biol Chem* **277**: 48115-48121.

117. Luo, C., H. Yang, C. Tang, G. Yao, L. Kong, H. He, and Y. Zhou. 2015. Kaempferol alleviates insulin resistance via hepatic IKK/NF-κB signal in type 2 diabetic rats. *Int Immunopharmacol* **28**: 744-750.

118. Yuan, Y. L., B. Q. Lin, C. F. Zhang, L. L. Cui, S. X. Ruan, Z. L. Yang, F. Li, and D. Ji. 2016. Timosaponin B-II Ameliorates Palmitate-Induced Insulin Resistance and Inflammation via IRS-1/PI3K/Akt and IKK/NF-[Formula: see text]B Pathways. *Am J Chin Med* **44**: 755-769.

119. Zhou, X., and S. You. 2014. Rosiglitazone inhibits hepatic insulin resistance induced by chronic pancreatitis and IKK-β/NF-κB expression in liver. *Pancreas* **43**: 1291-1298.

120. Gao, J., J. Song, M. Du, and X. Mao. 2018. Bovine α-Lactalbumin Hydrolysates (α-LAH) Ameliorate Adipose Insulin Resistance and Inflammation in High-Fat Diet-Fed C57BL/6J Mice. *Nutrients* **10**.

121. Hotamisligil, G. S. 2006. Inflammation and metabolic disorders. *Nature* **444**: 860-867.

122. Jiao, P., J. Ma, B. Feng, H. Zhang, J. Alan-Diehl, Y. Eugene-Chin, W. Yan, and H. Xu. 2011. FFA-Induced Adipocyte Inflammation and Insulin Resistance: Involvement of ER Stress and IKKβ Pathways. *Obesity* **19**: 483-491.

123. Wang, M., X. Chen, Z. Zheng, S. Yu, B. Zhou, Y. Liu, D. Liu, Y. Chen, and X. Qian. 2020. Beneficial effect of ER stress preconditioning in protection against FFA-induced adipocyte inflammation via XBP1 in 3T3-L1 adipocytes. *Mol Cell Biochem* **463**: 45-55.

124. Liu, J., D. Ibi, K. Taniguchi, J. Lee, H. Herrema, B. Akosman, P. Mucka, M. A. Salazar Hernandez, M. F. Uyar, S. W. Park, M. Karin, and U. Ozcan. 2016. Inflammation Improves Glucose Homeostasis through IKKβ-XBP1s Interaction. *Cell* **167**: 1052-1066.e1018.

125. Jiao, P., B. Feng, J. Ma, Y. Nie, E. Paul, Y. Li, and H. Xu. 2012. Constitutive Activation of IKKβ in Adipose Tissue Prevents Diet-Induced Obesity in Mice. *Endocrinology* **153**: 154-165.

126. Park, S.-H., Z. Liu, Y. Sui, R. N. Helsley, B. Zhu, D. K. Powell, P. A. Kern, and C. Zhou. 2016. IKKβ Is Essential for Adipocyte Survival and Adaptive Adipose Remodeling in Obesity. *Diabetes* **65**: 1616.

127. Kwon, H., S. Laurent, Y. Tang, H. Zong, P. Vemulapalli, and J. E. Pessin. 2014. Adipocyte-specific IKKβ signaling suppresses adipose tissue inflammation through an IL-13-dependent paracrine feedback pathway. *Cell Rep* **9**: 1574-1583.

128. Libby, P. 2002. Inflammation in atherosclerosis. *Nature* **420**: 868-874.

129. Libby, P., P. M. Ridker, and A. Maseri. 2002. Inflammation and atherosclerosis. *Circulation* **105**: 1135-1143.

130. Sage, A. P., and Z. Mallat. 2017. Readapting the adaptive immune response - therapeutic strategies for atherosclerosis. *Br J Pharmacol* **174**: 3926-3939.

131. Lu, W., S. H. Park, Z. Meng, F. Wang, and C. Zhou. 2019. Deficiency of Adipocyte IKKbeta Affects Atherosclerotic Plaque Vulnerability in Obese LDLR Deficient Mice. *Journal of the American Heart Association* **8**: e012009.

132. Gimbrone, M. A., and G. García-Cardeña. 2016. Endothelial Cell Dysfunction and the Pathobiology of Atherosclerosis. *Circ Res* **118**: 620-636.

133. Hernandez, R., and C. Zhou. 2021. Recent Advances in Understanding the Role of IKKbeta in Cardiometabolic Diseases. *Front Cardiovasc Med* **8**: 752337.

134. Ferreira, V., K. W. van Dijk, A. K. Groen, R. M. Vos, J. van der Kaa, M. J. Gijbels, L. M. Havekes, and H. Pannekoek. 2007. Macrophage-specific inhibition of NF-kappaB activation reduces foam-cell formation. *Atherosclerosis* **192**: 283-290.

135. Park, S. H., Y. Sui, F. Gizard, J. Xu, J. Rios-Pilier, R. N. Helsley, S. S. Han, and C. Zhou. 2012. Myeloid-specific IkappaB kinase beta deficiency decreases atherosclerosis in low-density lipoprotein receptor-deficient mice. *Arterioscler Thromb Vasc Biol* **32**: 2869-2876.

136. Lusis, A. J. 2000. Atherosclerosis. *Nature* **407**: 233-241.

137. Sui, Y., S. H. Park, R. N. Helsley, M. Sunkara, F. J. Gonzalez, A. J. Morris, and C. Zhou. 2014. Bisphenol A increases atherosclerosis in pregnane X receptor-humanized ApoE deficient mice. *Journal of the American Heart Association* **3**: e000492.

138. Liu, J., R. Hernandez, X. Li, Z. Meng, H. Chen, and C. Zhou. 2022. Pregnane X Receptor Mediates Atherosclerosis Induced by Dicyclohexyl Phthalate in LDL Receptor-Deficient Mice. *Cells* **11**: 1125.

139. Helsley, R. N., and C. Zhou. 2017. Epigenetic impact of endocrine disrupting chemicals on lipid homeostasis and atherosclerosis: a pregnane X receptor-centric view. *Environ Epigenet* **3**: dvx017.

140. Lind, L., J. A. Araujo, A. Barchowsky, S. Belcher, B. R. Berridge, N. Chiamvimonvat, W. A. Chiu, V. J. Cogliano, S. Elmore, A. K. Farraj, A. V. Gomes, C. M. McHale, K. B. Meyer-Tamaki, N. G. Posnack, H. M. Vargas, X. Yang, L. Zeise, C. Zhou, and M. T. Smith. 2021. Key Characteristics of Cardiovascular Toxicants. *Environ Health Perspect* **129**: 95001.

141. Wei, T., J. Liu, D. Zhang, X. Wang, G. Li, R. Ma, G. Chen, X. Lin, and X. Guo. 2021. The Relationship Between Nutrition and Atherosclerosis. *Front Bioeng Biotechnol* **9**: 635504.

142. Lu, Y., T. Thavarajah, W. Gu, J. Cai, and Q. Xu. 2018. Impact of miRNA in Atherosclerosis. *Arterioscler Thromb Vasc Biol* **38**: e159-e170.

143. Feinberg, M. W., and K. J. Moore. 2016. MicroRNA Regulation of Atherosclerosis. *Circ Res* **118**: 703-720.

144. Wysoczynski, M., J. Kim, J. B. t. Moore, and S. Uchida. 2020. Macrophage Long Non-Coding RNAs in Pathogenesis of Cardiovascular Disease. *Noncoding RNA* **6**.

145. Simion, V., H. Zhou, J. B. Pierce, D. Yang, S. Haemmig, Y. Tesmenitsky, G. Sukhova, P. H. Stone, P. Libby, and M. W. Feinberg. 2020. LncRNA VINAS regulates atherosclerosis by modulating NF-κB and MAPK signaling. *JCI Insight* **5**: e140627.

146. Shi, J., T. Zhou, and Q. Chen. 2022. Exploring the expanding universe of small RNAs. *Nat Cell Biol* **24**: 415-423.

147. Shi, J., Y. Zhang, D. Tan, X. Zhang, M. Yan, Y. Zhang, R. Franklin, M. Shahbazi, K. Mackinlay, S. Liu, B. Kuhle, E. R. James, L. Zhang, Y. Qu, Q. Zhai, W. Zhao, L. Zhao, C. Zhou, W. Gu, J. Murn, J. Guo, D. T. Carrell, Y. Wang, X. Chen, B. R. Cairns, X. L. Yang, P. Schimmel, M. Zernicka-Goetz, S. Cheloufi, Y. Zhang, T. Zhou, and Q. Chen. 2021. PANDORA-seq expands the repertoire of regulatory small RNAs by overcoming RNA modifications. *Nat Cell Biol* **23**: 424-436.

148. Rigoutsos, I., E. Londin, and Y. Kirino. 2019. Short RNA regulators: the past, the present, the future, and implications for precision medicine and health disparities. *Current Opinion in Biotechnology* **58**: 202-210.

149. Quintana, J. F., S. Kumar, A. Ivens, F. W. N. Chow, A. M. Hoy, A. Fulton, P. Dickinson, C. Martin, M. Taylor, S. A. Babayan, and A. H. Buck. 2019. Comparative analysis of small RNAs released by the filarial nematode Litomosoides sigmodontis in vitro and in vivo. *PLOS Neglected Tropical Diseases* **13**: e0007811.

150. Hoen, E. N. M., H. P. J. Buermans, M. Waasdorp, W. Stoorvogel, M. H. M. Wauben, and P. A. C. Hoen. 2012. Deep sequencing of RNA from immune cell-derived vesicles uncovers the selective incorporation of small non-coding RNA biotypes with potential regulatory functions. *Nucleic Acids Research* **40**: 9272-9285.

151. Sergiev, P. V., N. A. Aleksashin, A. A. Chugunova, Y. S. Polikanov, and O. A. Dontsova. 2018. Structural and evolutionary insights into ribosomal RNA methylation. *Nat Chem Biol* **14**: 226-235.

152. Phizicky, E. M., and A. K. Hopper. 2010. tRNA biology charges to the front. *Genes Dev* **24**: 1832-1860.

153. Schimmel, P. 2018. The emerging complexity of the tRNA world: mammalian tRNAs beyond protein synthesis. *Nature reviews. Molecular cell biology* **19**: 45-58.

154. Honda, S., P. Loher, M. Shigematsu, J. P. Palazzo, R. Suzuki, I. Imoto, I. Rigoutsos, and Y. Kirino. 2015. Sex hormone-dependent tRNA halves enhance cell proliferation in breast and prostate cancers. *Proc Natl Acad Sci U S A* **112**: E3816-3825.

155. Akiyama, Y., S. M. Lyons, M. M. Fay, T. Abe, P. Anderson, and P. Ivanov. 2019. Multiple ribonuclease A family members cleave transfer RNAs in response to stress. *biorxiv*.

156. Shigematsu, M., T. Kawamura, and Y. Kirino. 2018. Generation of 2',3'-Cyclic Phosphate-Containing RNAs as a Hidden Layer of the Transcriptome. *Front Genet* **9**: 562.

157. Zheng, G., Y. Qin, W. C. Clark, Q. Dai, C. Yi, C. He, A. M. Lambowitz, and T. Pan. 2015. Efficient and quantitative high-throughput tRNA sequencing. *Nature methods* **12**: 835-837.

158. Cozen, A. E., E. Quartley, A. D. Holmes, E. Hrabeta-Robinson, E. M. Phizicky, and T. M. Lowe. 2015. ARM-seq: AlkB-facilitated RNA methylation sequencing reveals a complex landscape of modified tRNA fragments. *Nature methods* **12**: 879-884.

159. Teupser, D., A. D. Persky, and J. L. Breslow. 2003. Induction of atherosclerosis by low-fat, semisynthetic diets in LDL receptor-deficient C57BL/6J and FVB/NJ mice: comparison of lesions of the aortic root, brachiocephalic artery, and whole aorta (en face measurement). *Arterioscler Thromb Vasc Biol* **23**: 1907-1913.

160. Meng, Z., R. Hernandez, J. Liu, T. Gwag, W. Lu, T. K. Hsiai, M. Kaul, T. Zhou, and C. Zhou. 2022. HIV Protein Tat Induces Macrophage Dysfunction and Atherosclerosis Development in Low-Density Lipoprotein Receptor-Deficient Mice. *Cardiovasc Drugs Ther* **36**: 201-215.

161. Sui, Y., S. H. Park, J. Xu, S. Monette, R. N. Helsley, S. S. Han, and C. Zhou. 2014. IKKbeta links vascular inflammation to obesity and atherosclerosis. *J Exp Med* **211**: 869-886.

162. Robinet, P., D. M. Milewicz, L. A. Cassis, N. J. Leeper, H. S. Lu, and J. D. Smith. 2018. Consideration of Sex Differences in Design and Reporting of Experimental Arterial Pathology Studies-Statement From ATVB Council. *Arterioscler Thromb Vasc Biol* **38**: 292-303.

163. Lu, W., Z. Meng, R. Hernandez, and C. Zhou. 2021. Fibroblast-specific IKK-beta deficiency ameliorates angiotensin II-induced adverse cardiac remodeling in mice. *JCI Insight* **6**: e150161.

164. Sui, Y., Z. Meng, J. Chen, J. Liu, R. Hernandez, M. B. Gonzales, T. Gwag, A. J. Morris, and C. Zhou. 2021. Effects of Dicyclohexyl Phthalate Exposure on PXR Activation and Lipid Homeostasis in Mice. *Environ Health Perspect* **129**: 127001.

165. Helsley, R. N., Y. Sui, S. H. Park, Z. Liu, R. G. Lee, B. Zhu, P. A. Kern, and C. Zhou. 2016. Targeting IkappaB kinase beta in Adipocyte Lineage Cells for Treatment of Obesity and Metabolic Dysfunctions. *Stem Cells* **34**: 1883-1895.

166. Satta, S., Z. Meng, R. Hernandez, S. Cavallero, T. Zhou, T. K. Hsiai, and C. Zhou. 2022. An engineered nano-liposome-human ACE2 decoy neutralizes SARS-CoV-2 Spike protein-induced inflammation in both murine and human macrophages. *Theranostics* **12**: 2639-2657.

167. Havel, R. J., H. A. Eder, and J. H. Bragdon. 1955. The distribution and chemical composition of ultracentrifugally separated lipoproteins in human serum. *J Clin Invest* **34**: 1345-1353.

168. Wang, F., Z. Liu, S. H. Park, T. Gwag, W. Lu, M. Ma, Y. Sui, and C. Zhou. 2018. Myeloid beta-Catenin Deficiency Exacerbates Atherosclerosis in Low-Density Lipoprotein Receptor-Deficient Mice. *Arterioscler Thromb Vasc Biol* **38**: 1468-1478.

169. Sui, Y., Z. Meng, S. H. Park, W. Lu, C. Livelo, Q. Chen, T. Zhou, and C. Zhou. 2020. Myeloid-specific deficiency of pregnane X receptor decreases atherosclerosis in LDL receptor-deficient mice. *J Lipid Res* **61**: 696-706.

170. Wong, T. W. Y., A. Ahmed, G. Yang, E. Maino, S. Steiman, E. Hyatt, P. Chan, K. Lindsay, N. Wong, D. Golebiowski, J. Schneider, P. Delgado-Olguín, E. A. Ivakine, and R. D. Cohn. 2020. A novel mouse model of Duchenne muscular dystrophy carrying a multi-exonic. *Dis Model Mech* **13**.

171. Pickering, R. J., C. Tikellis, C. J. Rosado, D. Tsorotes, A. Dimitropoulos, M. Smith, O. Huet, R. M. Seeber, R. Abhayawardana, E. K. Johnstone, J. Golledge, Y. Wang, K. A. Jandeleit-Dahm, M. E. Cooper, K. D. Pfleger, and M. C. Thomas. 2019. Transactivation of RAGE mediates angiotensin-induced inflammation and atherogenesis. *J Clin Invest* **129**: 406-421.

172. Ivanov, P., M. M. Emara, J. Villen, S. P. Gygi, and P. Anderson. 2011. Angiogenin-induced tRNA fragments inhibit translation initiation. *Mol Cell* **43**: 613-623.

173. Sun, X., S. He, A. K. M. Wara, B. Icli, E. Shvartz, Y. Tesmenitsky, N. Belkin, D. Li, T. S. Blackwell, G. K. Sukhova, K. Croce, and M. W. Feinberg. 2014. Systemic delivery of microRNA-181b inhibits nuclear factor-κB activation, vascular inflammation, and atherosclerosis in apolipoprotein E-deficient mice. *Circ Res* **114**: 32-40.

174. Robinson, M. D., D. J. McCarthy, and G. K. Smyth. 2010. edgeR: a Bioconductor package for differential expression analysis of digital gene expression data. *Bioinformatics* **26**: 139-140.

175. Levin, J. Z., M. Yassour, X. Adiconis, C. Nusbaum, D. A. Thompson, N. Friedman, A. Gnirke, and A. Regev. 2010. Comprehensive comparative analysis of strand-specific RNA sequencing methods. *Nature methods* **7**: 709-715.

176. Zhong, S., J. G. Joung, Y. Zheng, Y. R. Chen, B. Liu, Y. Shao, J. Z. Xiang, Z. Fei, and J. J. Giovannoni. 2011. High-throughput illumina strand-specific RNA sequencing library preparation. *Cold Spring Harb Protoc* **2011**: 940-949.

177. Yang, X., K. Regan, Y. Huang, Q. Zhang, J. Li, T. Y. Seiwert, E. E. Cohen, H. R. Xing, and Y. A. Lussier. 2012. Single sample expression-anchored mechanisms predict survival in head and neck cancer. *PLoS Comput Biol* **8**: e1002350.

178. Zhou, C., N. King, K. Y. Chen, and J. L. Breslow. 2009. Activation of PXR induces hypercholesterolemia in wild-type and accelerates atherosclerosis in apoE deficient mice. *J Lipid Res* **50**: 2004-2013.

179. Sui, Y., J. Xu, J. Rios-Pilier, and C. Zhou. 2011. Deficiency of PXR decreases atherosclerosis in apoE-deficient mice. *J Lipid Res* **52**: 1652-1659.

180. Hernandez, R., J. Shi, J. Liu, X. Li, J. Wu, L. Zhao, T. Zhou, Q. Chen, and C. Zhou. 2023. PANDORA-Seq unveils the hidden small noncoding RNA landscape in atherosclerosis of LDL receptor-deficient mice. *J Lipid Res* **64**: 100352.

181. Shi, J., E. A. Ko, K. M. Sanders, Q. Chen, and T. Zhou. 2018. SPORTS1.0: A Tool for Annotating and Profiling Non-coding RNAs Optimized for rRNA- and tRNA-derived Small RNAs. *Genomics Proteomics Bioinformatics* **16**: 144-151.

182. Ozata, D. M., I. Gainetdinov, A. Zoch, D. O'Carroll, and P. D. Zamore. 2019. PIWI-interacting RNAs: small RNAs with big functions. *Nat Rev Genet* **20**: 89-108.

183. Bartel, D. P. 2018. Metazoan MicroRNAs. *Cell* **173**: 20-51.

184. Kumar, P., C. Kuscu, and A. Dutta. 2016. Biogenesis and Function of Transfer RNA-Related Fragments (tRFs). *Trends in biochemical sciences* **41**: 679-689.

185. Lambert, M., A. Benmoussa, and P. Provost. 2019. Small Non-Coding RNAs Derived From Eukaryotic Ribosomal RNA. *Noncoding RNA* **5**.

186. Busnelli, M., S. Manzini, M. Chiara, A. Colombo, F. Fontana, R. Oleari, F. Potì, D. Horner, S. Bellosta, and G. Chiesa. 2021. Aortic Gene Expression Profiles Show How ApoA-I Levels Modulate Inflammation, Lysosomal Activity, and Sphingolipid Metabolism in Murine Atherosclerosis. *Arterioscler Thromb Vasc Biol* **41**: 651-667.

187. Xi, D., J. Zhao, M. Zhao, W. Fu, Z. Guo, and H. Chen. 2017. Identification of Gene Expression Changes in the Aorta of ApoE Null Mice Fed a High-Fat Diet. *Genes (Basel)* **8**.

188. Boräng, S., T. Andersson, A. Thelin, J. Odeberg, and J. Lundeberg. 2004. Vascular gene expression in atherosclerotic plaque-prone regions analyzed by representational difference analysis. *Pathobiology* **71**: 107-114.

189. Moore, K. J., and I. Tabas. 2011. Macrophages in the pathogenesis of atherosclerosis. *Cell* **145**: 341-355.

190. Lin, J., V. Kakkar, and X. Lu. 2014. Impact of MCP-1 in atherosclerosis. *Curr Pharm Des* **20**: 4580-4588.

191. Moos, M. P., N. John, R. Gräbner, S. Nossmann, B. Günther, R. Vollandt, C. D. Funk, B. Kaiser, and A. J. Habenicht. 2005. The lamina adventitia is the major site of immune cell accumulation in standard chow-fed apolipoprotein E-deficient mice. *Arterioscler Thromb Vasc Biol* **25**: 2386-2391.

192. Wang, I. M., B. Zhang, X. Yang, J. Zhu, S. Stepaniants, C. Zhang, Q. Meng, M. Peters, Y. He, C. Ni, D. Slipetz, M. A. Crackower, H. Houshyar, C. M. Tan, E. Asante-Appiah, G. O'Neill, M. J. Luo, R. Thieringer, J. Yuan, C. S. Chiu, P. Y. Lum, J. Lamb, Y. Boie, H. A. Wilkinson, E. E. Schadt, H. Dai, and C. Roberts. 2012. Systems analysis of eleven rodent disease models reveals an inflammatome signature and key drivers. *Mol Syst Biol* **8**: 594.

193. Berisha, S. Z., J. Hsu, P. Robinet, and J. D. Smith. 2013. Transcriptome analysis of genes regulated by cholesterol loading in two strains of mouse macrophages

associates lysosome pathway and ER stress response with atherosclerosis susceptibility. *PLoS One* **8**: e65003.

194. Raitoharju, E., L. P. Lyytikäinen, M. Levula, N. Oksala, A. Mennander, M. Tarkka, N. Klopp, T. Illig, M. Kähönen, P. J. Karhunen, R. Laaksonen, and T. Lehtimäki. 2011. miR-21, miR-210, miR-34a, and miR-146a/b are up-regulated in human atherosclerotic plaques in the Tampere Vascular Study. *Atherosclerosis* **219**: 211-217.

195. Takahashi, Y., M. Satoh, Y. Minami, T. Tabuchi, T. Itoh, and M. Nakamura. 2010. Expression of miR-146a/b is associated with the Toll-like receptor 4 signal in coronary artery disease: effect of renin-angiotensin system blockade and statins on miRNA-146a/b and Toll-like receptor 4 levels. *Clinical science* **119**: 395-405.

196. Suárez, Y., C. Wang, T. D. Manes, and J. S. Pober. 2010. Cutting edge: TNF-induced microRNAs regulate TNF-induced expression of E-selectin and intercellular adhesion molecule-1 on human endothelial cells: feedback control of inflammation. *J Immunol* **184**: 21-25.

197. Liu, D., L. Dejun, X. Sun, S. Xuelin, P. Ye, and Y. Ping. 2015. miR-31 Overexpression Exacerbates Atherosclerosis by Targeting NOX4 in apoE(-/-) Mice. *Clin Lab* **61**: 1617-1624.

198. Sun, X., N. Belkin, and M. W. Feinberg. 2013. Endothelial microRNAs and atherosclerosis. *Curr Atheroscler Rep* **15**: 372.

199. Shi, J., Y. Zhang, T. Zhou, and Q. Chen. 2019. tsRNAs: The Swiss Army Knife for Translational Regulation. *Trends in biochemical sciences* **44**: 185-189.

200. Li, X., X. Liu, D. Zhao, W. Cui, Y. Wu, C. Zhang, and C. Duan. 2021. tRNA-derived small RNAs: novel regulators of cancer hallmarks and targets of clinical application. *Cell Death Discov* **7**: 249.

201. Kim, H. K., G. Fuchs, S. Wang, W. Wei, Y. Zhang, H. Park, B. Roy-Chaudhuri, P. Li, J. Xu, K. Chu, F. Zhang, M. S. Chua, S. So, Q. C. Zhang, P. Sarnow, and M. A. Kay. 2017. A transfer-RNA-derived small RNA regulates ribosome biogenesis. *Nature* **552**: 57-62.

202. Glass, C. K., and J. L. Witztum. 2001. Atherosclerosis. the road ahead. *Cell* **104**: 503-516.

203. Bjorkegren, J. L. M., and A. J. Lusis. 2022. Atherosclerosis: Recent developments. *Cell* **185**: 1630-1645.

204. Herrington, W., B. Lacey, P. Sherliker, J. Armitage, and S. Lewington. 2016. Epidemiology of Atherosclerosis and the Potential to Reduce the Global Burden of Atherothrombotic Disease. *Circ Res* **118**: 535-546.

205. Roth, G. A., M. H. Forouzanfar, A. E. Moran, R. Barber, G. Nguyen, V. L. Feigin, M. Naghavi, G. A. Mensah, and C. J. Murray. 2015. Demographic and epidemiologic drivers of global cardiovascular mortality. *N Engl J Med* **372**: 1333-1341.

206. Eberle, C., M. F. Kirchner, R. Herden, and S. Stichling. 2020. Paternal metabolic and cardiovascular programming of their offspring: A systematic scoping review. *PLoS One* **15**: e0244826.

207. Perez, M. F., and B. Lehner. 2019. Intergenerational and transgenerational epigenetic inheritance in animals. *Nat Cell Biol* **21**: 143-151.

208. Sales, V. M., A. C. Ferguson-Smith, and M. E. Patti. 2017. Epigenetic Mechanisms of Transmission of Metabolic Disease across Generations. *Cell Metab* **25**: 559-571.

209. Ng, S.-F., R. C. Y. Lin, D. R. Laybutt, R. Barres, J. A. Owens, and M. J. Morris. 2010. Chronic high-fat diet in fathers programs β-cell dysfunction in female rat offspring. *Nature* **467**: 963-966.

210. De Jesus, D. F., K. Orime, D. Kaminska, T. Kimura, G. Basile, C. H. Wang, L. Haertle, R. Riemens, N. K. Brown, J. Hu, V. Männistö, A. M. Silva, E. Dirice, Y. H. Tseng, T. Haaf, J. Pihlajamäki, and R. N. Kulkarni. 2020. Parental metabolic syndrome epigenetically reprograms offspring hepatic lipid metabolism in mice. *J Clin Invest* **130**: 2391-2407.

211. Palinski, W., and C. Napoli. 2002. The fetal origins of atherosclerosis: maternal hypercholesterolemia, and cholesterol-lowering or antioxidant treatment during pregnancy influence in utero programming and postnatal susceptibility to atherogenesis. *FASEB J* **16**: 1348-1360.

212. Napoli, C., and W. Palinski. 2001. Maternal hypercholesterolemia during pregnancy influences the later development of atherosclerosis: clinical and pathogenic implications. *Eur Heart J* **22**: 4-9.

213. Khan, I. Y., V. Dekou, G. Douglas, R. Jensen, M. A. Hanson, L. Poston, and P. D. Taylor. 2005. A high-fat diet during rat pregnancy or suckling induces cardiovascular dysfunction in adult offspring. *Am J Physiol Regul Integr Comp Physiol* **288**: R127-133.

214. Trenteseaux, C., A. T. Gaston, A. Aguesse, G. Poupeau, P. de Coppet, R. Andriantsitohaina, J. Laschet, V. Amarger, M. Krempf, E. Nobecourt-Dupuy, and

K. Ouguerram. 2017. Perinatal Hypercholesterolemia Exacerbates Atherosclerosis Lesions in Offspring by Altering Metabolism of Trimethylamine-N-Oxide and Bile Acids. *Arterioscler Thromb Vasc Biol* **37**: 2053-2063.

215. Sui, Y., S. H. Park, F. Wang, and C. Zhou. 2018. Perinatal Bisphenol A Exposure Increases Atherosclerosis in Adult Male PXR-Humanized Mice. *Endocrinology* **159**: 1595-1608.

216. Carone, B. R., L. Fauquier, N. Habib, J. M. Shea, C. E. Hart, R. Li, C. Bock, C. Li, H. Gu, P. D. Zamore, A. Meissner, Z. Weng, H. A. Hofmann, N. Friedman, and O. J. Rando. 2010. Paternally induced transgenerational environmental reprogramming of metabolic gene expression in mammals. *Cell* **143**: 1084-1096.

217. Ost, A., A. Lempradl, E. Casas, M. Weigert, T. Tiko, M. Deniz, L. Pantano, U. Boenisch, P. M. Itskov, M. Stoeckius, M. Ruf, N. Rajewsky, G. Reuter, N. Iovino, C. Ribeiro, M. Alenius, S. Heyne, T. Vavouri, and J. A. Pospisilik. 2014. Paternal diet defines offspring chromatin state and intergenerational obesity. *Cell* **159**: 1352-1364.

218. Meng, Z., T. Gwag, Y. Sui, S. H. Park, X. Zhou, and C. Zhou. 2019. The atypical antipsychotic quetiapine induces hyperlipidemia by activating intestinal PXR signaling. *JCI Insight* **4**.

219. Sherman, B. T., M. Hao, J. Qiu, X. Jiao, M. W. Baseler, H. C. Lane, T. Imamichi, and W. Chang. 2022. DAVID: a web server for functional enrichment analysis and functional annotation of gene lists (2021 update). *Nucleic Acids Res* **50**: W216-W221.

220. Ashburner, M., C. A. Ball, J. A. Blake, D. Botstein, H. Butler, J. M. Cherry, A. P. Davis, K. Dolinski, S. S. Dwight, J. T. Eppig, M. A. Harris, D. P. Hill, L. Issel-Tarver, A. Kasarskis, S. Lewis, J. C. Matese, J. E. Richardson, M. Ringwald, G. M. Rubin, and G. Sherlock. 2000. Gene ontology: tool for the unification of biology. The Gene Ontology Consortium. *Nat Genet* **25**: 25-29.

221. Jun, J. I., and L. F. Lau. 2011. Taking aim at the extracellular matrix: CCN proteins as emerging therapeutic targets. *Nat Rev Drug Discov* **10**: 945-963.

222. Kular, L., J. Pakradouni, P. Kitabgi, M. Laurent, and C. Martinerie. 2011. The CCN family: a new class of inflammation modulators? *Biochimie* **93**: 377-388.

223. Hsu, P. L., J. S. Chen, C. Y. Wang, H. L. Wu, and F. E. Mo. 2019. Shear-Induced CCN1 Promotes Atheroprone Endothelial Phenotypes and Atherosclerosis. *Circulation* **139**: 2877-2891.

224. Ponticos, M. 2013. Connective tissue growth factor (CCN2) in blood vessels. *Vascular pharmacology* **58**: 189-193.

225. Jiang, R., J. Tang, X. Zhang, Y. He, Z. Yu, S. Chen, J. Xia, J. Lin, and Q. Ou. 2022. CCN1 Promotes Inflammation by Inducing IL-6 Production. *Front Immunol* **13**: 810671.

226. Gao, R., and D. R. Brigstock. 2005. Activation of nuclear factor kappa B (NF-kappaB) by connective tissue growth factor (CCN2) is involved in sustaining the survival of primary rat hepatic stellate cells. *Cell Commun Signal* **3**: 14.

227. Alata Jimenez, N., M. Castellano, E. M. Santillan, K. Boulias, A. Boan, L. F. Arias Padilla, J. I. Fernandino, E. L. Greer, J. P. Tosar, L. Cochella, and P. H. Strobl-Mazzulla. 2023. Paternal methotrexate exposure affects sperm small RNA content and causes craniofacial defects in the offspring. *Nat Commun* **14**: 1617.

228. Guo, Y., D. Bai, W. Liu, Y. Liu, Y. Zhang, X. Kou, J. Chen, H. Wang, X. Teng, J. Zuo, and S. Gao. 2021. Altered sperm tsRNAs in aged male contribute to anxiety-like behavior in offspring. *Aging Cell* **20**: e13466.

229. Liu, M., L. Zhang, G. Marsboom, A. Jambusaria, S. Xiong, P. T. Toth, E. V. Benevolenskaya, J. Rehman, and A. B. Malik. 2019. Sox17 is required for endothelial regeneration following inflammation-induced vascular injury. *Nat Commun* **10**: 2126.

230. Engert, S., I. Burtscher, W. P. Liao, S. Dulev, G. Schotta, and H. Lickert. 2013. Wnt/beta-catenin signalling regulates Sox17 expression and is essential for organizer and endoderm formation in the mouse. *Development* **140**: 3128-3138.

231. Daxinger, L., and E. Whitelaw. 2012. Understanding transgenerational epigenetic inheritance via the gametes in mammals. *Nat Rev Genet* **13**: 153-162.

232. Heard, E., and R. A. Martienssen. 2014. Transgenerational epigenetic inheritance: myths and mechanisms. *Cell* **157**: 95-109.

233. Gluckman, P. D., M. A. Hanson, T. Buklijas, F. M. Low, and A. S. Beedle. 2009. Epigenetic mechanisms that underpin metabolic and cardiovascular diseases. *Nat Rev Endocrinol* **5**: 401-408.

234. Fleming, T. P., A. J. Watkins, M. A. Velazquez, J. C. Mathers, A. M. Prentice, J. Stephenson, M. Barker, R. Saffery, C. S. Yajnik, J. J. Eckert, M. A. Hanson, T. Forrester, P. D. Gluckman, and K. M. Godfrey. 2018. Origins of lifetime health around the time of conception: causes and consequences. *Lancet* **391**: 1842-1852.

235. Khan, I. Y., P. D. Taylor, V. Dekou, P. T. Seed, L. Lakasing, D. Graham, A. F. Dominiczak, M. A. Hanson, and L. Poston. 2003. Gender-linked hypertension in offspring of lard-fed pregnant rats. *Hypertension* **41**: 168-175.

236. Oken, E., S. Y. Huh, E. M. Taveras, J. W. Rich-Edwards, and M. W. Gillman. 2005. Associations of maternal prenatal smoking with child adiposity and blood pressure. *Obes Res* **13**: 2021-2028.

237. Geerts, C. C., M. L. Bots, D. E. Grobbee, and C. S. Uiterwaal. 2008. Parental smoking and vascular damage in young adult offspring: is early life exposure critical? The atherosclerosis risk in young adults study. *Arterioscler Thromb Vasc Biol* **28**: 2296-2302.

238. Gunes, T., E. Koklu, A. Yikilmaz, M. A. Ozturk, M. Akcakus, S. Kurtoglu, A. Coskun, and S. Koklu. 2007. Influence of maternal smoking on neonatal aortic intima-media thickness, serum IGF-I and IGFBP-3 levels. *Eur J Pediatr* **166**: 1039-1044.

239. Power, C., K. Atherton, and C. Thomas. 2010. Maternal smoking in pregnancy, adult adiposity and other risk factors for cardiovascular disease. *Atherosclerosis* **211**: 643-648.

240. Raad, G., F. Serra, L. Martin, M. A. Derieppe, J. Gilleron, V. L. Costa, D. F. Pisani, E. Z. Amri, M. Trabucchi, and V. Grandjean. 2021. Paternal multigenerational exposure to an obesogenic diet drives epigenetic predisposition to metabolic diseases in mice. *eLife* **10**.

241. Sandovici, I., D. S. Fernandez-Twinn, A. Hufnagel, M. Constância, and S. E. Ozanne. 2022. Sex differences in the intergenerational inheritance of metabolic traits. *Nature Metabolism* **4**: 507-523.

242. Stein, A. D., H. S. Kahn, A. Rundle, P. A. Zybert, K. van der Pal-de Bruin, and L. H. Lumey. 2007. Anthropometric measures in middle age after exposure to famine during gestation: evidence from the Dutch famine. *Am J Clin Nutr* **85**: 869-876.

243. Tramunt, B., S. Smati, N. Grandgeorge, F. Lenfant, J. F. Arnal, A. Montagner, and P. Gourdy. 2020. Sex differences in metabolic regulation and diabetes susceptibility. *Diabetologia* **63**: 453-461.

244. Waxman, D. J., and C. O'Connor. 2006. Growth hormone regulation of sex-dependent liver gene expression. *Mol Endocrinol* **20**: 2613-2629.

245. Wiese, C. B., R. Avetisyan, and K. Reue. 2023. The impact of chromosomal sex on cardiometabolic health and disease. *Trends Endocrinol Metab* **34**: 652-665.

246. Wang, Y., X. Guo, X. Hong, G. Wang, C. Pearson, B. Zuckerman, A. G. Clark, K. O. O'Brien, X. Wang, and Z. Gu. 2022. Association of mitochondrial DNA content, heteroplasmies and inter-generational transmission with autism. *In* Nature communications. 3790.

247. Godschalk, R., A. Remels, C. Hoogendoorn, J. van Benthem, M. Luijten, N. Duale, G. Brunborg, A.-K. Olsen, F. G. Bouwman, A. Munnia, M. Peluso, E. Mariman, and F. J. van Schooten. 2017. Paternal Exposure to Environmental Chemical Stress Affects Male Offspring's Hepatic Mitochondria. *Toxicological Sciences* **162**: 241-250.

248. Nowogrodzki, J. 2024. A dad's diet affects his sperm - and his sons' health. *Nature*: doi:10.1038/d41586-41024-01623-41582.

249. Chen, C. C., and L. F. Lau. 2009. Functions and mechanisms of action of CCN matricellular proteins. *Int J Biochem Cell Biol* **41**: 771-783.

250. Mo, F. E., and L. F. Lau. 2006. The matricellular protein CCN1 is essential for cardiac development. *Circ Res* **99**: 961-969.

251. Sigala, F., S. Georgopoulos, E. Papalambros, D. Chasiotis, G. Vourliotakis, A. Niforou, A. Kotsinas, N. Kavantzas, E. Patsouris, V. G. Gorgoulis, and E. Bastounis. 2006. Heregulin, cysteine rich-61 and matrix metalloproteinase 9 expression in human carotid atherosclerotic plaques: relationship with clinical data. *Eur J Vasc Endovasc Surg* **32**: 238-245.

252. Hilfiker, A., D. Hilfiker-Kleiner, M. Fuchs, K. Kaminski, A. Lichtenberg, H. J. Rothkötter, B. Schieffer, and H. Drexler. 2002. Expression of CYR61, an angiogenic immediate early gene, in arteriosclerosis and its regulation by angiotensin II. *Circulation* **106**: 254-260.

253. Bai, T., C. C. Chen, and L. F. Lau. 2010. Matricellular protein CCN1 activates a proinflammatory genetic program in murine macrophages. *J Immunol* **184**: 3223-3232.

254. Imhof, B. A., S. Jemelin, R. Ballet, C. Vesin, M. Schapira, M. Karaca, and Y. Emre. 2016. CCN1/CYR61-mediated meticulous patrolling by Ly6Clow monocytes fuels vascular inflammation. *Proc Natl Acad Sci U S A* **113**: E4847-4856.

255. Wang, Y., Z.-P. Chen, H. Hu, J. Lei, Z. Zhou, B. Yao, L. Chen, G. Liang, S. Zhan, and X. Zhu. 2021. Sperm microRNAs confer depression susceptibility to offspring. *Science Advances* **7**: eabd7605.

256. Sarker, G., W. Sun, D. Rosenkranz, P. Pelczar, L. Opitz, V. Efthymiou, C. Wolfrum, and D. Peleg-Raibstein. 2019. Maternal overnutrition programs hedonic

and metabolic phenotypes across generations through sperm tsRNAs. *Proc Natl Acad Sci U S A* **116**: 10547-10556.

257. Gapp, K., A. Jawaid, P. Sarkies, J. Bohacek, P. Pelczar, J. Prados, L. Farinelli, E. Miska, and I. M. Mansuy. 2014. Implication of sperm RNAs in transgenerational inheritance of the effects of early trauma in mice. *Nature neuroscience* **17**: 667-669.

258. Rodgers, A. B., C. P. Morgan, N. A. Leu, and T. L. Bale. 2015. Transgenerational epigenetic programming via sperm microRNA recapitulates effects of paternal stress. *Proceedings of the National Academy of Sciences* **112**: 13699-13704.

259. Zheng, X., Z. Li, G. Wang, H. Wang, Y. Zhou, X. Zhao, C. Y. Cheng, Y. Qiao, and F. Sun. 2021. Sperm epigenetic alterations contribute to inter- and transgenerational effects of paternal exposure to long-term psychological stress via evading offspring embryonic reprogramming. *Cell Discov* **7**: 101.

260. Chen, Q., and T. Zhou. 2023. Emerging functional principles of tRNA-derived small RNAs and other regulatory small RNAs. *J Biol Chem* **299**: 105225.

261. Kuhle, B., Q. Chen, and P. Schimmel. 2023. tRNA renovatio: Rebirth through fragmentation. *Mol Cell* **83**: 3953-3971.

262. Cai, C., and Q. Chen. 2024. Father's diet influences son's metabolic health through sperm RNA. *Nature*: doi:10.1038/d41586-41024-01502-w.

263. Yanagisawa, M., H. Kurihara, S. Kimura, Y. Tomobe, M. Kobayashi, Y. Mitsui, Y. Yazaki, K. Goto, and T. Masaki. 1988. A novel potent vasoconstrictor peptide produced by vascular endothelial cells. *Nature* **332**: 411-415.

264. Dhaun, N., and D. J. Webb. 2019. Endothelins in cardiovascular biology and therapeutics. *Nat Rev Cardiol* **16**: 491-502.

265. Dong, Z. M., S. M. Chapman, A. A. Brown, P. S. Frenette, R. O. Hynes, and D. D. Wagner. 1998. The combined role of P- and E-selectins in atherosclerosis. *J Clin Invest* **102**: 145-152.

266. Ma, S., X. Y. Tian, Y. Zhang, C. Mu, H. Shen, J. Bismuth, H. J. Pownall, Y. Huang, and W. T. Wong. 2016. E-selectin-targeting delivery of microRNAs by microparticles ameliorates endothelial inflammation and atherosclerosis. *Sci Rep* **6**: 22910.

267. Fu, H., J. Feng, Q. Liu, F. Sun, Y. Tie, J. Zhu, R. Xing, Z. Sun, and X. Zheng. 2009. Stress induces tRNA cleavage by angiogenin in mammalian cells. *FEBS Lett* **583**: 437-442.

268. Liu, S., L. Zhuo, J. Wang, Q. Zhang, Q. Li, G. Li, L. Yan, T. Jin, T. Pan, X. Sui, Q. Lv, and T. Xie. 2020. METTL3 plays multiple functions in biological processes. *American journal of cancer research* **10**: 1631-1646.

269. Bentzon, J. F., F. Otsuka, R. Virmani, and E. Falk. 2014. Mechanisms of plaque formation and rupture. *Circ Res* **114**: 1852-1866.

270. Virmani, R., A. P. Burke, A. Farb, and F. D. Kolodgie. 2006. Pathology of the vulnerable plaque. *J Am Coll Cardiol* **47**: C13-18.

271. Harman, J. L., and H. F. Jørgensen. 2019. The role of smooth muscle cells in plaque stability: Therapeutic targeting potential. *Br J Pharmacol* **176**: 3741-3753.

272. Grootaert, M. O. J., and M. R. Bennett. 2021. Vascular smooth muscle cells in atherosclerosis: time for a re-assessment. *Cardiovasc Res* **117**: 2326-2339.

273. Milutinović, A., D. Šuput, and R. Zorc-Pleskovič. 2020. Pathogenesis of atherosclerosis in the tunica intima, media, and adventitia of coronary arteries: An updated review. *Bosnian Journal of Basic Medical Sciences* **20**: 21-30.

274. Haurani, M. J., and P. J. Pagano. 2007. Adventitial fibroblast reactive oxygen species as autacrine and paracrine mediators of remodeling: bellwether for vascular disease? *Cardiovasc Res* **75**: 679-689.

275. Xu, F., J. Ji, L. Li, R. Chen, and W.-c. Hu. 2007. Adventitial fibroblasts are activated in the early stages of atherosclerosis in the apolipoprotein E knockout mouse. *Biochemical and Biophysical Research Communications* **352**: 681-688.

276. Maiellaro, K., and W. R. Taylor. 2007. The role of the adventitia in vascular inflammation. *Cardiovascular research* **75**: 640-648.

277. Schwartz C, J., and A. Mitchell J. R. 1962. Cellular Infiltration of the Human Arterial Adventitia Associated with Atheromatous Plaques. *Circulation* **26**: 73-78.

278. Tieu, B. C., X. Ju, C. Lee, H. Sun, W. Lejeune, I. A. Recinos, A. R. Brasier, and R. G. Tilton. 2011. Aortic Adventitial Fibroblasts Participate in Angiotensin-Induced Vascular Wall Inflammation and Remodeling. *Journal of Vascular Research* **48**: 261-272.

279. Lu, W., Z. Meng, R. Hernandez, and C. Zhou. 2021. Fibroblast-specific IKK-β deficiency ameliorates angiotensin II-induced adverse cardiac remodeling in mice. *JCI Insight* **6**.

280. Hao, Y., S. Hao, E. Andersen-Nissen, W. M. Mauck, S. Zheng, A. Butler, M. J. Lee, A. J. Wilk, C. Darby, M. Zager, P. Hoffman, M. Stoeckius, E. Papalexi, E. P.

Mimitou, J. Jain, A. Srivastava, T. Stuart, L. M. Fleming, B. Yeung, A. J. Rogers, J. M. McElrath, C. A. Blish, R. Gottardo, P. Smibert, and R. Satija. 2021. Integrated analysis of multimodal single-cell data. *Cell* **184**: 3573-3587.e3529.

281. Young, M. D., and S. Behjati. 2020. SoupX removes ambient RNA contamination from droplet-based single-cell RNA sequencing data. *Gigascience* **9**.

282. DePasquale, E. A. K., D. J. Schnell, P. J. Van Camp, Í. Valiente-Alandí, B. C. Blaxall, H. L. Grimes, H. Singh, and N. Salomonis. 2019. DoubletDecon: Deconvoluting Doublets from Single-Cell RNA-Sequencing Data. *Cell Rep* **29**: 1718-1727.e1718.

283. Korsunsky, I., N. Millard, J. Fan, K. Slowikowski, F. Zhang, K. Wei, Y. Baglaenko, M. Brenner, P. R. Loh, and S. Raychaudhuri. 2019. Fast, sensitive and accurate integration of single-cell data with Harmony. *Nat Methods* **16**: 1289-1296.

284. Wu, T., E. Hu, S. Xu, M. Chen, P. Guo, Z. Dai, T. Feng, L. Zhou, W. Tang, L. Zhan, X. Fu, S. Liu, X. Bo, and G. Yu. 2021. clusterProfiler 4.0: A universal enrichment tool for interpreting omics data. *Innovation (Camb)* **2**: 100141.

285. Newman, A. A. C., V. Serbulea, R. A. Baylis, L. S. Shankman, X. Bradley, G. F. Alencar, K. Owsiany, R. A. Deaton, S. Karnewar, S. Shamsuzzaman, A. Salamon, M. S. Reddy, L. Guo, A. Finn, R. Virmani, O. A. Cherepanova, and G. K. Owens. 2021. Multiple cell types contribute to the atherosclerotic lesion fibrous cap by PDGFRβ and bioenergetic mechanisms. *Nat Metab* **3**: 166-181.

286. Tinajero, M. G., and A. I. Gotlieb. 2020. Recent Developments in Vascular Adventitial Pathobiology: The Dynamic Adventitia as a Complex Regulator of Vascular Disease. *The American Journal of Pathology* **190**: 520-534.

287. Zalewski, A., Y. Shi, and A. G. Johnson. 2002. Diverse origin of intimal cells: smooth muscle cells, myofibroblasts, fibroblasts, and beyond? *Circ Res* **91**: 652-655.

288. Shi, Y., J. E. O'Brien, A. Fard, J. D. Mannion, D. Wang, and A. Zalewski. 1996. Adventitial myofibroblasts contribute to neointimal formation in injured porcine coronary arteries. *Circulation* **94**: 1655-1664.

289. Majesky, M. W., X. R. Dong, V. Hoglund, W. M. Mahoney, and G. Daum. 2011. The adventitia: a dynamic interface containing resident progenitor cells. *Arterioscler Thromb Vasc Biol* **31**: 1530-1539.

290. Sakamoto, S., T. Tsuruda, K. Hatakeyama, T. Imamura, Y. Asada, and K. Kitamura. 2014. Impact of age-dependent adventitia inflammation on structural alteration of abdominal aorta in hyperlipidemic mice. *PLoS One* **9**: e105739.

291. Akhavanpoor, M., C. A. Gleissner, H. Akhavanpoor, F. Lasitschka, A. O. Doesch, H. A. Katus, and C. Erbel. 2018. Adventitial tertiary lymphoid organ classification in human atherosclerosis. *Cardiovasc Pathol* **32**: 8-14.

292. Ngwenyama, N., K. Kaur, D. Bugg, B. Theall, M. Aronovitz, R. Berland, S. Panagiotidou, C. Genco, M. A. Perrin, J. Davis, and P. Alcaide. 2022. Antigen presentation by cardiac fibroblasts promotes cardiac dysfunction. *Nat Cardiovasc Res* **1**: 761-774.

293. Lee, S., J. Kim, P. N. Valdmanis, and H. K. Kim. 2023. Emerging roles of tRNA-derived small RNAs in cancer biology. *Exp Mol Med* **55**: 1293-1304.

294. Qin, C., P. P. Xu, X. Zhang, C. Zhang, C. B. Liu, D. G. Yang, F. Gao, M. L. Yang, L. J. Du, and J. J. Li. 2020. Pathological significance of tRNA-derived small RNAs in neurological disorders. *Neural Regen Res* **15**: 212-221.

295. Guzzi, N., M. Cieśla, P. C. T. Ngoc, S. Lang, S. Arora, M. Dimitriou, K. Pimková, M. N. E. Sommarin, R. Munita, M. Lubas, Y. Lim, K. Okuyama, S. Soneji, G. Karlsson, J. Hansson, G. Jönsson, A. H. Lund, M. Sigvardsson, E. Hellström-Lindberg, A. C. Hsieh, and C. Bellodi. 2018. Pseudouridylation of tRNA-Derived Fragments Steers Translational Control in Stem Cells. *Cell* **173**: 1204-1216.e1226.

296. Ying, S., P. Li, J. Wang, K. Chen, Y. Zou, M. Dai, K. Xu, G. Feng, C. Zhang, H. Jiang, W. Li, Y. Zhang, and Q. Zhou. 2023. tRF-Gln-CTG-026 ameliorates liver injury by alleviating global protein synthesis. *Signal Transduct Target Ther* **8**: 144.

297. Li, D., X. Gao, X. Ma, M. Wang, C. Cheng, T. Xue, F. Gao, Y. Shen, J. Zhang, and Q. Liu. 2024. Aging-induced $tRNA^{Glu}$-derived fragment impairs glutamate biosynthesis by targeting mitochondrial translation-dependent crustal organization. *Cell Metab* **36**: 1059-1075.e1059.

298. Wang, B., L. Xia, D. Zhu, H. Zeng, B. Wei, L. Lu, W. Li, Y. Shi, J. Liu, Y. Zhang, and M. Sun. 2022. Paternal High-Fat Diet Altered Sperm 5'tsRNA-Gly-GCC Is Associated With Enhanced Gluconeogenesis in the Offspring. *Front Mol Biosci* **9**: 857875.

299. Frye, M., B. T. Harada, M. Behm, and C. He. 2018. RNA modifications modulate gene expression during development. *Science* **361**: 1346-1349.

300. Gapp, K., G. van Steenwyk, P. L. Germain, W. Matsushima, K. L. M. Rudolph, F. Manuella, M. Roszkowski, G. Vernaz, T. Ghosh, P. Pelczar, I. M. Mansuy, and E. A. Miska. 2018. Alterations in sperm long RNA contribute to the epigenetic inheritance of the effects of postnatal trauma. *Molecular psychiatry*.

301. Grandjean, V., S. Fourre, D. A. De Abreu, M. A. Derieppe, J. J. Remy, and M. Rassoulzadegan. 2015. RNA-mediated paternal heredity of diet-induced obesity and metabolic disorders. *Sci Rep* **5**: 18193.